Academician Evgene Kharadze

Vice - President of International Union of Astronomy (1976-82)

I would like to give you brief information you about a great Georgian scientist, academician and public person Eugene Kharadze. He was born on October 31, 1907. In 1930, he graduated from Tbilisi State University and in 1931-1934, was a postgraduate student at Leningrad Astronomical Institute. In 1932, he founded Abastumani Astrophysical Observatory, headed it until 1992 (for 60 years!) and was an honorable director of the Observatory for 10 years before he deceased.

In 1937-1998, Eugene Kharadze was the head of the Faculty of Astronomy of Tbilisi State University. In 1959-1966, he was the rector of Tbilisi State University. In 1992-2001, he closely cooperated with Samtskhe-Javakheti State University. His works were dedicated to different astronomical fields. Eugene Kharadze was given a title of a Doctor of Physical and Mathematical Sciences (1948) and Professor (1949), Vice-President (1972-77) and President (1978-86) of Georgian Science Academy, Vice-President of International Astronomical Union (1976-82) and Member of Georgian Encyclopedia Council.

Academician Eugene Kharadze was awarded with a number of prizes, including an Order of Honor. His painstaking efforts to support the development and success of astrophysical research are indeed invaluable.

Today, Abastumani Astrophysical Observatory founded by Eugene Kharadze is engaged in active scientific work.

Abastumani Astrophysical Observatory was named after Eugene Kharadze in 2001. The great scientist died on October 10, 2001.

R. Chigladze

The III volume of Journal
"Astronomy & Astrophysics (Caucasus)" was dedicated to the
110th Anniversary of Academician Eugene Kharadze.

Astronomy & Astrophysics (Caucasus) 3, (2018)

ABOUT THE PROBABILITY OF RECURRENCE SUPERNOVAE OUTBURSTS IN DIFFERENT GALAXIES

I.R. Salmanov [1]
[1] N. Tusi Shamakhy Astrophysical Observatory of NAS of Azerbaijan, city Baku, Azerbaijan;
Email: salmanov1940@mail.ru
P.N. Shustarev [2]
[2] N. Tusi Shamakhy Astrophysical Observatory of NAS of Azerbaijan, city Baku, Azerbaijan;
Email: petersh50@mail.ru

Abstract

The characteristic peculiarities of galaxies with multiple (nSN ≥ 3) outbursts of supernova (SN) have been considered in the article. It has been revealed that such usual spiral galaxies and nSN ≥ 5, SN of II type with overwhelming majority burst out. It has been noted that the medium large stellar mass, high rate of stellar formation and less massive black hole (in the nucleus) and less importance of the surface density of the galaxies are typical to the galaxies with multiple outbursts of SN. Probability of multiple outbursts of galaxies increases with the growth of the deviation of the color- index from the mean value.

Key words: nucleus of galaxies, rate of star formation, multiple supernovae outbursts

1. Introduction

As it is known, in some galaxies (including our Galaxy) supernova outbursts occur from time to time. At the same time, there is a considerable number of galaxies, in which no outbursts were generally observed during the whole observation period (~50-100 years), in others only one outburst was observed, while in some (but few) galaxies, there were several outbursts (up to 9) observed, following each other with different time intervals. Unfortunately, this phenomenon is related to the structure and physical properties of these galaxies, or is it a random process related to the observational selection? – It is extremely difficult to answer this question now.

For example, the fact opposing the first assertion is that among the galaxies, in which there were both, single and multiple outbursts, there are almost all presently known types of galaxies (including quasars and blazars). The fact opposing the second assertion is that as we have seen, quite weak outbursts of brightness in rather distant galaxies (called anonymous), then, naturally, we have to see them in close, long-observed galaxies. Indeed, we should mention the fact that the ratio of the number of I-type supernovae to II-type supernovae for anonymous galaxies equals 4.05, while for nearer galaxies (e.g. of NGC catalog), this ratio is 1.39, which is likely to be due to the fact that a I-type of supernova is brighter than the II-type one.

2. Outburstrs of I and II Type SNe

Probable observational selection, a relatively small collected observational data on supernova outbursts and small time interval, during which more or less regular observations of supernova are carried out, make it very difficult to find any regularities both in general supernova outbursts, and in the nature of the multiplicity of outbursts. For example, analysis of data from the catalogue (Barbon 1999) showed that, as a rule, due to multiple outbursts ($n \geq 4$), the outbursts of the II type are more common. However, this property of multiple outbursts is not universal. At this point, one can give both examples and counterexamples as well; we do not know what happened in those galaxies before, like we do not know what will happen to them in the future.

Nevertheless, as the observational data accumulate and various hypotheses appear from time to time, an explanation of one or another fact is done (see e.g. (Hakobyan et al.2014)). However, we will not consider them as it is not the subject of the present article.

The authors in (Sullivan et al. 2006) concluded (on the basis of observational data for more than 120 galaxies) that the probability of outbursts recurrence increases with the increase of weight (log $M*$) of stellar component of these galaxies, as well as with the increase of the star formation (logSFR) in them. In this article (in Figure 5) logSFR vs logM^* graph was constructed, which clearly shows the change in the rate of star formation with the change in the mass of the stellar component. In Fig. 1 of the article, we constructed a similar graph using the data from article (Rowan-Robinson 2008). In order not to overload the drawing, we took only points belonging to the first observation area and only for the galaxies of morphological type Sab. There were total 5192 points. The resulting figure is very similar to Figure 5 of the article (Sullivan et al. 2006.), except a small shift along axis logM^* towards larger mass values.

Thus, the probability of recurrence of outbursts apparently depends on such fundamental parameters of galaxies as the star formation rate and stellar mass of its component.

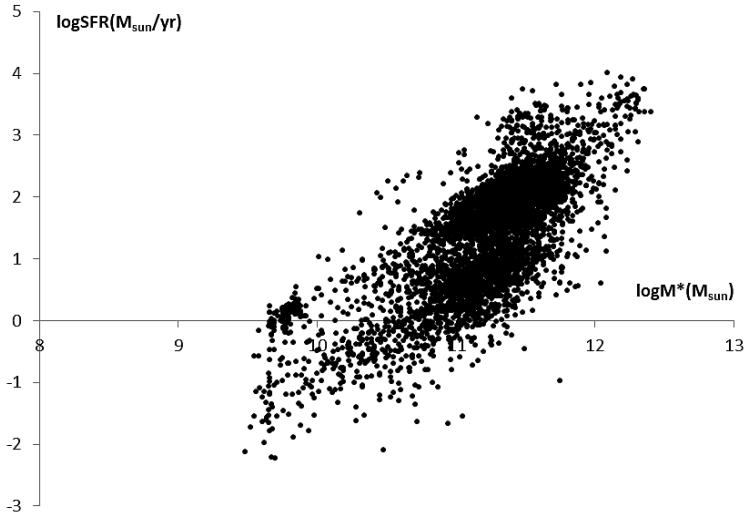

Figure 1. Change in the star formation rate, depending on the mass of the stellar component for the galaxies of morphological type Sab from the article (Rowan-Robinson 2008).

This fact drew our attention to other fundamental parameters of galaxies, such as the mass of the nucleus. From article (Beifiori et al. 2009.) , in which for the case of the Keplerian model of the galactic disk, the upper limits of the masses of supermassive black holes in these galaxies were calculated by using the observational data obtained with telescope "Hubble", for two cases of disc inclination of 33° and 81°. Fig. 2 shows the graph of these masses (as marked in the article (Beifiori et al. 2009.) . We denote them as MBH1 from the number of supernovae in these galaxies.

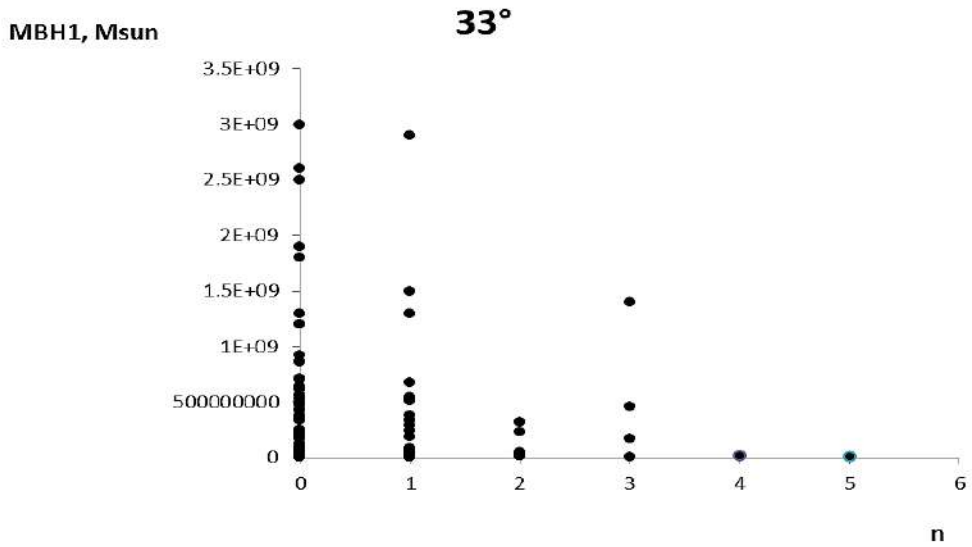

Figure 2. The number of multiple outbursts, as well as a single one and galaxies without any outbursts, depending on the masses of supermassive black holes in these galaxies. The slope of the disc plane is 1 =33°

A similar graph for 1 = 81°is not apparently different from Figure 2, but only at a zero-point. Thus, this figure shows that the smaller the mass from the supermassive black hole, the greater the probability that multiple supernova outbursts in this galaxy. A similar figure has been drawn by us individually for the spiral and elliptical galaxies (see Fig. 3). This figure shows that multiple supernovae outbursts are inherent to spiral galaxies, and in case of elliptical galaxies, they are possible only with a more massive black hole. We can conclude from the aforesaid that it is most likely that the galaxies with multiple supernovae outbursts have really somehow different physical conditions. In particular, on average, there is a big star mass, the larger star formation rate, and less massive black hole (the nucleus).

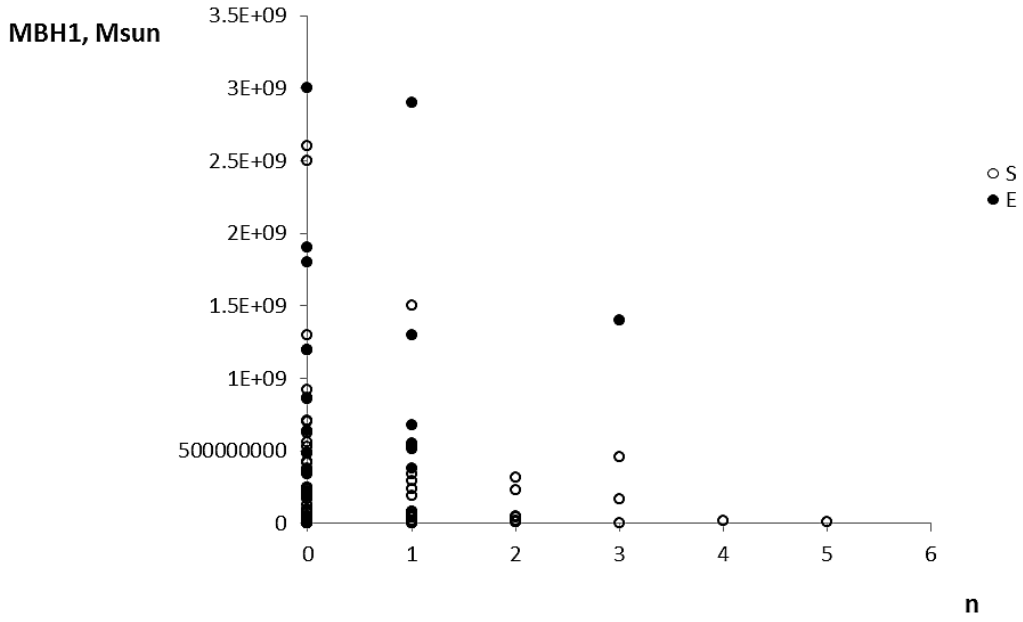

Figure 3. The dependence of the number of outbursts from the mass of a super- massive black hole in galaxies of two different morphological types.

For further analysis, we calculated the value of $\log M_d/R_{eff}^2$, where value M_d for our galaxies is taken from the catalogue (William et al. 2013.) and is determined based on the analysis of the dynamics of galactic matter. We obtained the value of effective radius - R_{eff}, measured in kpc from the same catalogue. We contingently called this value planar density (PD), which is measured in kps^{-1} and a graph constructed for this parameter is similar to that in Fig. 2. As it is seen in Fig. 4, it is similar to Fig. 2 and moreover, the higher the value of the PD, the lower the probability of multiple supernovae outbursts.

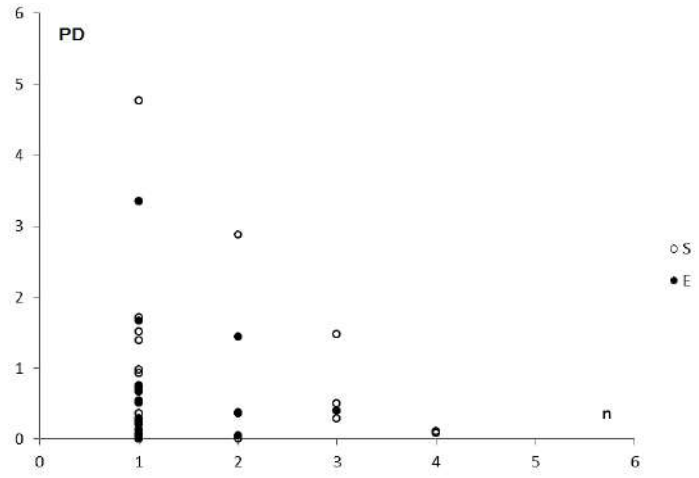

Figure 4. Multiplicity of supernovae outbursts, depending on the values of PD

Hence, naturally, it implies the necessity for constructing another graph. From Fig. 5, it is clear that only for sufficiently small values of PD there may be sufficiently massive nuclei of galaxies, and on the contrary, as the probability of multiple outbursts relies on the aforesaid, it is the highest for small PD and small mass of nuclei. As for another graph (see Fig. 6), where D is the distance to the respective galaxy in Mpc from the article (William et al. 2013.) , the figure shows that galaxies with large PD - are mainly close galaxies.

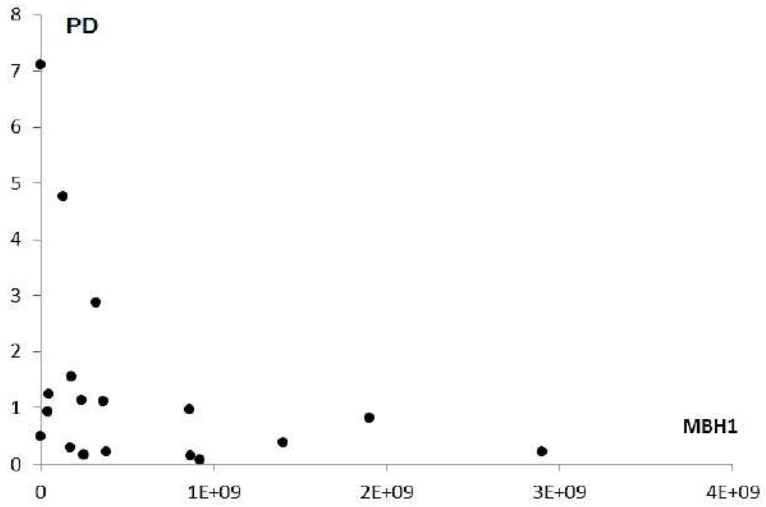

Figure 5. Change of the values of PD for galaxies with different values of super- massive black holes.

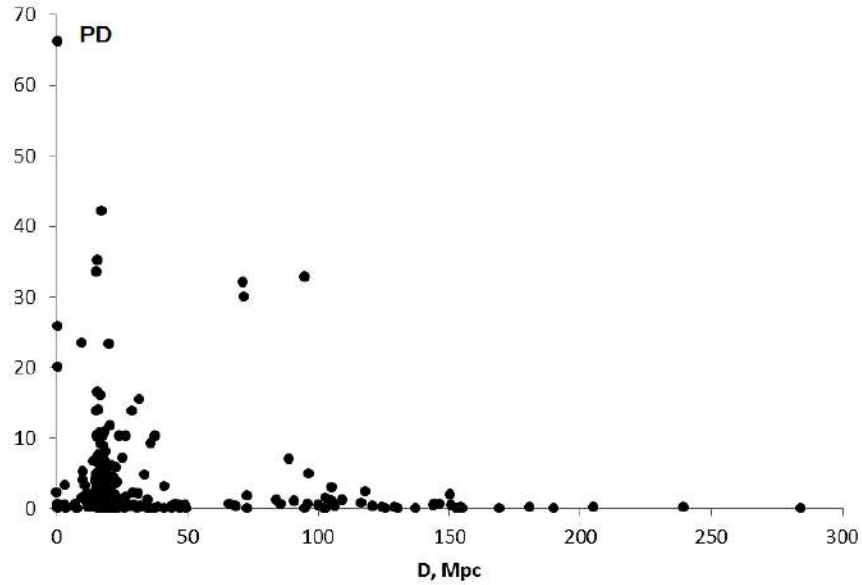

Figure 6. Change the values of PD of galaxies depending on the distance to these galaxies.

From Fig. 6 it can be concluded that the farther the galaxy is, the less its PD values are (for close galaxies from the NGC catalog). In addition, the absence of the points at the top - right side of the graphs in Fig. 5 and Fig. 6 are worthwhile. Unfortunately, no final conclusions can be made as we have few data, i.e. the statistics is relatively poor.

Let us now analyze the possible connection of photometric indexes with the mass of nucleus. As for searcher SIMBAD (Strasbourg astronomical date center), the largest number of data is provided for the values J, H, K, but, unfortunately, their bandwidth is too close to each other and, moreover, all of them are in the infrared area of spectrum. Therefore, we calculated the color-index (V-J) for the galaxies with different numbers of multiple outbursts (app. from 0 to 5), and the graph of mass of nucleus (MBHI) - color index (V-J) is constructed separately. It is clear from Fig. 7 that the greater the multiple outbursts are in the galaxy, the less the value of color-index is on average (V-J).

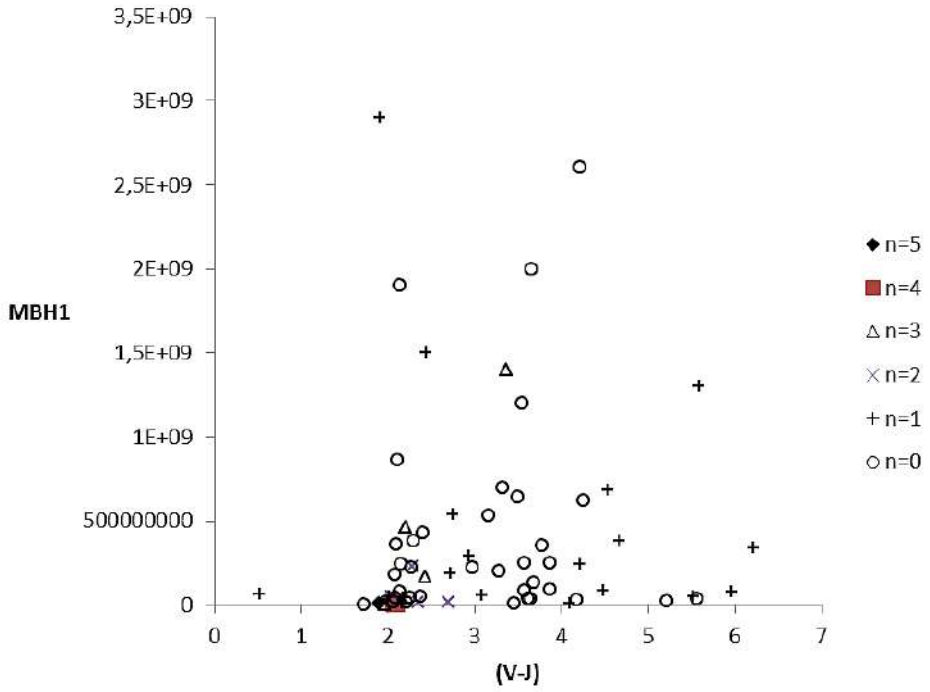

Figure 7. Graph of mass of nucleus-color-index (PD) for considered galaxies separately for different number of multiple outbursts.

Moreover, the analysis of a large number of different color-indexes shows that they are distributed in the normal (or close to similar) regardless the morphological type of galaxies.

3. Conclusions

Thus, the following conclusion can be made from the present article: it is confirmed that the probability of multiple outbursts in galaxies increases with an increase in the mass of the stellar component and star formation rate; it shows that the probability of multiple outbursts in galaxies increases with a decrease of the mass of supermassive black holes in them, as well as with a decrease of the values of PD in the galaxies; the probability of supernovae outburst in the galaxy increases with its color-index deviation from the average value of the index as it decreases.

We consider it our duty to express our sincere gratitude and appreciation to D.Y. Tsvetkov for his valuable remarks and productive discussions of the article.

References

Beifiori A., M. Sarzi, E. M. Corsini et al, Upper Limits On the Masses Of 105 Supermassive Black Holes from Hubble Space Telescope/Space Telescope Imaging Spectrograph Archival Data, Ap. J., 2009, v. 692, p. 856-868.

Hakobyan A. A., T. A. Nazaryan, V. Zh. Adibekyan, A. R. Petrosian, L. S. Aramyan, D. Kunth, G. A. Mamon, V. de Lapparent, E. Bertin, J. M. Gomes, M. Turatto. Supernovae and their host galaxies - II.The relative frequencies of super-novae types in spirals, MNRAS, 2014, v. 444, p. 2428-2441.

James D. Neill, Mark Sullivan, D. Andrew Howell, et al, The Local Hosts of Type Ia Supernovae, Ap. J, 2009, v. 707, p. 1449-1465.

Sullivan M., D. Le Borgne, C. J. Pritchet et al, Rates And Properties Of Type Ia Supernovae As a Function of Mass And Star Formation in Their Host Galaxies, Ap. J, 2006, v. 648, p. 868-883.

SWIRE Photometric Redshift Catalogue (Rowan-Robinson +,2008)/11/290.

The Asiago Supernova Catalogue 1999 (Barbon+, 1999)/II/227.

William E. Harris, Gretchen L. H. Harris, Matthew Alessi, A Catalog Of Globular Cluster Systems: What Determines The Size of a Galaxy's Globular Cluster Population, , Ap. J, 2013, v. 772, p. 82 (1-13).

Astronomy & Astrophysics (Caucasus) 3, (2018)

THE FRAUNHOFERS LINES CLASSIFICATIONS ON ASYMMETRY CHANGES INSIDE THE PROFILES IN SPECTRUM OF THE SUN

D.M. Kuli-Zade, S.N.Gulahmedova, S.Sh. Rajabova

Baku State University

E-mail: ckulizade@mail.ru

Abstract

The article offers the method of asymmetry change inside Fraunhofer lines profiles and uses the new digital spectra with high resolution. It was shown that asymmetry may change repeatedly in value and sign inside the spectral line profile. The lines can be classified in three groups on asymmetry changes inside the profiles.

Key words: Solar spectrum, Line profiles, Asymmetry, Asymmetry changes, Classification.

1. Introduction

The use of new digital spectral devices with high resolution and high dispersion (Fourier spectrometers and double monochromators) helped finally establish that in the spectrum of the Sun, most Fraunhover lines are asymmetric [1-8]. However, all the works dedicated to this problem so far have been qualitative and do not allow thoroughly studying the asymmetry of Fraunhofer lines profiles. The problem could be solved by using a quantitative method, which allows measuring asymmetry more thoroughly and expressing it by physical dimensional values. Besides, the earlier works did not consider the change of asymmetry inside the spectral line profile at all. The investigation of this problem may play a certain role in the study of the stratification of the solar photosphere.

In this work we propose the new quantitative method to investigate the asymmetry change inside the weak and moderate Fraunhofer lines profiles in the spectrum of the Sun.

2. Spectral material

We used high-dispersion digital spectral materials with high resolution by Kurucz and others [9], obtained by Fourier- spectrometer. The residual intensity in [9] is given by step 2mÅ. This allows drawing weak and moderate Fraunhofer lines profiles in the spectrum of the Sun as a star.

For the investigation purposes, the clearest, non-mixed lines in the spectral region λλ5000-7000Å were selected. Mostly lines FeI, TiI, CrI, NiI and others were used. Excitation potential of lower levels of the used lines varied from ε=3.2 ev to ε=5.0 ev. The construction of the studied Fraunhofer lines profiles and determination of their spectrophotometric properties were done by means of program ORIGIN.

3. Method

The key point in the study of change of asymmetry inside Fraunhofer lines profiles is the determination of the center of the line prolife. Usually, the profile center is determined by maximum value of central depth R_0. It is admitted in advance that the nucleus of profile is symmetrical. Another objective is the determination of the line center at a half-width of the profile. This allows studying the change of asymmetry not only in the wings, but also in the nucleus of lines profiles. But due to this, the line profile in the region of $R=1/2R_0$ may be symmetrical. The analysis of profiles evidences that more visible asymmetry is observed in the wings of profiles. That is why the different researchers determine the center of profile differently: either on central nucleus, or on the half width of the profiles. In the present work, the center of the line is determined on the maximum value of central depth R_0.

At different distances from the center of the lines profiles, i.e. for different depths of lines profiles, the value is determined as follows:

$$\delta(R)=\Delta\lambda_{\upsilon i}- \Delta\lambda_{ri} \ ,$$

where $\Delta\lambda_{\upsilon i}$ and $\Delta\lambda_{ri}$ are the distances from the center at the same depths of the profile in the violet and red wings of the lines, respectively. This value determines the quantitative value of asymmetry at the given depth of the profile in mÅ. We call it differential asymmetry. It is quite a low value, which is measured in mÅ and which can be determined only by the digital high-dispersion spectra.

If $\delta(R)>0$, we will call the asymmetry a violet one, but if $\delta(R)<0$, the asymmetry is red. If $\delta(R)=0$, then line profile at the given depth is symmetrical.

The dependence of differential asymmetry $\delta(R)$ on depth R shows the change of asymmetry inside the line profile.

It turned out that at some depths of the given line profile $\delta(R)>0$, i.e. violet asymmetry is observed, but at other depths $\delta(R)<0$, i.e. the asymmetry is red. Thus, within the range of a line profile, differential asymmetry changes both by value and sign. This determines a

complex, fine structure of Fraunhofer lines profiles in the spectrum of the Sun and stars.

Figure 1 shows asymmetry change inside the profiles of infrared O I lines. In this case $\delta(R)>0$, i.e. violet asymmetry is observed, and asymmetry changes only by value.

Figure 2 shows asymmetry change inside the line profiles for λ5845.294Å and λ5922.123Å. In this case, for all line profiles $\delta(R)<0$, i.e. only red asymmetry is observed; asymmetry changes only by value.

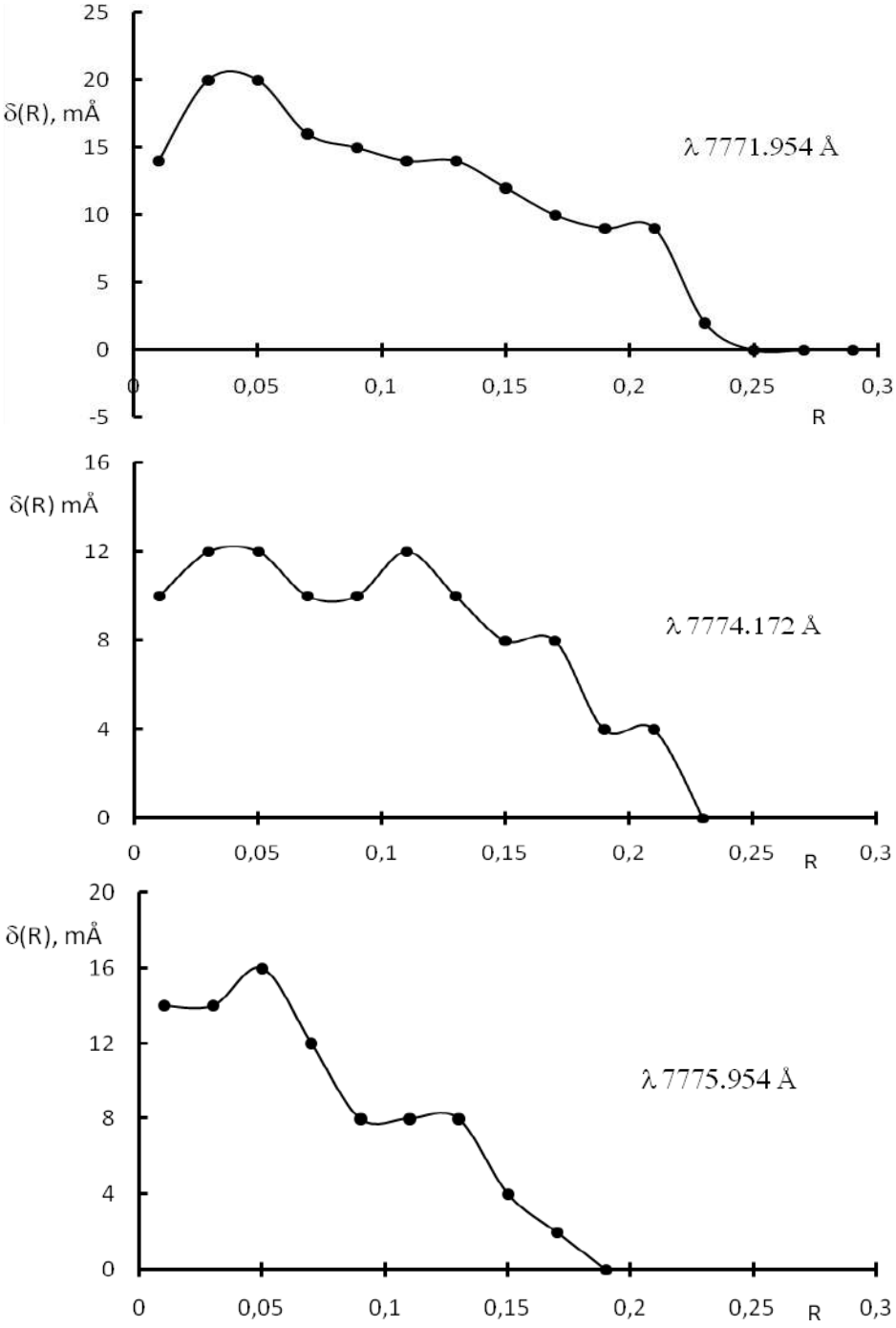

Figure.1. Asymmetry dependence for infrared triplet lines OI on line depth R

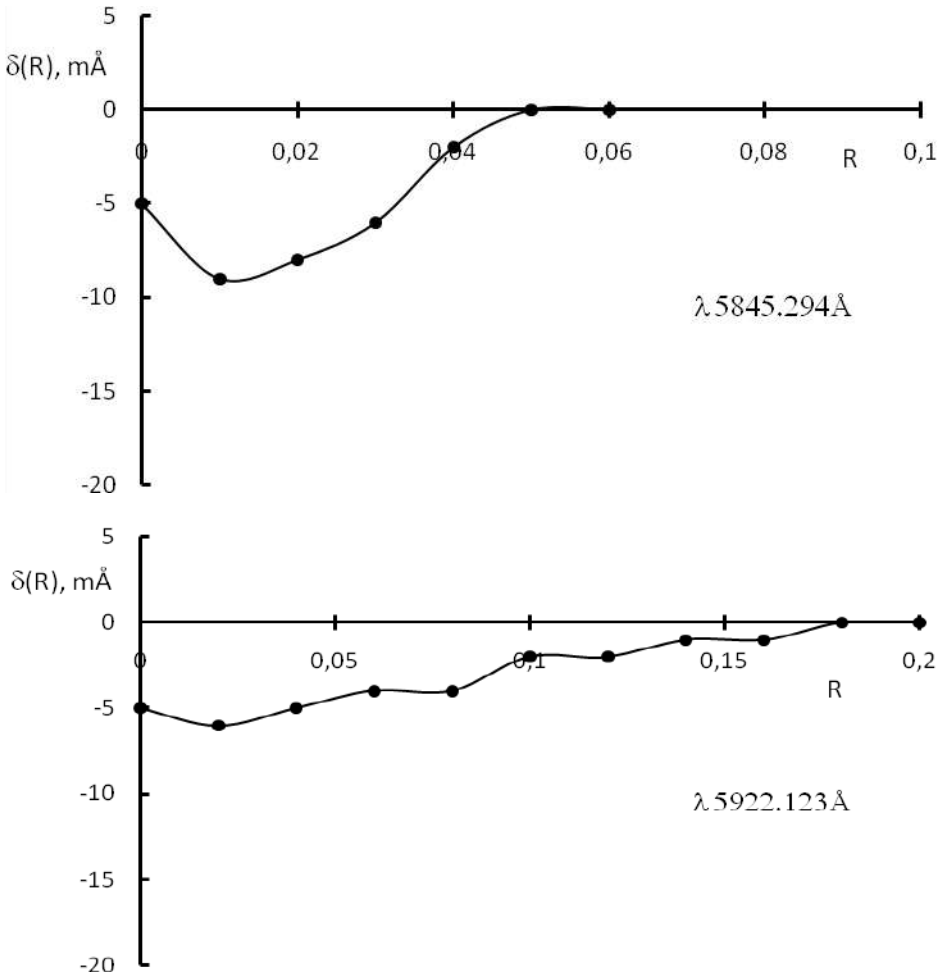

Figure.2. Asymmetry dependence λ 5845.294 Å and λ 5922.123 Å on line depth R

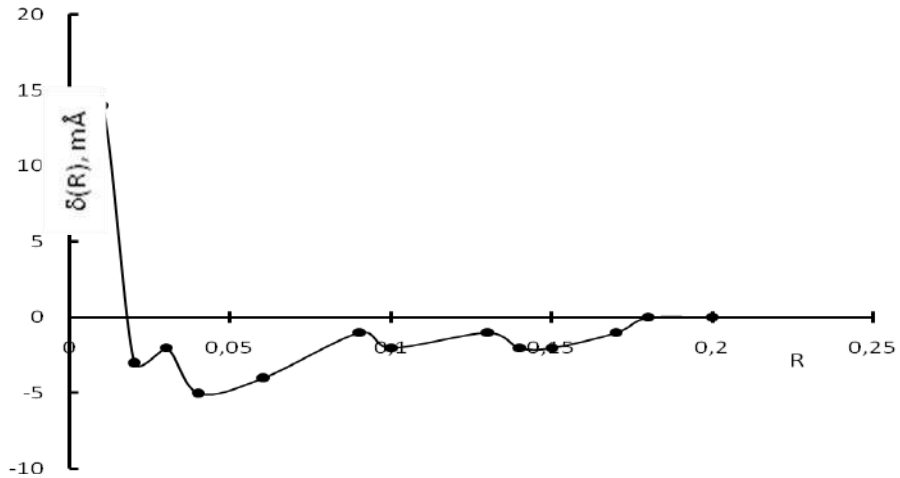

Figure.3. Asymmetry dependence for λ5342.708 Å on line depth R

The change of asymmetry inside line profile λ5342.708ÅFeI in the spectrum of the Sun as stars, i.e. in the flux spectrum of the Sun is shown in Fig.3. As in the case of the Sun stars in the far wings of lines in $R<0.02$, $\delta(R)>0$,violet asymmetry is observed. At the depth of $R\approx0.17$ $\delta(R)\approx0$, asymmetry is not observed. At $R>0.02$, $\delta(R)<0$ i.e. red asymmetry is observed. It turns out that, violet asymmetry is observed in wings and is replaced by red asymmetry in the central parts. In this case, asymmetry changes both by value and sign.

4. Classification

The experimental results of a number of Fraunhofer lines profiles in the spectrum of the Sun revealed that the profiles of most lines are asymmetrical. An asymmetry of lines profiles has a complex, fine structure. In the range of the given line profile, the asymmetry may change its value and sign repeatedly, i.e. a violet asymmetry [$\delta(R)<0$] observed at one depth, can be changed by a red asymmetry [$\delta(R)<0$], and vice versa, a red asymmetry may change to the violet one. At some depths of the profile, $\delta(R)\approx0$ can be observed, i.e. asymmetry does not occur. This is probably associated with the change of physical conditions in the photosphere as the depth increases.

The lines can be classified in three groups on a nature of change of asymmetry inside the profile:

1. Throughout the depth of profile $\delta(R)>0$, i.e. only violet asymmetry is observed and asymmetry changes only by value; Fig.1.
2. Along the whole depth of profile $\delta(R)<0$, i.e. only red asymmetry is observed and asymmetry changes only by value; Fig.2.
3. At some depths of profile $\delta(R)>0$, but at other depths of profile $\delta(R)<0$. Inside the line, asymmetry changes both by value and sign. Fig.3.

References

1. Kostyk R.I. The fine structure of the Fraunhofer lines and the structure of the atmosphere of the Sun. Astron. Zh. 1985, 62, no. 1, p.112-122.
2. Kuli-Zade DM Dependence of the asymmetry of the profiles of Fraunhofer lines on intensity. Astron. Zh., 2001, N1, p.87-90.
3. Cavallini F., Ceppatelli G., Righini A. Interpretation of shifts and asymmetries of FeI lines in solar facular areas. Astron. And Astrophys., 1987, 173, №1, p. 155-160.
4. Dravins D. Photospheric spectrum line asymmetries and wavelength shifts. Ann. Rev. Astron. and. Astrophys., 1982, v. p. 61-89.
5. Higgs L.A. Asymmetry of solar line profiles. Month. Not RAS, 1962, v. 24, N21, 51-59.

6. Kuli-Zade D.M. Intensity Dependence of the asymmetry of Fraunhofer Line Profiles. Astronomy Reports, 2001, v.45, №1, p. 75-78.

7. Kostyk R.I., Orlova T.V. On the asymmetry of selected Fraunhofer lines. V. Solar Phys., 1977, v. 53, №2, p. 353-358.

8. Balthasar H. On the contribution of horizontal granular motions to observed limb - effect curves. Solar Phys, 1985, v. 99, №1/2, p. 31-38.

9. Kurucz R.L., Furenlid I., Brault J., Testerman L. Solar flux atlas from 296 to 1300 nm. New Mexico, National Solar Observatory, 1984, 293 p.

Astronomy & Astrophysics (Caucasus) 3, (2018)

ON THE FULL ASYMMETRY OF THE WHOLE FRAUNHOFER LINES PROFILE IN SPECTRUM OF THE SUN

D.M. Kuli-Zade[1], S.G. Mamedov[2], Z.F. Aliyeva[1], K.İ. Alısheva[1], R.K. Sartipzade[1]

[1]Baku State University
[2] Shamakhy Astrophysical Observatory

E-mail:ckulizade@mail.ru

Abstract

New quantitative method was proposed to determine full asymmetry of whole Fraunhofer lines profile in the spectrum of the Sun. New dimensional physical unit called full asymmetry of whole lines profile was introduced. Full asymmetry of whole profile and its positive and negative fractions for 94 Fraunhofer lines in resolved and unresolved solar spectrum were defined. It was shown that with the increase of lines intensity the full asymmetry increases significantly.

Key words: The Sun. Spectrum. Fraunhofer lines. Profiles . Full asymmetry.

1. Introduction

Different methods are often used for the description of asymmetry of Fraunhofer lines profiles in the spectra of the Sun stars: asymmetry coefficient, the third moment of distribution function of lines profiles, bisector – geometric locus of mid-chord which connects profile points on violet and red wings with similar intensity and others. However, these methods are not quantitative and have a descriptive character. This does not allow us to study the dependence of asymmetry of profiles on atomic and photospheric values what is very important for the analysis of mechanisms leading to the asymmetry of Fraunhofer lines profiles in stellar atmosphere. Besides, there was not a definite value for the determination of asymmetry of whole Fraunhofer lines profiles.

The overview of Atreshenko I.N. and Gadun A.S. [1] made a special emphasis on this point: «There are no generally recognized characteristics for finding statistic dependences of asymmetry of lines on, for example, atomic parameters to describe asymmetry of whole profile ».

At the Astrophysics chair of Baku State University, a new quantitative method to determine the full asymmetry of whole Fraunhofer lines profiles in the spectra of the Sun and stars, was introduced [2-4].

2. Method

The method to determine the asymmetry of whole lines profile is as follows: taking two points with similar intensity on violet and red wings of line profile. The distance differences of these points from the center of a profile for various profile depths are determined as:

$$\delta(R_i)=\Delta\lambda_{vi}-\Delta\lambda_{ri}. \quad (1)$$

The line center is determined at half-width of the profiles, which is a differential asymmetry and determines asymmetry on depth of a profile. The differential asymmetry $\delta(R_i)$ within the range of lines profile varies in value and in sign. In other words, within the range of the given line profile, the violet asymmetry ($\delta(R)>0$) is repeatedly replaced with the red one ($\delta(R)<0$) and vice versa. Further, the dependence $\delta(R_i)$ on profile depth R_i is plotted (see Fig.1).

Fig. 1 shows the dependence $\delta(R_i)$ on R for lines λ5367,476 Å FeI in the spectrum of the solar disc center. As it is seen, within the range of the given line profile $\delta(R)$ the sign repeatedly changes $\delta(R) >0$ (violet asymmetry) to $\delta(R_i)<0$ (red asymmetry).

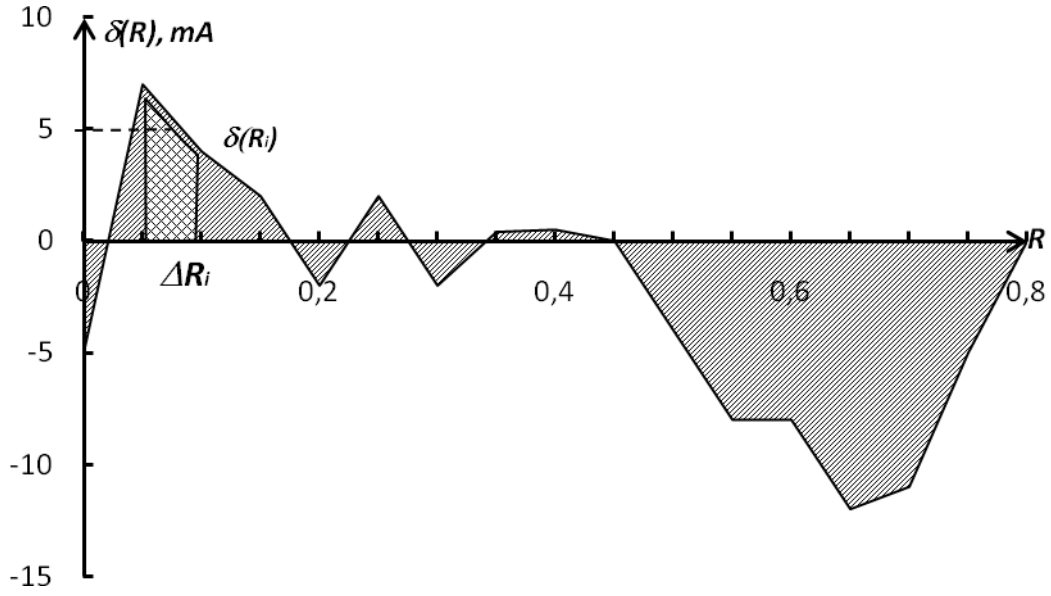

Fig. 1 .Determination of full asymmetry of whole profile

The shaded area, which is limited by line dependence $\delta(R)$ on R with axis of abscissa can be expressed with the value:

$$\Lambda = \sum_{i}^{n} |\delta(R_i)| \Delta R = \sum_{\delta(R)_i > 0} |\delta(R_i)| \Delta R_i + \sum_{\delta(R) < 0} |\delta(R_i) \Delta R_i| , \qquad (2)$$

Which is called full asymmetry and determines the asymmetry of whole Fraunhofer line profile. This value is determined from the observed lines profiles and is measured in mÅ.

In (2), the first member determines the positive,

$$\Lambda_+ = \sum_{\delta(R)>0} |\delta(R_i)| \Delta R_i , \qquad (3)$$

but the second member determines the negative

$$\Lambda_- = \sum_{\delta(R)<0} |\delta(R_i)| \Delta R_i \qquad (4)$$

share of full asymmetry of line profile.

The double shaded area in fig. 1 shows the component of summation in determining the asymmetry of whole Fraunhofer line profile. It should be noted that the full asymmetry and its positive and negative shares are rather small values (several mÅ). That is why, in such studies, it is necessary to select only non-blended lines with few isotopic shifts and practically free from hyperfine structure. In this regard, it is convenient to use Fev lines of spectral region λλ5000-7000Å.

Besides, for this task, the spectral devices of high spectral dispersion and high resolution must be used. That is why, the study of thin structure of Fraunhofer lines profiles have started only since the digital double monochromators and Fourier spectrometers were in use.

3. Determination of full asymmetry

We determined the full asymmetry of whole profiles of 94 Fraunhofer lines in the spectrum of Solar disc center and the Sun as a star. Digital spectra obtained with the help of double monochromators for disk center [5] and Fourier spectrometer of high-resolution for Sun as a star [6] were used. Construction of lines profiles, determination of equivalent widths W and full asymmetry Λ were conducted by program ORIGIN.

The results are given in the table 1, where in the first column the wavelengths of lines λÅ are presented, the second column shows the equivalent widths mÅ, and the last three columns show full asymmetry ΛmÅ of the whole profile and its positive and negative shares.

Table 1

Full asymmetry of the whole Fraunhofer line profiles

λ,Å	Element	ε	Resolved Sun				Unresolved Sun			
			W	Λ_+	Λ_-	Λ	W	Λ_+	Λ_-	Λ
1	**2**	**3**	**4**	**5**	**6**	**7**	**8**	**9**	**10**	**11**
5010,943	Ni I	3,63	49	0,41	-0,03	0,44	51	0,34	-0,68	1,02
5197,170	Ni I	3,9	28	0,03	-1,27	1,3	27	0,04	-1,32	1,36
5197,576	FeII	3,23	84	0,017	-0,04	3,21	81	1,42	-1,5	2,92
5197,942	FeI	4,3	37	0,03	-0,62	0,65	37	0	-0,75	0,75
5198,718	FeI	2,22	94	3,38	-0,06	3,44	97	1,82	-2,74	4,56
5223,190	FeI	3,63	29	0,05	-0,25	0,3	30	0	-1	1
5234,630	FeII	3,22	89	2,28	-0,6	2,88	86	0,22	-2,1	2,32
5246,777	CrII	3,71	19	0,03	-0,57	0,6	16	0,13	-0,22	0,35
5247,058	FeI	0,09	65	2,4	-0,02	2,42	65	0,1	-0,36	0,46
5247,574	CrI	0,96	82	1,42	-0,32	1,74	79	0,3	-0,92	1,22
5250,216	FeI	0,12	66	0,81	-0,43	1,24	68	1,59	-0,52	2,11
5264,808	FeII	3,33	48	0,96	-0,25	0,71	48	0,45	-1,04	1,49
5287,183	CrI	3,44	12	0,1	-0,28	0,28	11	0,07	-0,22	0,29
5293,375	CrI	3,37	7	0,01	-0,2	0,21	5	0	-0,2	0,2
5295,321	FeI	4,41	29	0	-0,75	0,75	29	0,66	-0,66	1,32
5296,702	CrII	0,98	92	1,72	-0,39	2,11	91	1,02	-1,56	2,58
5300,751	CrI	0,98	57	0,85	-0,32	1,17	59	0,06	-2,26	2,32
5305,866	CrII	3,83	26	0,02	-0,68	0,7	27	0,01	-1,32	1,33
5320,040	FeI	3,64	21	0,1	-0,4	0,5	22	0	-0,53	0,53
5342,708	CoI	4,02	30	0,17	0	0,17	32	0,14	-0,33	0,47
5376,836	FeI	4,29	17	0,02	-0,58	0,56	17	0,02	-0,45	0,47
5379,381	FeI	3,69	61	1,28	-0,13	1,41	60	0,26	-0,72	0,98
5386,340	FeI	4,15	33	0	-0,44	0,44	32	0,08	-0,48	0,56
5436,302	FeI	4,39	41	0,09	-0,68	0,77	42	0,15	-2,22	2,37
5522,454	FeI	4,21	44	0,27	-0,04	0,31	43	0,58	0	0,58
5560,220	FeI	4,43	55	0,75	-0,42	1,17	52	0,12	-1,02	1,14
5576,099	FeI	3,43	123	2,1	-0,64	2,74	123	3,12	-0,58	3,7
5608,981	FeI	4,21	14	0,03	-0,9	0,93	12	0	-3,41	3,41
5643,087	Ni I	4,16	17	0,02	-0,57	0,59	18	0,02	-0,48	0,5
5646,689	FeI	4,26	9	0,02	-0,05	0,07	8	0,03	-0,13	0,16
5648,279	CrI	3,82	7	0,07	-0,01	0,08	7	0,02	-0,49	0,51
5651,477	FeI	4,47	10	0,04	-0,56	0,6	19	0,11	-0,2	0,31
5661,354	FeI	4,28	23	0,01	-0,54	0,53	25	0	-0,79	0,79
5662,524	FeI	4,18	97	3,11	-0,09	3,2	95	1,18	-0,72	1,9
5677,695	FeI	4,1	8	0,01	-0,3	0,31	10	0,06	-0,677	0,73
5679,032	FeI	4,65	62	1,61	-0,1	1,71	61	0,08	-0,42	0,5

5719,828	CrI	3,01	7	0,01	-0,29	0,3	12	0,22	-0,23	0,45
5731,772	FeI	4,26	59	1,15	-0,24	1,39	61	0,03	-0,57	0,6
5741,856	FeI	4,26	32	0,21	-0,17	0,38	38	0,27	-0,35	0,62
5778,463	FeI	2,59	21	0,06	-0,45	0,51	28	0	-1,11	1,11
5783,073	CrI	3,32	33	0,09	-1,09	1,18	41	0,03	-1,88	1,91
5805,226	Ni I	4,17	43	0,66	-0,03	0,69	47	0,2	-0,1	0,3
5811,919	FeI	4,14	12	0,01	-0,46	0,47	13	0,19	-0,2	0,39
5814,815	FeI	4,28	24	0,05	-0,27	0,32	28	0,33	-0,41	0,74
5844,608	CrI	3,01	6	0,01	-0,08	0,09	6	0,01	-0,3	0,31
5844,933	FeI	4,15	6	0,01	-0,17	0,18	5	0,03	-0,57	0,6
5845,294	FeI	5,03	9	0	-0,3	0,3	8	0	-0,47	0,47
5880,270	TiI	1,05	8	0,07	-0,09	0,16	8	0,03	-0,36	0,39
5922,123	TiI	1,05	20	0,02	-0,45	0,47	22	0	-0,4	0,4
5927,797	FeI	4,65	43	0,18	-0,26	0,44	43	0,14	-0,56	0,7
5929,682	FeI	4,55	41	0,34	-0,17	0,51	43	0	-0,98	0,98
5930,191	FeI	4,65	92	2,69	-0,17	2,86	89	1,83	-1,11	3,04
5934,665	FeI	3,93	78	1,49	-0,31	1,8	80	1,43	-0,12	1,55
5969,578	FeI	4,28	6	0	-0,05	0,05	6	0,41	-0,01	0,42
6065,494	FeI	2,61	117	2,94	-0,1	3,04	116	1,81	-0,82	2,63
6093,649	FeI	4,61	31	0,11	-0,4	0,51	30	0,04	-0,62	0,66
6098,250	FeI	4,56	17	0,01	-0,62	0,63	17	0,01	-1,24	1,25
6098,664	TiI	3,06	8	0	-0,22	0,22	7	0	-0,24	0,24
6126,224	TiI	1,07	21	0	-0,39	0,39	23	2,85	-0,04	2,89
6151,623	FeI	2,18	48	0,39	-0,42	0,81	47	0,02	-0,8	0,82
6159,382	FeI	4,61	14	0	-0,56	0,56	13	0,03	-0,21	0,24
6176,816	Ni I	4,09	66	2,92	-0,01	2,93	63	0,83	-0,45	1,28
6177,253	Ni I	1,83	16	0,06	-0,22	0,28	15	0,05	-0,22	0,27
6186,717	Ni I	4,1	30	0,13	0	0,13	31	0,06	-1,67	1,73
6187,995	FeI	3,94	48	0,28	-0,22	0,5	47	0,18	-0,57	0,75
6213,437	FeI	2,22	82	2,76	-0,02	2,78	79	0,95	-0,16	1,11
6226,740	FeI	3,88	28	0	-0,07	0,07	29	0,29	-0,27	0,56
6246,327	FeI	3,6	119	3,98	-1,01	4,09	119	3,52	0	3,52
6252,565	FeI	2,4	118	2,82	-0,01	2,83	118	1,2	-0,09	1,29
6258,110	TiI	1,44	51	1,13	-0,11	1,24	50	0,42	-0,6	1,02
6297,799	FeI	2,22	73	1,46	-0,4	1,86	74	0,18	-1,32	1,5
6301,508	FeI	3,65	121	4,28	-0,07	4,35	124	2,65	-0,13	2,78
6302,499	FeI	3,69	86	1,94	-0,3	2,24	87	0,04	-1,73	1,77
6303,461	FeI	4,32	7	0,06	-0,03	0,09	8	0,7	0	0,7
6303,767	TiI	1,44	9	0,03	-0,01	0,04	11	0,05	-0,03	0,08
6315,814	FeI	4,07	41	0,02	-0,54	0,56	43	0,03	-1,08	1,11
6327,604	NiI	1,68	37	0,82	-0,03	0,85	40	0,21	-0,02	0,23

4. Discussion

As it was noted in the overview of Atrosehnko and Gadun[1], the method of bisector does not allow us to study the dependence of asymmetry on atomic and photospheric values, but the method of asymmetry coefficient gives the results, which cannot be physically grounded. A number of authors arrived at the conclusion that the intensity of fraunhofer lines of the asymmetry coefficient, which is determined by central moments of the second and third order, decreases and approaches zero for rather strong lines.

We consider that this is a false result related to the description method.

As it is seen from (2), when determining the full asymmetry of whole Fraunhofer line profile modules of components are summed. Otherwise, inside the lines profile, positive and negative shares of asymmetry can compensate each other fully or partially, and asymmetrical line might seem symmetrical.

Previous methods fail to consider the compensation of violet asymmetries in the same depths of line profile with red asymmetry in other depths. With our method, this condition is accounted with summing not the components but $\delta(R_i)\Delta R_i$, but their modules.

If asymmetry is related to dynamic processes in the Solar photosphere, then it should influence more strongly the strong lines, the formation of which covers the entire photosphere and chromospheres even partially, than the weak lines, which occur in rather thin layer of the photosphere.

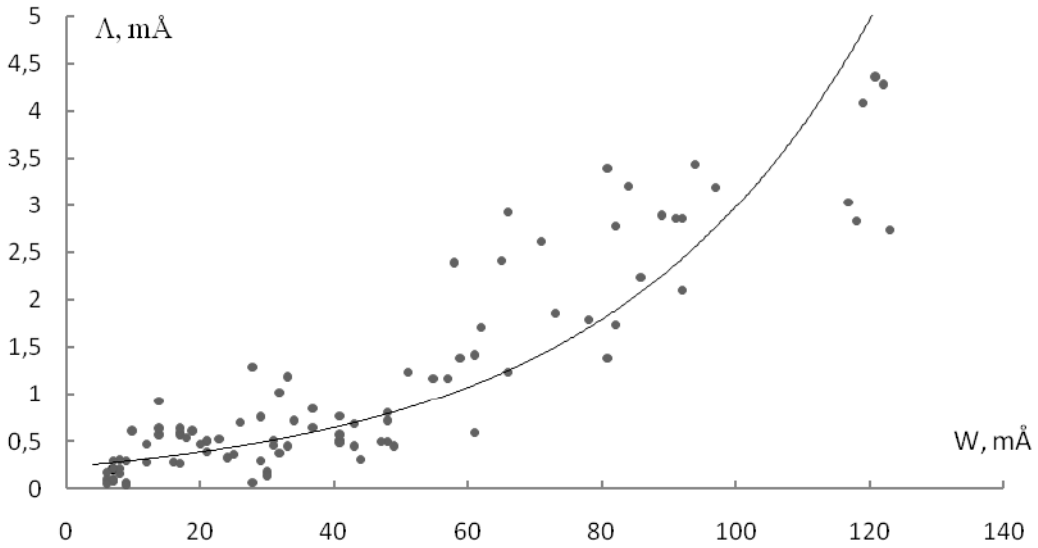

Fig. 2. Intensity dependence full asymmetry for resolved spectrum of the Sun

In fig. 2, the dependence of full asymmetry of whole line profile on equivalent widths of the studied lines is presented. As it can be seen, with an increase of lines intensity, the full asymmetry increases clearly and significantly, what is expected following the physical considerations.

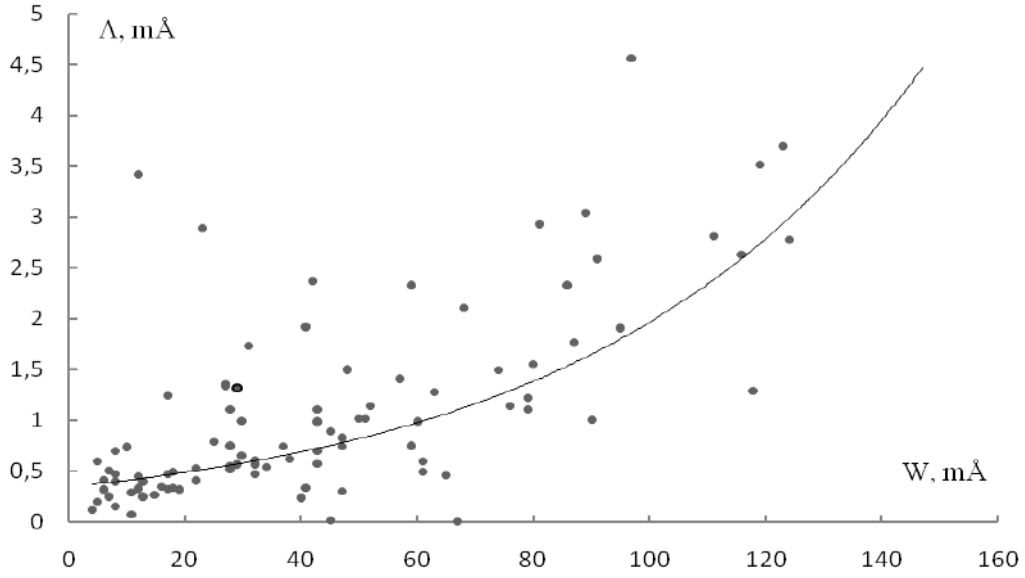

Fig. 3.. Intensity dependence full asymmetry for unresolved spectrum of the Sun

References:

1. Atroshenko I. N., Gadun A.S. Asymmetry and absolute shifts of Solar photospheric lines, VINITI, 1990, №1676.B 90.

2. Kuli – Zade D.M., On the quantitative method for measurement and analysis of the fine structure of Fraunhofer line profiles, Astron. and Astrophys. Transaction. 2014. v. 28, №4, 384-404.

3. Kuli-Zade D.M. Dependence of asymmetry of Fraunhofer lines profiles on intensity, Astron. jour. 2001, №1, 87-90.

4. Kuli-Zade D.M., Intensity Dependence of the asymmetry of Fraunhofer line Profiles, Astronomy Reports, 2001, v 45, №1, 75-78.

5. Del bouille L., Neven L., Roland G. Photometric Atlas of the Solar spectrum from λ3000 *to* 10000*Å , Lige, 1973; p. 241.*

6. Kurucz R.L., Furenlid I. , Brault J., Testerman L., Solar flux atlas from 296 to 1300 nm, New ,Mexico, National Solar Observatory, 1984, p. 239.

Astronomy & Astrophysics (Caucasus) 3, (2018)

Results of Observations over Jupiter's Galilean Satellites

R. Chigladze,[1, 2] M. Tateshvili [1]

[1] Samtskhe-Javakheti State University,

[2] Kharadze Abastumani Astrophysical Observatory, Georgia

Email: revazchigladze@ yahoo.com
Email: tateshvilimaia @gmail.com

Abstract

The work describes the polarization properties of the light reflected from the surfaces of Galileo Jupiter's satellites, with their physical characteristics studied based on their analysis. Europe turned out to have the most homogeneous, and Callisto has the least homogeneous. Time variations are the most typical to satellite Io what must be the result of the volcanic actions on the satellite surface.

Keywords: polarization, degree of polarization, front and rear hemispheres

1. Introduction

Since 1981, at Abastumani Astrophysical Observatory, the electropolarimetric and electrofotometric observations over the Galilean satellites of Jupiter in the optical-spectral regions (4200 – 7800 A) have been performed. Polarimeter ASEP – 78, in combination with different telescopes was used (Chigladze. 1987, 2006, 2012).

In general, the magnitude of the degree of polarization of the light reflected from the satellite's surface must vary depending on α-phase angle, satellite orbital longitude L, wave length λ and observation period t, or P = P (α, L, λ, t). (Dolffus A, 1975., Geake, K, A. Dollfus 1979., Veverka, I 1971., Zaitsev et al 2012., Chigladze. 2006, 2012, 2015). See the schematic picture in Fig. 1.

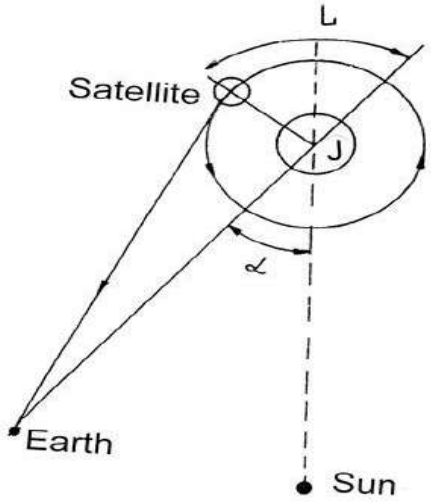

Fig. 1.

2. Observations

The following conclusions can be drawn based on the analysis of the obtained results:

1. Degree of polarization of Jupiter's Galilean satellites near the opposition significantly differs from zero (Table 1): L – Orbital longitude and P% - Linear polarization.

Table 1

For Io	$L = 93^0$ P = 0. 35%
For Europe	$L = 269^0$ P = 0. 27%
For Ganymede	$L = 90^0$ P = 0. 35%
For Callisto	$L = 333^0$ P = 0. 46%
	$(\sigma_\rho \leq 0,05\%)$

2. Dependence between the degree of polarization and the phase angle (Fig. 2, 3).

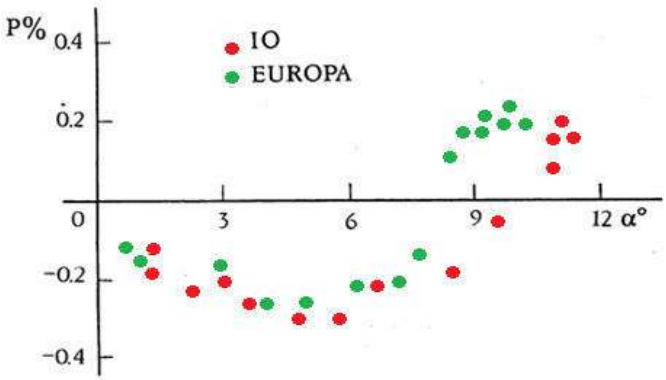

Fig. 2. For EUROPA , α (inv) = 10^0 , For IO , α (inv) = 8^0

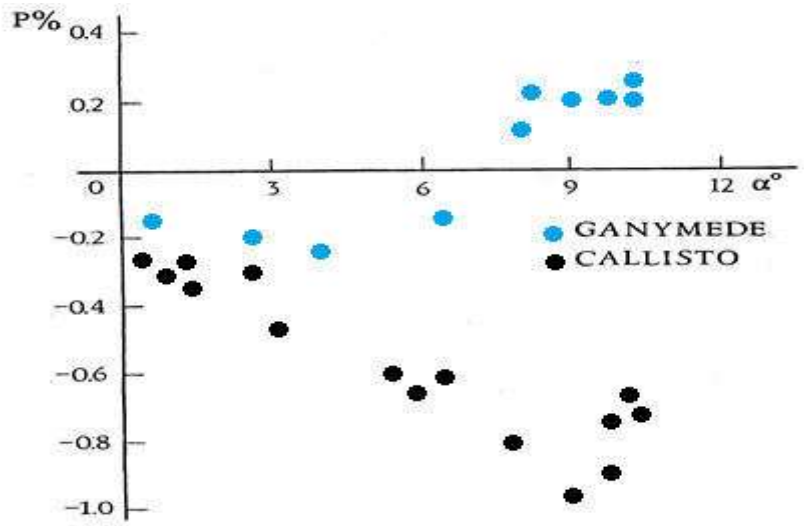

Fig. 3. For GANYMEDE , α (inv) = 8^0 , For CALLISTO, α (inv) > 11^0

3. Orbital variations of Galilean satellites Europe (Fig. 5) (reaches the maximum at minimum).

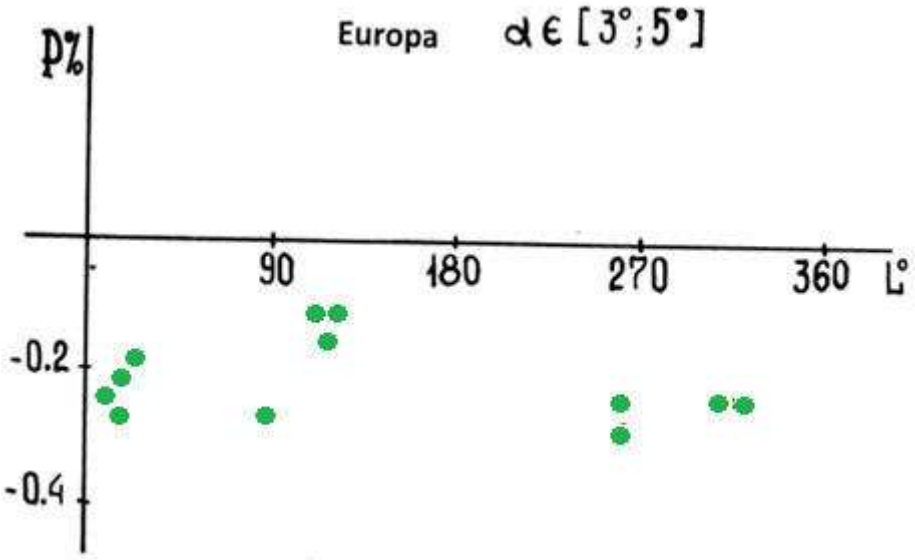

Fig. 4. Dependence between the degree of polarization and the orbital longitude

As it is seen from the drawings, Europe has the most homogeneous surface and Callisto has the least homogeneous surface.

4. Time variations are most typical to satellite Io evidencing the existence of a volcanic activity on its surface (Fig. 5),

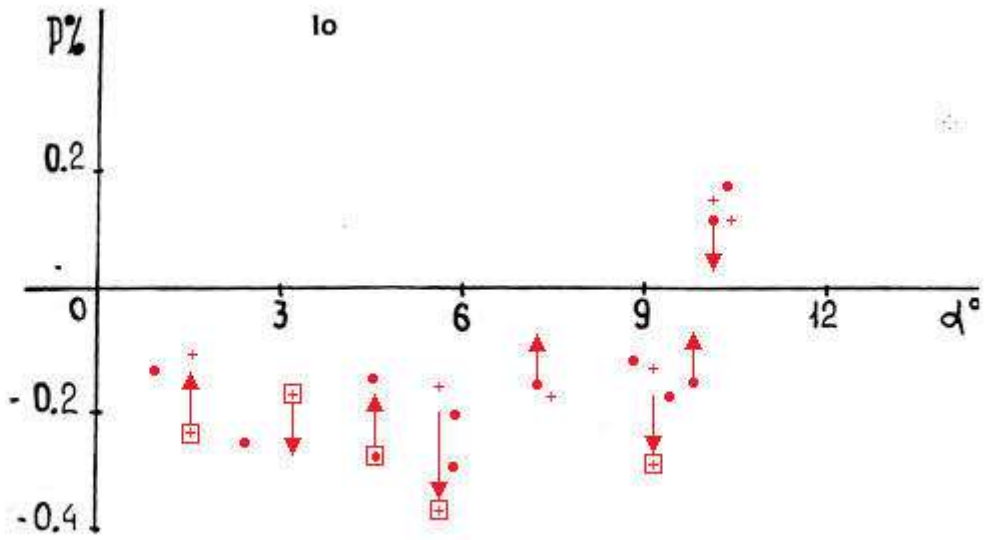

Fig. 5. The length of the arrow points to the scale of change.

5. Dependence between the degree of polarization and the wave length

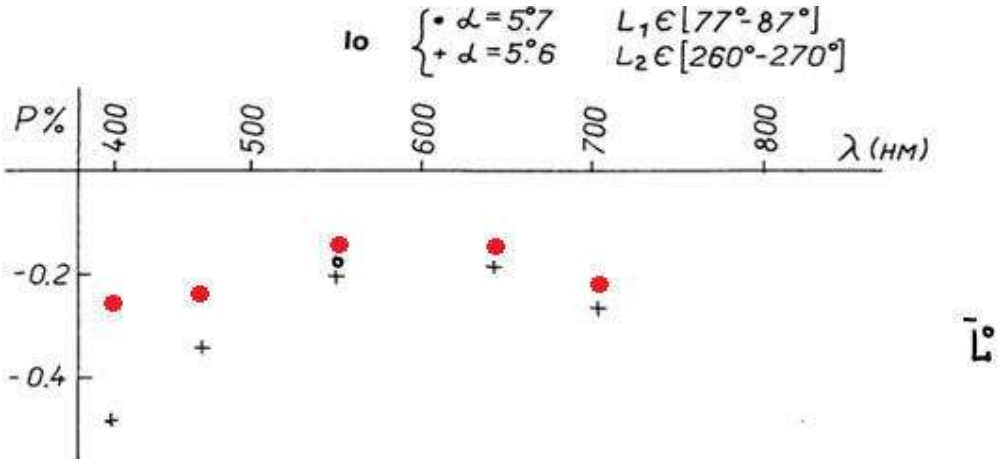

Fig. 6.

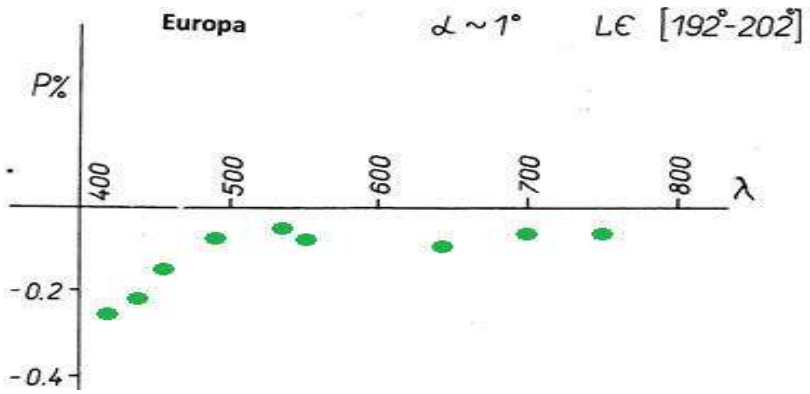

Fig. 7

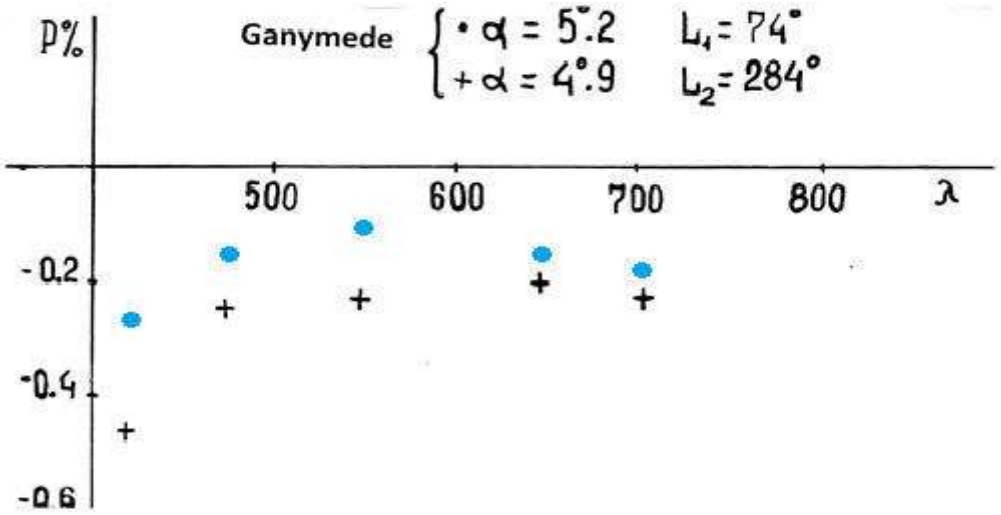

Fig. 8

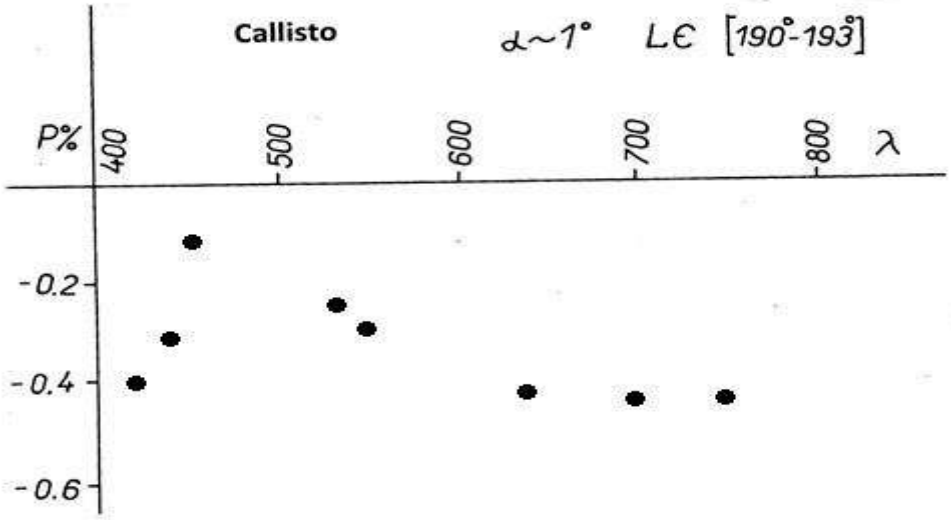

Fig. 9

3. Conclusions

1. As it is seen from the drawings, Europe has the most homogeneous surface and Callisto has the least homogeneous surface.

$(P_{max.} - P_{min})_{Europe} < (P_{max.} - P_{min})_{Io} < (P_{max.} - P_{min})_{Ganymede} < (P_{max.} - P_{min})_{Callisto}$

2. Polarization curve of satellite Callisto is similar to the polarization curve of the Moon.

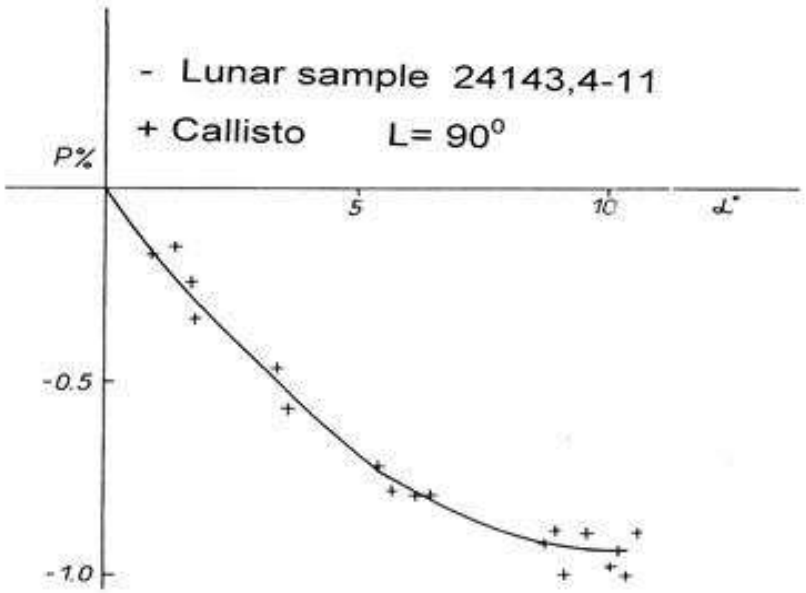

Fig. 10

3. The empirical formulas for each object are as follows:

For Io: $\begin{cases} P(\alpha) = 20.31\,\alpha^2 - 3.72\alpha - 0.07 \\ m(\alpha) = -0.001\alpha^2 + 0.046\alpha + 4^m.80 \end{cases}$

Second-degree polynomial and the relationship $P(\alpha) = m(\alpha) - 4^m.8 + 20.311\alpha^2 - 3.766\alpha - 0.07$

For Europe:

For Europe: $\begin{cases} P(\alpha) = 54.55\alpha^2 - 6.57\alpha - 0.05 \\ m(\alpha) = -0.00125\alpha^2 + 0.0312\alpha + 5^m.17 \end{cases}$

and the relationship

$P(\alpha) = m(\alpha) - 5^m.17 + 54.55\alpha^2 - 6.60\alpha - 0.05$

For Ganymede: $\begin{cases} P(\alpha) = 72.33\,\alpha^2 - 10.09\alpha - 0.05 \\ m(\alpha) = -0.00066\alpha^2 + 0.323\alpha + 4^m.54 \end{cases}$

and the relationship

$P(\alpha) = m(\alpha) - 4^m.54 + 72.33\alpha^2 - 6.89\alpha - 0.05$

For Callisto: $\begin{cases} P(\alpha) = 62.39\,\alpha^2 - 13.07\alpha - 0.05 \\ m(\alpha) = -20.00274\alpha^2 + 0.078\alpha + 5^m.5 \end{cases}$

and the relationship $P(\alpha) = m(\alpha) - 5^m.5 + 82.4\alpha^2 - 0.0463\alpha - 0.05$

References

Chigladze R, Proceedings of Tbilisi University, 1987. 270, 240.

Chigladze R, Dissertation Thesis. Abastumani, 2006. 186.

Chigladze R, Bull. Georgian National Sciences, 2012. 6 , 96.

ChigladzeR, Electropolarimetric and Electrofotometric Investigation of Jupirer's Galilian Setellites". International Scientific Conference, Problems of Modern Astrophysics" Akhaltsikhe. 2015.

Dolffus A, Icarus., 1975. 25, 416.

Geake, K, A. Dollfus. Icarus., 1979. 343.

Veverka I., Icarus, 1971. 14, 355.

Zaitsev et al, Advances in Astronomy and Space Physics, 2012. 2. 177.

Astronomy & Astrophysics (Caucasus) 3, (2018)

Spectral and Photometric Data of Be star, EM Cep

N. Kochiashvili[1], R. Natsvlishvili[1], I. Kochiashvili[1], M. Vardosanidze[1,2], S. Beradze[1,2], A. Pannicke[1,3]

[1]E. Kharadze Abastumani Astrophysical Observatory, Ilia State University.
[2]Samtskhe-Javakheti State University
[3]Astrophysical Institute and University Observatory Friedrich Schiller University Jena

E-mail: nino.kochiashvili@iliauni.edu.ge

Abstract

The subject of investigation in this project is a Be spectral type giant variable star EM Cep. It was established that the star has a double nature: 1. when emission lines are seen in its spectrum and 2. when only absorption lines are observable and emission lines are not seen. This means that the star is not always in Be state. Be state continues existing during a few months. EM Cep shows flare activity too. The causes of photometric and spectral variability are to be established. The existence of different mechanisms, which provokes Be phenomenon, is possible.

The character of light curves' variability gives us possibility to propose that it is not excluded that the star could be a short-period Cepheid of λ Eri type. However, we do not have sufficient data to exclude its binarity.

On the basis of the observations carried out at Abastumani observatory, the light curve with two minima and two maxima were revealed, but these data, too accord with the half-period – we can also consider a light curve with one minimum and one maximum. Both cases suggest a good agreement with the characters of variability. For the case of binarity in Abastumani observatory, a set of orbital elements by using the Wilson-Devinney code is already obtained. The elements correspond to the model of acceptable, real close binary star. However, notwithstanding this situation, the true nature of the star is not established for the moment. To solve this problem, we need to get high-resolution spectral data, when by using radial velocity curves, it would be possible to answer the question of binarity of the star. It is not excluded to reveal spectral lines of the second component in case of binarity of the star.

Since 2014, we have renewed UBVRI photometric observations of EM Cep in Abastumani using a 48-cm telescope with CCD device. Spectral observations are made in Azerbaijan, Shamakhy Observatory. Our German Colleagues have been observing the star since March of 2017 at the Observatory of the Jena University. We plan to carry out a joint analysis of the observations of the three observatories to explain the observational peculiarities of the star.

Subject headings: stars, emission-line, eclipsing, stars, oblique rotator.

Introduction: Be stars

Be stars are defined as non-supergiant stars with temperatures between about 10000K and 30000K, which have shown emission lines in their spectra on at least one occasion. As the definition suggests, the spectra of Be stars can vary with time, like their brightness. About 20 % of B stars are Be stars and, because these stars are very luminous, there are about 200 of them as the naked-eye stars. This makes them one of the most conspicuous classes of variables (Percy 2007). Be stars were discovered almost 150 years ago by Secchi (1866).

The periodic variability of early type Be stars has been well known since more than 30 years. While initially, both the rotation and the pulsation were proposed as an underlying mechanism, first spectroscopy, then space-based photometry provided increasing evidence for pulsation, in most cases in grouped multiperiodicity. The great accuracy of dedicated space missions make it possible to identify pulsational variability for all observed Be stars, including late type ones, though only at millimagnitude level and below. At present, it seems that detecting pulsation in Be stars is only limited by the detection threshold, not by the physical absence of pulsation (Rivinius et al. 2013). Opinion exists that about 70% of Be stars are binaries (see for example, Zorec et al. (2016)).

EM Cep

We have observed a B spectral type giant star EM Cep at Abastumani Observatory since 1991 (Kochiashvili 1999). For that time, it was known as a bright ($m(V) = 7.03$) short period variable with spectral class BI IV+?. The amplitude of its variability is 0.15 magnitudes and period – $P = 0.806187$ days. Some of its investigators considered the star as a close binary system (Lynds 1959a,b; Johnston 1970; Rachkovskaya 1972, 1976; Bakos & Tremko 1975; Tremko & Bakos 1980; Karimie 1979; Breinhorst & Karimie 1980; Cristescu et al. 1981), while some of them regarded it as a non-radial pulsator (Hilditch et al. 1982). According to her observations, Rachkovskaya (1977) made a conclusion that EM Cep is either a β Cep type variable or an oblique rotator. As Hα emission lines were observed in its spectra (Plaskett & Pearce 1931; Merrill et al. 1932; Rachkovskaya 1977), so EM Cep is a Be spectral type star. The character of the light curves' changing allows suggesting that the variable maybe a λ Eri type short-period Cepheid (Kochiashvili et al. 2007; Bakis et al. 2007; Kochiashvili & Kochiashvili 2008). We also examined the case of binarity for the star (Kochiashvili & Kochiashvili 2008).

The Flare

As it is known today, O and B stars show the flare activity. Two or three decades ago, they were rarely mentioned in regard of flares of early spectral type stars, but according to the latest data, such a type of stars belongs to the most active class in the Universe. A very interesting "unusual" flare was revealed for the Be star EM Cep in 1991. During UBVR electrophotometric observations using 48-cm reflector of Abastumani Astrophysical Observatory, a flare in R pass-band was detected with simultaneously anti-flare in U band (Figure 1).

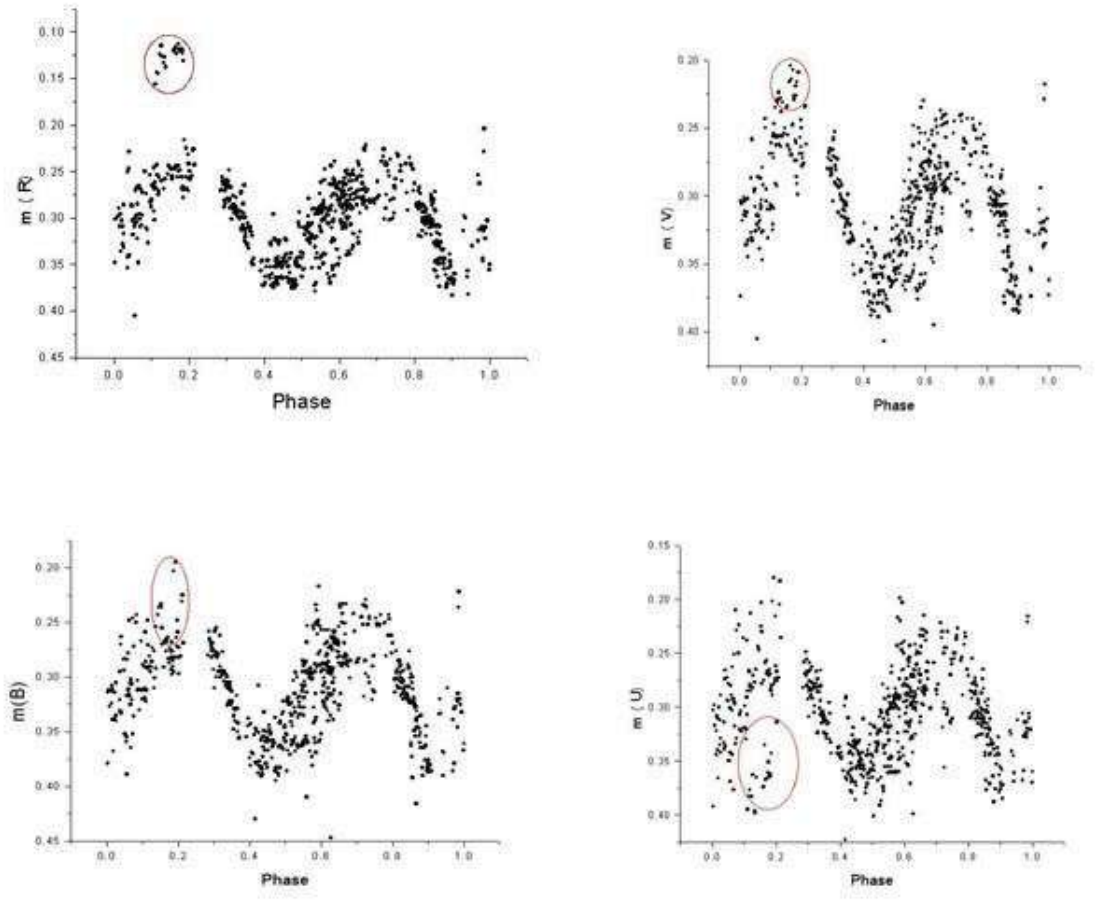

Figure 1. "Unusual" flare of EM Cep (Kochiashvili, 1999).

Energetics of the flare

We use the following relationship:

$$2.5 \lg L/L_{\odot} = M_{\odot} - M.$$

Where $M_{\odot}$ and M are Absolute stellar magnitudes of the Sun and EM Cep consequently. Energy of the flare in the solar luminosity units is: $\log L = 0.4(M_{\odot} - M)$ and $L_{\odot} = 3.86 \cdot 10^{33}$ erg/sec. Solar absolute magnitudes in U, B, V and R bands are: $M_{\odot U} = 5.^m58$; $M_{\odot B} = 5.^m43$; $M_{\odot V} = 4.^m77$; $M_{\odot R} = 4.^m24$. And the same values for EM Cep are: $M_U = -5.^m9$; $M_B = -4.^m9$; $M_V = -4.^m6$; $M_R = 4.^m5$

The mean amplitude of EM Cep's flare in R band was approximately $0.^m13$, and the one of the anti-flare in U band was approximately $-0.^m11$. Consequently, the absolute values during the flare were: $M_R = -4.^m63$ and $M_U = -5.^m79$. The luminosity of EM Cep in the solar units would be $L_R = 3133 L_{\odot}$. Analogically, the luminosity of EM Cep during the flare in solar units: $L_{Rf} = 3872 L_{\odot}$. Therefore an increase in luminosity during the flare in R band was approximately 24 %.

Antiflare

The luminosity in U band during the anti-flare was: $L_{Uf} = 35318$. Mean luminosity in U band for EM Cep: $L_U = 39084 L_{\odot}$. Therefore, the luminosity decrease in U band during the flare was 10%.

Mass Loss

During the flare, the luminosity increase in R band was $L_R = 739 L_{\odot}$. We calculate the equivalent mass loss during 2 hours of flare using $E = mc^2$ relationship: $M_{Rf} = 10^{-14} M_{\odot}$. Analogically, the equivalent mass of the energy of anti-flare would be: $M_{Uf} = 5 \cdot 10-14 M_{\odot}$.

Two Possible Scenarios

We decided to examine the star either as an eclipsing close binary or as a short period Cepheid.

The first case

We tried to get a formal solution of the light curves of EM Cep using the Wilson-Devinney code (Bradstreet 1993). Due to the unstable character of EM Cep light curves, we used observations of 1999 only - during this period the star did not show significant changes of light curves. Those are data of August (4 nights) and October (5 nights). Orbital elements of Cristescu et al. (1981) were used as input data. We took a fillout=0.17 for the system. This is a case of W UMa type eclipsing binary. The Model is presented for R band (Figure 2).

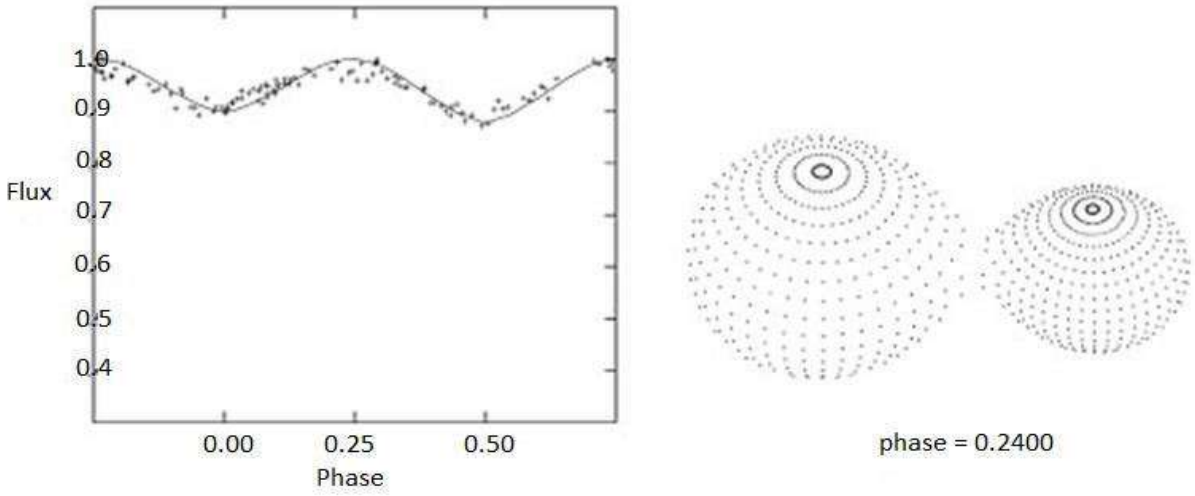

Figure 2. Model of EM Cep according to Binary Maker (Kochiashvili & Kochiashvili, 2008)

The second case

By its light variation character, EM Cep shows certain similarity with λ Eri variable (Kochiashvili et al. 2007). Consequently, we calculated our photoelectric data for half-period (see Bakis et al. (2007)). The results are presented for R band in Figure 3.

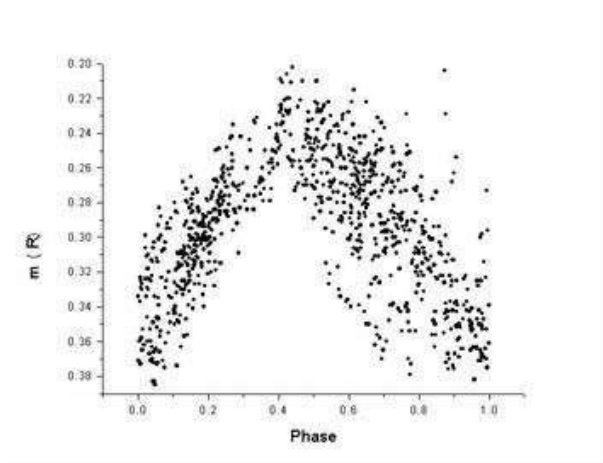

Figure 3. Electrophotometric data of EM Cep for a half-period (*P* = 0.403 days; Kochiashvili & Kochiashvili, 2008).

The orbital elements estimated for the first case are absolutely acceptable, but they do not correspond to the existing spectral data. We have got 0.4 contribution of the secondary component in the total luminosity. So, we would see spectral lines of the both stars for this solution. However, later, we learned that spectral lines of only one component were visible in

the existing spectral data. Even in such a situation, we would not exclude that in certain conditions, spectral lines of one component are screened by a gaseous envelope (see for example Djuraševi´c et al. (2008)). The true nature of the star remained unknown. High resolution spectral observations were needed to finally solve this problem (Kochiashvili & Kochiashvili 2008).

We decided to get high resolution spectral data of EM Cep and to try to resolve the binarity problem of the star. Our Armenian colleague, Arthur Karapetian observed the star using a 2.6-m telescope of Byurakan Astrophysical Observatory. No spectral lines of a companion star were found. We could neither reveal a sign of radial velocities. The still-unpublished examples of EM Cep Hα lines according to A. Karapetian are shown in Figure 4.

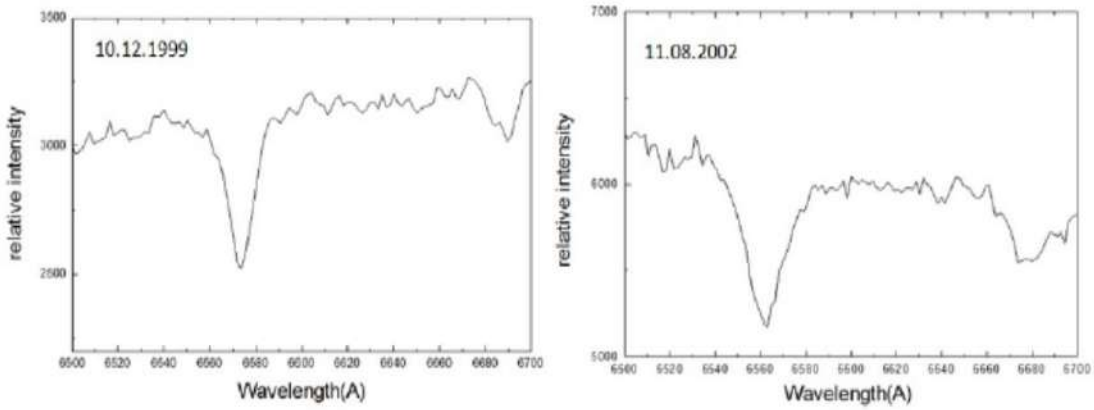

Figure 4. Hα lines of EM Cep, obtained by Arthur Karapetyan using a 2.6-m telescope of Byurakan Astrophysical Observatory

New findings of Bulgarian astronomers

New spectral observations were carried out by the 2m RCC telescope of the National Astronomical Observatory at Rozhen, Bulgaria, in 2004-2015. The resolution of the spectra is 16400, and most spectra have an S/N ratio in the range of 150-250. Initially, EM Cep was observed in the spectral range centered on Hα, but after July of 2005, the spectral range was changed to include the He I λ6678 line (Kjurkchieva et al. 2016). According to the new spectral data, EM Cep switches between B and Be star states, as revealed by the level of Hα emission, but spends most of its time in a B star state. The authors made the following estimations: disk masses in the order of $(3 - 10) \cdot 10{-}11\ M_{\mathrm{EM}\ Cep}$; mass loss rate of $\sim 3 \cdot 10{-}9 M_{\odot}$/yr; $M_{EM\ Ce\mathrm{p}} = 12.5\ M_{\odot}$; $R_{polar} = 6.3\ R_{\odot}$; $R_{equatorial} = 9.5\ R_{\odot}$; $T_{eff} = 26000K$.

So, the star has the Be character for a certain time interval and it has not emission at all in the remaining period (Figure 5). The transition from B to Be and then to B state again lasted for up to 7 months. The classical Be star model can satisfactorily reproduce the Hα line profiles of EM Cep with disk density parameters and disk masses that are typical of the Be

stars (Kjurkchieva et al. 2016). The profiles of the absorption line He I λ6678 have also a remarkable short-time variability.

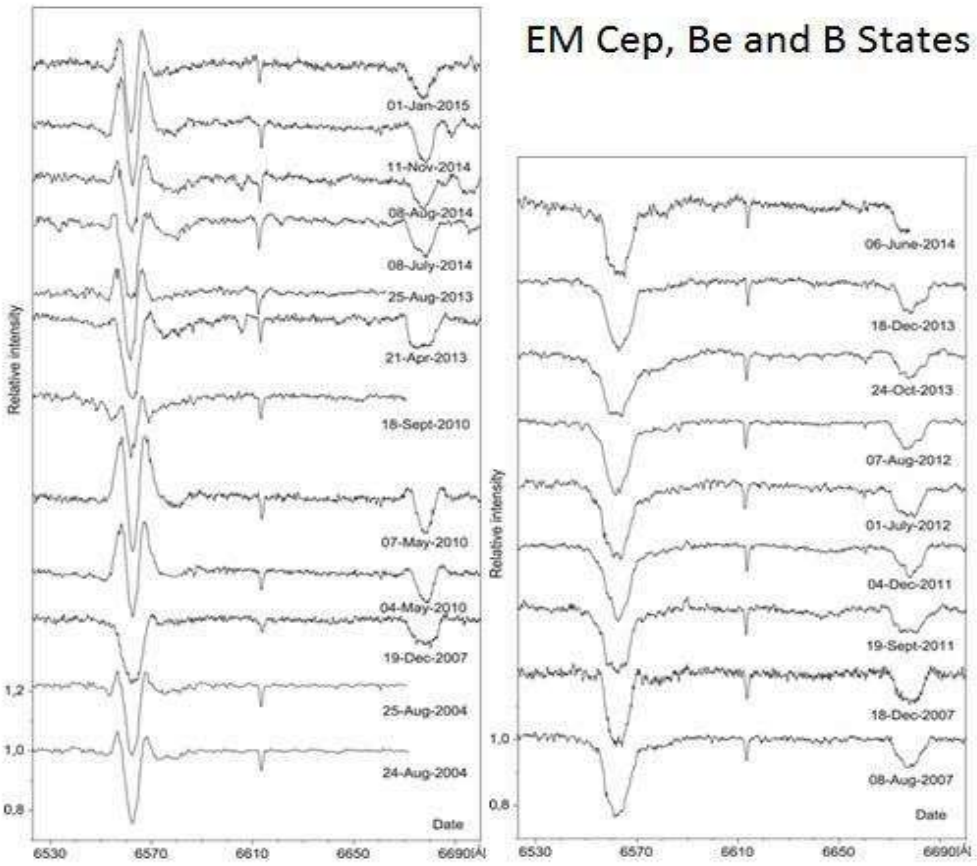

Figure 5. Be and B states of EM Cep. The Hα profile of EM Cep in the Be state is doubly-peaked with a central absorption core and two emission wings (Kjurkchieva et al. 2016)

Recent Spectral Observations of EM Cep

In 2017, several spectral observations have been obtained with the spectrograph FLECHAS on the 0.9 m telescope of the University Observatory Jena. The H_α region in the spectra clearly shows the Be state (black, orange and blue graphs) and the B state (green). We found out that the switch from the B to Be state occurs within a few days.

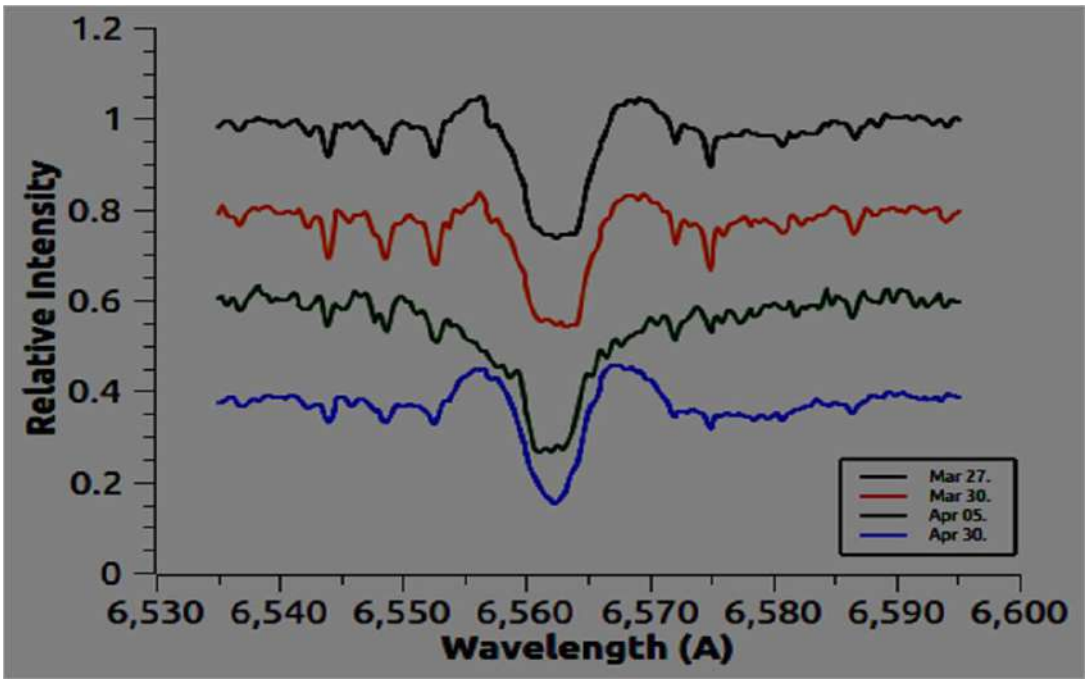

Fig. 6: Hα region in the spectra of EM Cep. The B phase is clearly visible in the green colored graph.
In other three cases the star is in a Be state

Conclusions

Be stars and their massive extension, the Oe stars, may prove to be progenitors of late stages of massive star evolution connected to rapid rotation, such as S Dor variables, or even the long GRBs. A full extension of Be star research to extragalactic environments will only be reached with future facilities, such as extremely large telescopes (Rivinius et al. 2013).

We have interesting results for one of the S Dor star, the LBV, P Cygni, which is also a B spectral type star. There are some unsolved problems as for S Dor so for Be stars that could be related to each other. We think that the possibility to observe bright stars of both types using small telescopes is an advantage. Therefore, we are continuing observations of EM Cep using the same 48 cm Cassegrain telescope and a new CCD with standard U, B, V, R, I and the additional Hα filters. We hope to find observational evidence for stellar pulsations, if any. One of the aims for these observations is to monitor flare activity of EM Cep.

References

1. Bakis, H., Bakis, V., Demircan, O., Budding, E., & Tanriver, M. 2007, Solar and Stellar Physics Through Eclipses, 370, 225
2. Bakos, G. A., & Tremko, J. 1975, JRASC, 69, 307
3. Breinhorst, R. A., & Karimie, M. T. 1980, PASP, 92, 432
4. Bradstreet, D. H. 1993, IAU Commission on Close Binary Stars, 21, 151
5. Cristescu, C., Oprescu, G., &Suran, M. D. 1981, Information Bulletin on Variable Stars, 2050,1
6. Djuraševi´c, G., Vince, I., Antokhin, I., Zakirov, M., & Eshankulova, M. 2008, Romanian Astronomical, Journal, 18, 126
7. Hilditch, R. W., McLean, B. J., & Reid, I. N. 1982, MNRAS, 200, 1153
8. Johnston, K. 1970, PASP, 82, 1093
9. Karimie, M. T. 1979, Information Bulletin on Variable Stars, 1594, 1
10. Kochiashvili, I., &Kochiashvili, N. 2008, Romanian Astronomical Journal, 18, 61
11. Kochiashvili, N. T. 1999, Astrophysics, 42, 399
12. Kochiashvili, N., Natsvlishvili, R., Bakis, H., & Tanriver, M. 2007, Astronomical and Astrophysical Transactions, 26, 113
13. Lynds, C. R. 1959, ApJ, 130, 577
14. Lynds, C. R. 1959, ApJ, 130, 603
15. Rachkovskaya, T. M. 1972, Izvestiya Ordena Trudovogo Krasnogo Znameni Krymskoj Astrofizicheskoj Observatorii, 46, 35
16. Rachkovskaya, T. M. 1976, Izvestiya Ordena Trudovogo Krasnogo Znameni Krymskoj Astrofizicheskoj Observatorii, 55, 100
17. Rachkovskaya, T. M. 1977, Izvestiya Ordena Trudovogo Krasnogo Znameni Krymskoj Astrofizicheskoj Observatorii, 56, 11
18. Rivinius, T., Carciofi, A. C., & Martayan, C. 2013, A&A Rev., 21, 69
19. Tremko, J., & Bakos, G. A. 1980, JRASC, 74, 321.

Astronomy & Astrophysics (Caucasus) 3, (2018)

Photometric and Spectral Observations of P Cygni, the Luminous Blue Variable

N. Kochiashvili[1], S. Beradze[1,2], R. Natsvlishvili[1], I. Kochiashvili[1],
M. Vardosanidze[1,2], A. Pannicke[1,3]

[1]E. Kharadze Abastumani Astrophysical Observatory, Ilia State University

[2]Samtskhe-Javakheti State University

[3]Astrophysical Institute and University Observatory of Friedrich Schiller University, Jena

E-mail: nino.kochiashvili@iliauni.edu.ge

Abstract

We found original observations by E. Kharadze and N. Magalashvili of P Cygni in the archives of Abastumani Astrophysical Observatory. These observations were carried out during 1951-1983 period. Initially, they used 29 Cygni as comparison star and all observations of P Cygni were processed using this star. On the basis of their calculations, authors decided that P Cygni may be a W UMa type binary with orbital period of 0.500565, but this hypothesis was not confirmed. There is a whole set of observational data. So, we recalculated all data (where it was possible) using 36 Cygni as a comparison star. Besides, we are going to present the results of the new photometric observations of the P Cygni and new spectral observation. New photometric observations were obtained in 2014 using 48 cm Cassegrain telescope of Abastumani Observatory. Some interesting behaviors of the light curves were revealed. New spectral observation was obtained of the University Observatory Jena, in Germany where we clearly can see stellar variability.

Key Words: UBV photometry, Luminous Blue Variable Stars, P Cygni

1. Introduction.

Non W-R stars, but other known hot and luminous variable stars, such as η Car, P Cyg, R71, R122, the S Doradus stars and the Hubble-Sandage variables, are clearly related to massive stars and undoubtedly represent an advanced evolutionary stage (Maeder, 1984), in 1984 P. Conti combined them as Luminous Blue Variables (LBV). Luminous Blue Variables

are descendants of massive O stars, which are nearly to the end of the core hydrogen burning. They undergo episodic mass-loss and probably represent a transition between the most massive O star and the red supergiant and/or W-R stage (Massey 2006). Extremely high luminosities of these stars place them near or above the Eddington limit. They are characterized by a large variability of amplitudes and violent mass ejections. They have unusually high mass loss rates ranging from 10^{-6} to 10^{-3} $M_{\odot}$/yr.

The following three types of variability of Luminous Blue Variables are known: 1. Micro-variations with 0.1 mag. amplitude and comparatively small time-scale variations from days to weeks or months. 2. S Dor type variations or outbursts with amplitudes of 0.5 mag., and 3. Large sporadic outbursts with amplitude >2 mag. on a time-scale of 100 years.

Luminous Blue Variables are extraordinary because of the fact that they can show different type of photometric and spectroscopic variations.

P Cygni (34 Cyg,) is one of the most luminous stars of the Galaxy. It has been classified as a Luminous Blue Variable (LBV) after two major outbursts in 1600 and 1660. After remaining at its maximum for about 6 years, the brightness started to decrease and the star became invisible to the naked eye in 1626. It reappeared in 1654 and remained at 3-rd magnitude until 1659. The visual magnitude of the star was varying between 1660 and 1683 and started to increase slowly until it reached the value of 5.2 in 1780. Except for a few observations by Herschel in the 1780s, there is no record of variations between 1780 and 1870. Since then, the brightness of P Cygni has been increasing slowly by 0.4 magnitudes to bring it to its current value of V=4.83. Analysis of historical observations of P Cygni has shown that between 1700 and 1988, its overall brightness slowly increased by 0.15±0.02 mag/century (de Groot and Lamers 1992). The light curve of P Cygni after 1600 AD is displayed in Fig. 1.

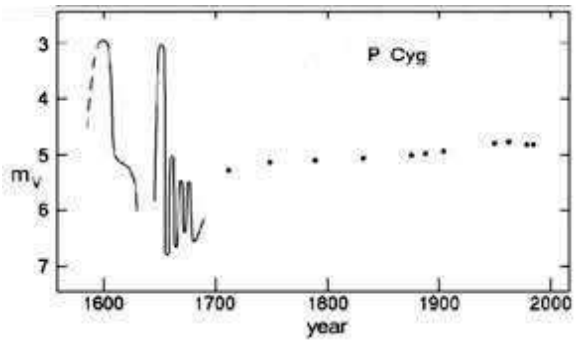

Fig. 1. The historical light curve of P Cygni from 1600 up to 2000 (de Groot 1983).

The first spectra of P Cygni obtained as early as in 1897 already show the famous P Cygni-type spectral lines - an undisplaced emission accompanied by a shortward displaced absorption core (Maury& Pickering, 1897). Initially, this was interpreted as a blend of two different lines. McCrea (1929) and Beals (1930, 1932) were the first to interpret P Cygni-type profiles in novae, Wolf-Rayet stars and P Cygni itself as due to a radially expanding stellar envelope.

Stars with extended envelopes are divided into two broad classes according to the so called “P Cygni emission line profiles”. First class of stars shows mass ejection or global expansion of shell – the emission-line structures of such stars are similar to those of P Cygni. The second class of stars is characterized by accretion of material or global contraction of the shell. The structure of their emission lines is inversely to the structure of P Cygni emission line profiles. These are so-called “P Cygni profile” and “inverse P Cygni profile” objects consequently (Fig. 2).

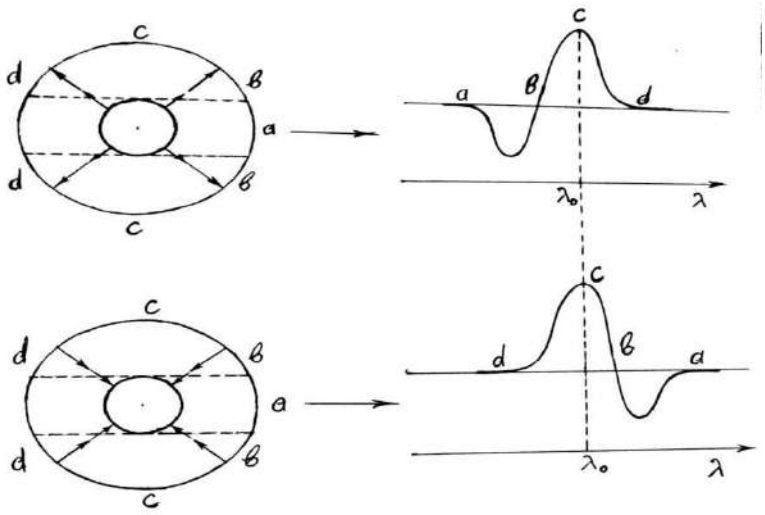

Fig.2. “P Cygni profile” and “inverse P Cygni profile

Early serious, detailed analysis of P Cygni spectrum was carried out by Beals (1950), Hutchings (1969) and de Groot (1969). More recently, Stahl et al. (1993) and Markova (1994) published spectral atlases with identifications of many weak lines in the visual spectral region.

The Copernicus satellite obtained the first spectra of P Cygni in the non-visible ultraviolet region (Hutchings 1976.). Near-IR and IR observations have been reported by Barlow and Cohen (1977), Waters and Wesselius (1986), and Lamers et al. (1996). P Cygni is located on the upper part of the Hertzprung-Russell (HR) diagram populated by different

types of emission-line stars, including supergiants, O3If/WN6, Ofpe/WN9, B[e], LBVs and WR stars. It is clear that all these classes represent different phases in the evolution of stars with zero-age main-sequence (ZAMS) masses of more than $40M_{\odot}$. It was found that P cygni has three different type variations: 1. Short, 17-days variation; 2. 100-days variation, which is also observed in LBVs, and 3. Long-period variation of a several-year-long period. For today, it is known that P Cygni is the nearest LBV, at a distance of 1.7 kpc. It is estimated that its mass is 30 $M_{\odot}$. The effective temperature is T_{eff}=18200 K, the radius - R=75 $R_{\odot}$, the mass loss rate – 1.5×10^{-5} $M_{\odot}$/year (Barlow & Cohen, 1977) and Luminosity of $L=5.6 \times 10^{5}L_{\odot}$ (Kashi, Amit, 2010).

2.UBV Observations at Abastumani Observatory

Investigations of variable stars have been done at Abastumani observatory from the very beginning of its establishment (1932). Photoelectric observations of P Cygni were made using a 33 cm reflector of Abastumani observatory. The observations were carried out from September 11 up to October 8, 1935. The amplitude of light variability attained 0.16 magnitudes. Observations of September 7-November 11, 1936, revealed the variation of brightness of 0.10 mag. And observations during September 8 and October 8, 1937, show light fluctuations of 0.08 mag.

Nikonov's observations cover 758 days. We have clear evidence that the stellar brightness rose by about 0.3 mag. (0.298) during approximately one year and then it has almost the same level of 0.08 mag. fluctuations in two observational runs. Two sharp minima of stellar brightness are clearly seen

HJD_{min}=2428074.83andHJD_{min}=2428449.34. Besides, two maxima moments were fixed: HJD_{max}=2428444.31 andHJD_{max}=2428480.26. The corresponding time intervals are 374.51 and 35.95 days.

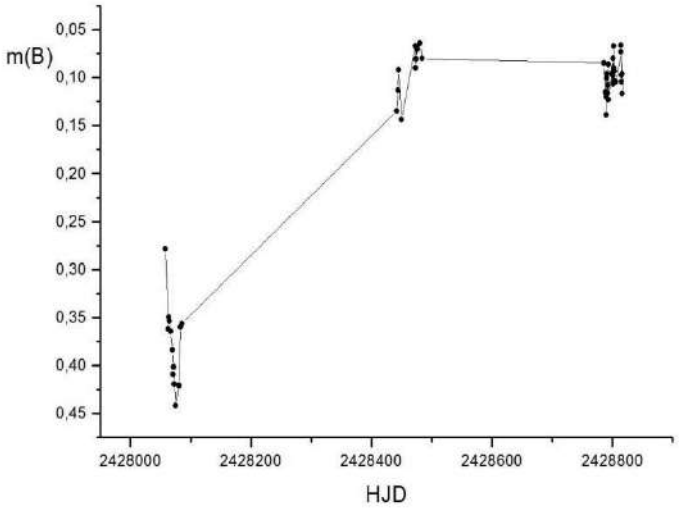

Fig. 3. Observations of P Cygni made by Nikonov during 1935-1937, using the 33 cm reflector of Abastumani observatory.

Since 1951, Nino Magalashvili and Eugene Kharadze had been regularly observing P Cyg using 33 cm. reflector with an electro-photometer. B and V filters were used during 1951-1960 and then, after 1961, U, B and V filters instead. On the basis of the above-mentioned observations, Magalashvili and Kharadze made a conclusion suggesting that the behavior of the star was similar to W Uma variability, with the period of 0.500565 d and 0.10-0.08 mag. The article was paid great attention of the investigators of variable stars, but W Uma variability was not confirmed. Presumably, one of the reasons of Magalashvili – Kharadze erroneous conclusions is the complex variability of this interesting star. Possibly, the variability of 12-14 hours really exists. However, the current revision of the observational material assured us that fortunately, 1951-1967 and 1974-1983 observations were carried out in a way making it possible to re-process them and estimate the true variability picture of P Cygni. It turned out that observers Eugene Kharadze and Nino Magalashvili used 29 Cyg and 36 Cyg as comparison and check stars. Light reduction of variable P Cygni was conducted using 29 Cyg, which in turn, is a variable of δSct type.

We have the opportunity to process the observations and calculate difference of brightness of variable and 36Cyg, which will give us a real light variation of P Cyg and are giving these UBV data in Fig. 4.

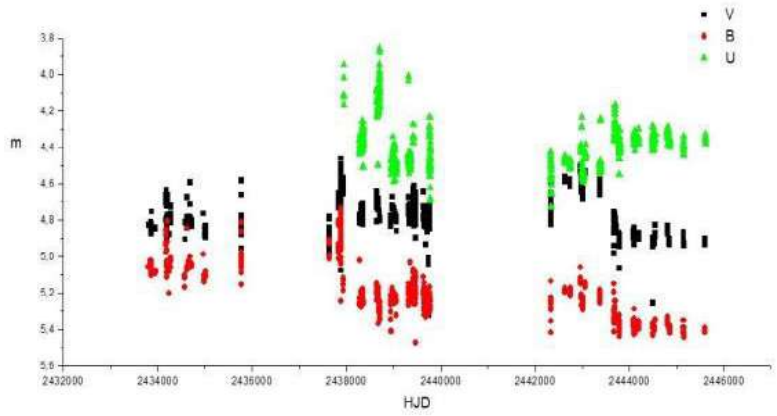

Fig. 4. UBV observations of P Cygni made by E. Kharadze and N. Magalashvili during 1951-1983. 36 Cygni = HD 193369 used as a comparison star

At the first glance, we can see that in 1974-1983, the star was dimmed in U band while brightened in B and V bands (the last third part of Fig. 4). The middle part of the figure represents a time interval of 1961-1967 and at this point, the colour behavior of the star is different: during brightening in V band the star is fainter in B and U.

Observations of P Cygni obtained by Kharadze and Magalashvili at Abastumani observatory are unique: 1. they represent homogenous data of more than 30 years and probably, it would be possible to reveal periodicity(ies) in brightness variations; 2. there are UBV observations and we can trace colour behavior of the star; 3. the observations by Kharadze and Magalashvili are unique because they are the only existing data of P Cygni observed with filters in the period of 1951-1983.(Fig. 5)

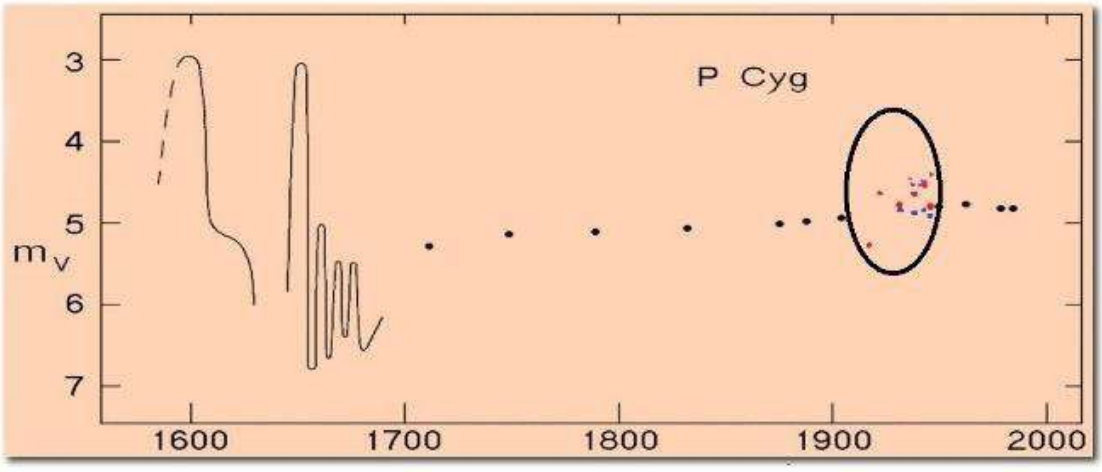

Fig: 5. The light curve of P Cygni during 1600 - 2000 AD with Abastumani data. Red points – V filter, blue – B and purple – U.

3. Photometric observations of P Cygni in 2014

We observed P Cygni on July 23 - October 20, 2014 with a 48 cm Cassegrain telescope and standard B, V, R, I filters. HD 228793 (V=9.9, B=10.16) has been used as a comparison star (see Fig. 6). We revealed that during our observations the star underwent light variations with the mean amplitude of approximately 0.1 magnitudes in all pass-bands and the period of this change was approximately 68 days. (Fig. 6)

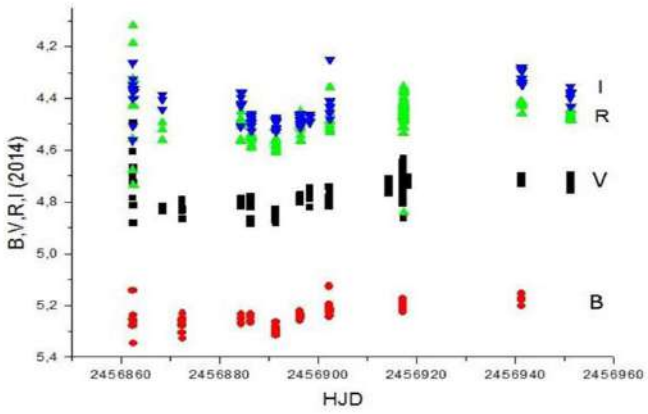

Fig. 6. BVRI photometric Observations of P Cygni during 2014

4. Spectral Observations of P Cyg

In 2017, several spectral observations have been obtained with the spectrograph FLECHAS on the 0.9 m telescope of the University Observatory Jena. The Hα region in the spectra clearly shows the P Cygni profile and variability within one month.

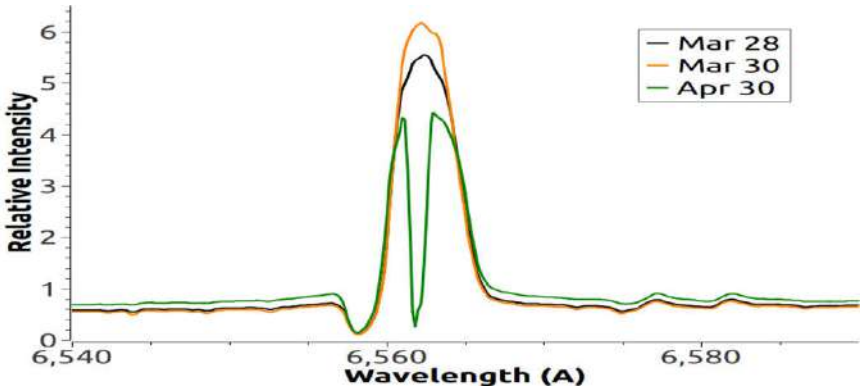

Fig. 7. H_α region in the spectra of P Cyg from three different observations in 2017. The stellar variability is clearly seen: in March we have dominant emission line; in April - absorption component instead.

5. Discussion

We revised observational data of P Cyg obtained at Abastumani Astrophysical Observatory. We would like to mention that according de Groot and Lamers 1992, observations of P Cygni have shown that from 1700 to 1988, its overall brightness slowly increased by 0.15±0.02 mag./century (de Groot and Lamers 1992). However, interesting and valuable light variations were revealed in Abastumani. Particularly, 0.3 mag. brightness increase was observed in the period of 1935-1936.

So, the further detailed analysis and publication of the data is needed as we still have some unanswered questions like, for example, the binarity of P Cyg. This star has very strong stellar wind and perhaps this is the reason for the stellar variability in P Cygni spectra. Besides, the mechanism of great eruptions has not been established yet, and the connection between the stellar rotation, the pulsation and the magnetic fields of P Cyg are not so clear so far.

References

1. Barlow, M.J; Cohen, M. Infrared photometry and mass loss rates for OBA supergiants and Of stars. Astrophys. J., 1977, 213, p. 737-755.

2. Beals, C.S. The Atmospheres of the Early Type Stars (with Plates XVII to IX), Journal of the Royal Astronomical Society of Canada. 1950, 44, p. 221-240

3. Beradze, S; Kochiashvili, N; Kochiashvili, I; Natsvlishvili, R. Hypergiant P Cygni. Instability and Evolution of Stars, Proceedings of the Byurakan-Abastumani Colloquium dedicated to Ludwik Mirzoyan's 90th anniversary, held on 26-28 August 2013 in Byurakan Astrophysical Observatory, Armenia. Eds.: Harutyunian, H. A.; Nikoghosyan, E. H.; Melikian, N. D., Yerevan, "Gitutyun" Publishing House of the National Academy of Sciences of the Republic of Armenia (NAS RA), p. 10-13. 2014

4. de Groot. Spectral variations of P Cygni. Communications of the Konkoly Observatory. 1969, 65 p. 203-214

5. de Groot, M.; Lamers, H. J. G. L. M., 1992, Nonisotropic and Variable Outflows from Stars, ASP Conference Series, Vol. 22, Laurent Drissen, Claus Leitherer, and Antonella Nota, Eds., p. 360.

6. Hutchings, J.B. Expanding atmospheres in OB supergiants-III. P. Cygni. MNRAS, 1969, 144, p. 235-243

7. Kashi, Amit., 2010, INTERNATIONAL CONFERENCE ON BINARIES: In celebration of Ron Webbink's 65th Birthday. AIP Conference Proceedings, Volume 1314, pp. 55-56. .

8. Kochiashvili et al. New Photometric Observations of P Cygni. Wolf-Rayet Stars: Proceedings of an International Workshop held in Potsdam, Germany, 1-5 June 2015. Edited by Wolf-Rainer Hamann, Andreas Sander, HelgeTodt. Universitätsverlag Potsdam, 2015., p.360

9. Kochiashvil, N; Beradze, S; Kochiashvili, I; Janiashvili, E; Natsvlishvili, R; Urishadze, T; Vardosanidze, M. UBV Photometry of P Cygni at Abastumani observatory. Azerbaijani Astronomical Journal, v. 9; p. 18-21. 2014.

10. Lamers H. J. G. l. M; de Groot; Cassatella, A. The distance, temperature and luminosity of the hypergiant P Cygni (B1 Ia+). Astron. Astrophys., 1983, 128. p. 299-310.

11. Maeder, A. Evolution of Massive Stars Supergiants and Wolf-Rayet Stars. Observational Tests of the Stellar Evolution Theory. International Astronomical Union

Symposium No. 105, held in Geneva, Switzerland, September 12-16, 1983. Editors, Andre Maeder, Alvio Renzini; Publisher, D. Reidel Publishing Company, Dordrecht, The Netherlands, Boston, MA, Hingham, MA. Sold and distributed in the U.S.A. and Canada by Kluwer Academic Publishers, 1984. LC # QB806 .O27 1984. ISBN # 90-277-1774-5. P.299, 1984

12. Markova, N. VizieR On-line Data Catalog: J/A+AS/108/561. Originally published in: 1994, A&AS. 108. 561M

13. Massey, Philip. The Discovery of a P Cygni Analog in M31. Astrophys.J., 2006, 238, p. L93-L96

14. McCrea, W.H., 1929, The Observatory, Vol. 52, pp. 267-274

15. Magalashvili N; Kharadze E: Periodicity of the Light Variation of P Cygni. IBVS, 1967, 210,

16. Maury, Antonia C., Pickering, Edward C. Spectra of bright stars photographed with the 11-inch Draper Telescope as part of the Henry Draper Memorial. Annals of Harvard College Observatory. 1897, 28, p.1-128.

17. Najarro, F., Spectroscopy of P Cygni. *P Cygni 2000: 400 Years of Progress* 233: 133, 2001

18. Nikonov V.B. Photoelectric Observation of P Cygni. 1937, Bull. AbAO, 1, p. 35-38

19. Stahl, Otmar. Luminous Blue Variables of the Magellanic Clouds. In: New Aspects of Magellanic Cloud research; European meeting on the Magellanic Cloud, 2nd, SFB No. 328 'Evolution of Galaxies', Heidelberg, Germany, June 15-17, 1992. 1993. A95-88790, p. 263-270.

20. van Genderen A.M., S Doradusvariable sinthe Galaxy and the Mage llanic Clouds, A&A, v. 366, p. 508. 2001.

21. van Genderen A.M., Sterken C., de Groot M.J.H., New perceptions on the S Doradus phenomenon and the micro variations of five Luminous Blue Variables (LBVs), Astron. Astrophys. Suppl., 1997, 124, p. 517-531.

Observations of Supernovae associated with Gamma-Ray Bursts

Alina Volnova[1], Alexei Pozanenko[1, 2], Maria Pruzhinskaya[3, 4], Sergei Blinnikov[5, 6, 7], Elena Mazaeva[1], Raguli Inasaridze[8] , Vova Ayvazyan[8], Gulnazi Inasaridze[8] , Inna Reva[9], Otabek Burkhonov[10] , Shukhrat Ehgamberdiev[10], Otari Kvaratskhelia[8] , Vasilij Rumyantsev[11], Yuri Krugly[12], Evgeny Klunko[13], and Igor Molotov[14]

[1] Space Research Institute of the Russian Academy of Sciences, Moscow, Russia
E-mail: alinusss@gmail. com
[2] National Research Nuclear University MEPhI (Moscow Engineering Physics Institute), Moscow, Russia
E-mail: apozanen@iki. rssi. ru
[3] Lomonosov Moscow State University, Sternberg Astronomical Institute, Moscow, Russia
[4] Laboratoire de Physique Corpusculaire, Université Clermont Auvergne, Université Blaise Pascal, CNRS/IN2P3, Clermont-Ferrand, France
[5] Institute for Theoretical and Experimental Physics, Moscow, Russia
[6] All-Russia Research Institute of Automatics, Moscow, Russia
[7] Kavli Institute for the Physics and Mathematics of the Universe (WPI), The University of Tokyo Institutes for Advanced Study, The University of Tokyo, Kashiwa, Japan
[8] Abastumani Astrophysical observatory, Ilia State University, Tbilisi, Georgia
[9] Fesenkov Astrophysical Institute, Almaty, Kazakhstan
[10] Ulugh Beg Astronomical Institute of the Uzbek Academy of Sciences, Tashkent, Uzbekistan
[11] Crimean Astrophysical Observatory, Nauchniy, Crimea, Russia
[12] Institute of Astronomy of Kharkiv National University, Kharkiv, Ukraine
[13] Institute of Solar-Terrestrial Physics, Russian Academy of Sciences, Siberian branch, Irkutsk, Russia
[14] Keldysh Institute of Applied Mathematics, Moscow, Russia

Abstract

In this paper, we present an overview of the observational properties of supernovae (SNe) associated with long-duration gamma- ray bursts (GRBs). We summarise the statistics of GRB-SNe physical properties and consider different modelling methods. We report the results of the numerical modelling of the GRB 130702A/SN 2013dx multicolour light curve using a spherically symmetrical multi-group radiation hydrodynamics code STELLA. We have obtained main bolometric parameters of the SN and compare our results with those of analytical modelling.

1. Introduction

The two last decades of observations and investigations of gamma-ray bursts (GRBs) and their optical counterparts led to the unam- biguous association between at least some long GRBs and the death of massive stars. The observational connection of long GRBs with type Ib/c supernovae (SNe) supports this evidence. The first reliable association between GRB 980425 and type Ic SN 1998bw with broad spectral lines was both positional and temporal, and spectral data of the two events showed the same redshift of 0.0085 ($\sim$ 40 Mpc) (Galama et al. 1998; Iwamoto et al. 1998; Kulkarni et al. 1998). However, the γ-ray properties of GRB 980425, in particular, its relatively low γ-ray luminosity, made this event a sort of outlier in the range of all long GRBs. The next confirmation of GRB-SNe associations occurred in 2003, with the discovery of very bright GRB 030329 associated with type Ic SN 2003dh (Hjorth et al. 2003; Stanek et al. 2003; Matheson et al. 2003). The kinetic energy of both these SNe exceeded 10^{52} erg, so they were hypernovae (the name of unusual SN suggested by Paczyński 1998). The launch of the *Swift* space observatory (Gehrels et al. 2004) changed the way of GRBs investigation dramatically. An early discovery of GRBs optical counterparts and their fast follow-up with ground-based telescopes allowed to build detailed multicolour light curves and obtain valuable spectroscopic data.

The light curve (LC) of the long GRB optical counterpart may be roughly divided by three main phases (Fig. 1): (i) the phase of the *prompt emission* when the optical radiation is registered simultaneously with the γ-rays and is a result of the central engine activity; (ii) the *afterglow* phase which is mostly connected to the relativistic jet emission and its interaction with a circumburst medium; (iii) the relaxation of the afterglow to the host galaxy flux level. At a later moment of the afterglow phase the SN feature may appear as a bump on the monotonous LC supporting the photometric evidence of the SN component presence. However, the only way to confirm whether the bump is indeed the SN is to do spectroscopic observations. The detection of broad lines in the spectra indicates the rapid outflow of the material and allows securing the nature of the LC bump as a SN. Up to the end of 2016 there are 20 GRB-SNe associations with the spectroscopic confirmation and additionally about 30 GRB-SNe with the only photometric

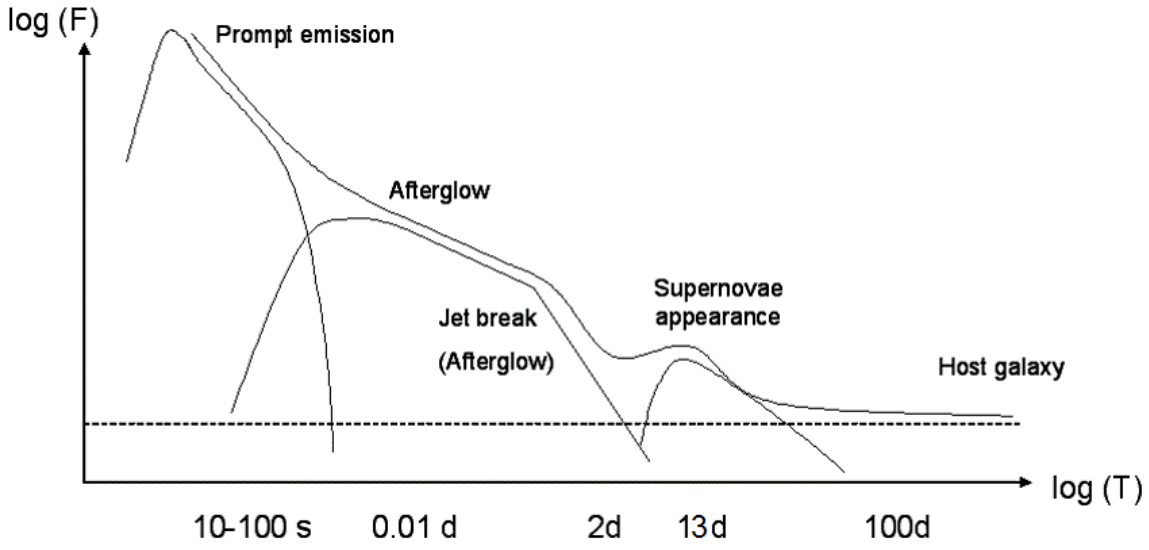

Fig. 1. The schematic light curve of the long GRB optical counterpart in a rest frame. The phases of the prompt emission, afterglow and host galaxy are depicted. The observational

appearance of the SN feature begins at a later time of the afterglow phase and lasts till the flux of the source is not distinguishable from the host galaxy flux.

SN-like feature in the LC. In addition to SN 1998bw and SN 2003dh we may note a few more interesting spectroscopic GRB-SNe: SN 2006aj (Ic; Ferrero et al. 2007); SN 2010bh (Ic; Bufano et al. 2011); SN 2013cq (Ic; Perley et al. 2014); SN 2013fu (Ib/c; Cano et al. 2014); SN 2016jca (Ic; de Ugarte-Postigo et al. 2016).

The observed flux from the GRB-SN is composed of the afterglow flux, the SN itself and the constant flux of the host galaxy. A careful decomposition of the three components is necessary to obtain the LC of the SN for further determination of its bolometric properties. The temporal behaviour of the multicolour LC of the optical afterglow and the host galaxy contribution should be carefully modelled and quantified. The decomposition should also take into account the line-of-sight extinction in the Milky Way (e. g. by using the extinction maps by Schlafly & Finkbeiner 2011) and in the host galaxy (e. g., by modelling its spectral energy distribution and comparing it with models of the well-studied galaxies). Every listed component may be included in the fitting procedure as an additional parameter or a set of parameters (Thöne et al. 2011; Sollerman et al. 2007; Greiner et al. 2015). This phenomenological approach is based on the standard GRB theory that states that the light powering the AG is synchrotron in origin, and therefore follows a power-law behaviour in both time and frequency ($f_\nu \propto (t - t_0)^{-\alpha} \nu^{-\beta}$, where the respective decay and energy spectral indices are α and β, while $t0$ is the trigger time of the GRB (Sari et al. 1998).

Once the SN LC has been obtained, the most common way to estimate its bolometric properties is to compare it with a template known GRB-SN LC. The proximity of GRB 980425/SN 1998bw event allowed to build detailed multicolour LCs (Clocchiatti et al. 2011), which became the most usable template LCs for the phenomenological investigations of GRB-SNe. The spectral data of the SN 1998bw were modelled carefully (Nakamura et al. 2001; Maeda et al. 2002) and also became the template spectra for other GRB-SNe investigations. The other good spectroscopic GRB-SN is SN 2003dh (GRB 030329, Mazzali et al. 2003; Deng et al. 2005), but the exceptional brightness and inhomogeneity of the GRB afterglow does not allow to build a reliable SN LC. SN 2006aj associated with GRB 060218 (Ferrero et al. 2006) is also used as a template for other GRB-SNe both in photometric and spectroscopic studies.

The spectra of GRB-SNe usually exhibit broad lines of O I, Ca II, Si II and Fe II. The line velocities calculated by modelling two specific lines (Si II λ6355 and Fe II λ5169) indicate that the ejecta containing these elements move with the speed of order $15,000 - 40,000$ kilometres per second. SN 1998bw has been spectroscopically observed in detail during its nebular phase due to its close proximity. The nebular lines include O I, O II, Ca II, Mg I, Na I, Fe II, Fe III, Co II, C I (Mazzali et al. 2001). Nebular O I was also observed for nearby GRB-SNe 2006aj (Maeda et al. 2007) and 2010bh (Bufano et al. 2012).

SN 1998bw was studied with unprecedented details, and its bolometric properties were modelled numerically (see, e. g., Maeda 2006). In cases when the bolometric (or quazibolometric) LC of the particular GRB-SN may be built, a simple scaling of the SN 1998bw bolometric LC and fitting it to the LC of interest may help to estimate bolometric properties of the investigated GRB-SN. For many years the SN 1998bw LC was used for this purpose in its numerical form, and in 2013, a new analytical method has appeared (Cano 2013). The main idea of this method is the same – the comparison of bolometric LCs with that of SN 1998bw – but it uses the simple one-dimetional Arnett (1982) model to fit the bolometric LC of the SN 1998bw with an analytical

function, containing all bolometric quantifiable properties as free parameters. To compare the two LCs in these terms means to find the luminosity scaling k and time-stretch s factors of the SN of interest. However, this method may involve some

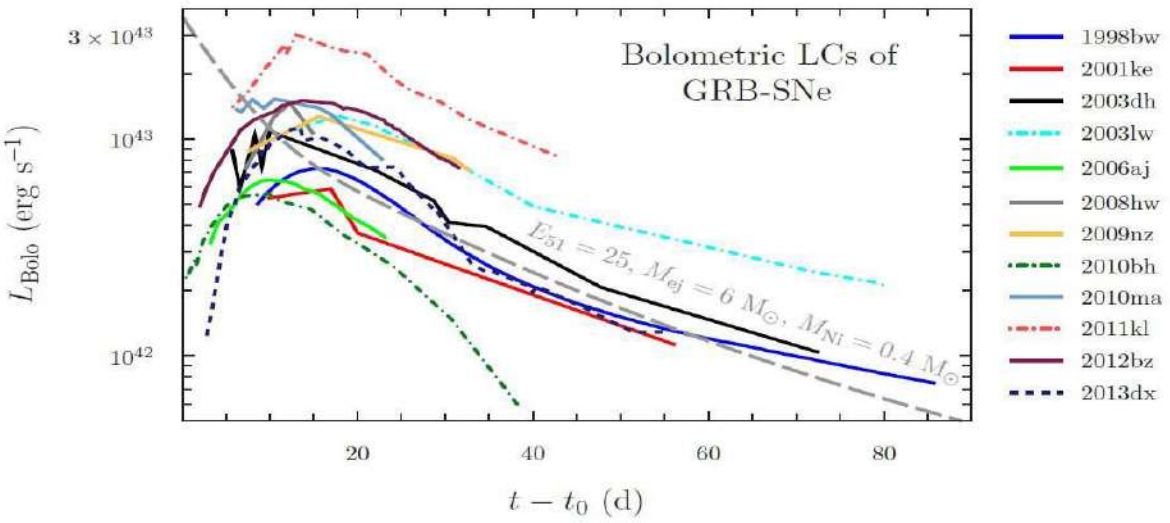

Fig. 2. The bolometric LCs of 12 GRB-SNe with well-sampled observational data (adopted from Cano et al. (2016)). Times are given in the rest-frame. The average peak luminosity of all GRB-SNe except SN 2011kl is $\bar{L}_p = 1.0 \times 10^{43}$ ergs /s, with a standard deviation of $\sigma_{\bar{L}_p} = 0.4 \times 10^{43}$ ergs/s, and the average peak time is $t_p = 13.2\ d$ ($\sigma_{\bar{L}_p} = 2.6\ d$). Plotted for reference is an analytical model that considers the luminosity produsedby an average GRB-SN (grey dashed line; $E_K = 2.5 \times 10^{52}$) erg , $M_{ej} = 6M_\odot, M_{56Ni} = 0.4M_\odot$).

additional uncertainties if there are no enough data in different colours of multicolour observations to build a good bolometric LC. Another case may take place if SN 1998bw is not a unique type of SN associated with GRBs.

The comparison of a particular SN LC with that of the "classical" SN 1998bw allows estimating the main observational prop- erties: the peak luminosity Lp and the time corresponding to the maximum in the LC tp. The analytical model of Cano (2013) allowed to estimate the main physical properties for the sample of 28 GRB-SNe (Cano et al. 2016). The average peak luminosity of this GRB-SN sample is $\bar{L}\mathrm{p} = 1.0 \times 10^{43}$ erg/s, with a standard deviation of $\sigma_{\bar{L}_p} = 0.4 \times 10^{43}$ erg/s, and the average peak is $t\mathrm{p} = 13.2$ d ($\sigma t\mathrm{p} = 2.6$ d). The average GRB-SN (grey dashed line in Fig. 2) has a kinetic energy of $E_K = 2.5 \times 10^{52}$ erg ($\sigma_{EK} = 1.8 \times 10^{52}$ erg), an ejecta mass of $M\mathrm{ej} = 6\mathrm{M}_\odot$ ($\sigma Mej = 4\ \mathrm{M}_\odot$), a nickel 56 mass of $M_{56\,\mathrm{Ni}} = 0.4\ \mathrm{M}_\odot$ ($\sigma M_{56\mathrm{Ni}} = 0.2\ \mathrm{M}_\odot$) and a peak photospheric velocity of $v_{\mathrm{ph}} = 21,000$ km/s ($\sigma_{v\mathrm{ph}} = 8,000$ km/s).

The numerical 1D, 2D, and 3D simulations of the GRB-SNe LCs allows determining the bolometric physical properties of the event in every particular case, but it is rather sophisticated and requires good observational data in order to estimate the quality of the model. The numerically calculated model should be based on hydrodynamical equations and a radiative transfer theory. Since 1998, many codes have been used for the purpose of GRB-SNe LCs modelling, but all of them were built for the particular GRB-SN study (SN 1998bw, Mazzali et al. (2001); Maeda

(2006); Nagataki et al. (2006); SN 2003dh, Mazzali et al. (2003); Nagataki et al. (2006); SN 2006aj, Maeda et al. (2007); SN 2011kl, Bersten et al. (2016)).

In the next Section we discuss the case of GRB 130702A/SN 2013dx and the numerical modelling of its multicolour LC realized by the 1D spherically symmetrical multi-group radiation hydrodynamics code STELLA (Blinnikov et al. 1998, 2006) which treats non-equilibrium radiative transfer according to chemical composition and inner structure of a pre-supernova star. The code has been used successfully for LC modelling of different types of SNe (Ia, Blinnikov et al. 2006; Ib/Ic, Folatelli et al. 2006; Tauris et al. 2013; IIb, Blinnikov et al. 1998; IIn, Chugai et al. 2004; IIP, Baklanov et al. 2005; Tominaga et al. 2009). The STELLA code was applied for GRB-SN modelling for the first time by Volnova et al. (2017), and here we present an abridged version of our studies.

2. GRB 130702A/SN 2013dx

2.1 Observations

GRB 130702A was detected by the Gamma-ray Burst Monitor (GBM; Meegan et al. 2009) on-board the space observatory *Fermi* at 00:05:23.079 UT on July 2, 2013 (Cheung et al. 2013; Collazzi & Connaughton 2013) at the position of R. A. = 218.°81, Dec= +12.°25 with 1σ uncertainty of 4.° and duration of $T90$ [1] of about 59 s in the GBM energy range of 50–300 keV. The gamma-rayemission of the burst was also detected by SPI-ACS/*INTEGRAL* (Hurley et al. 2013), Konus-*Wind* (Golenetskii et al. 2013), and *Fermi*/LAT detected more than 5 photons above 100 MeV up to t = 2200 s after the GBM trigger (Cheung et al. 2013).

The X-ray counterpart of GRB 130702A was discovered by the X-Ray Telescope (XRT; Burrows et al. 2005) aboard the *Swift* space observatory only in t = 1.03 d (D'Avanzo et al. 2013b) and was observed up to 225 d after the trigger [2].

The optical counterpart of the GRB 130702A was discovered by the intermediate Palomar Transient Factory (Law et al. 2009; Rau et al. 2009) with the Palomar 48-inch Oschin telescope (P48) (Singer et al. 2013a,b), its spectroscopic redshift is z =0.145 (Mulchaey et al. 2013a,b; D'Avanzo et al. 2013a). The afterglow position coincided with that of a faint source SDSS J142914.75+154626.0 that was suggested to be the host galaxy of the burst in subsequent studies (Kelly et al. 2013; D'Elia et al. 2015; Toy et al. 2016).

The radio counterpart of GRB 130702A was observed by Combined Array for Research in Millimeter Astronomy (CARMA) (Perley & Kasliwal 2013), by the Westerbork Synthesis Radio Telescope (van der Horst 2013), by the Karl G. Jansky Very Large Array (Corsi et al. 2013), and by the 22-m radio-telescope RT-22 of the Crimean Astrophysical observatory (Volnova et al. 2017).

The emerging SN associated with the optical afterglow was discovered photometrically about 6 days after the burst trigger with the 2.5-m Nordic Optical Telescope (NOT) based on obvious brightening of the afterglow (Schulze et al. 2013). Later the SN was confirmed spectroscopically (Cenko et al. 2013; D'Elia et al. 2013) and got name SN 2013dx.

The GRB observational collaboration of IKI RAS started to monitor the optical afterglow of GRB 130702A with 1.5-m AZT-22 telescope of Maidanak astronomical observatory (MAO) on July 3, 2013, i. e. one and a half days after the *Fermi* trigger (Pozanenko et al. 2013), and continued the

[1] The time during which the cumulative counts increase from 5% to 95% above background (Kouveliotou et al. 1993).

[2] http://www.swift.ac.uk/xrt_curves/00032876/

observations of the afterglow and rising SN in *R*-band on July 4-12, 14-16, 18, 19, 21, 23 and August 15, 18, 28. We also took several frames in *B*-band on July 7, 10, 12, 15. The afterglow was observed by 0.7-m AS-32 telescope of Abastumani Astrophysical Observatory (AbAO) taking unfiltered images on July 3, 4, 15 and 16. The 1-m Zeiss-1000 telescope of Simeiz branch of the Crimean Astrophysical Observatory took several frames of the afterglow and emerging SN in *B* and *R* filters on July 13, 15-16. The 2.6-m Shajn telescope of the Crimean Astrophysical Observatory (CrAO) observed the optical counterpart in *R* filter on July 5. The instrument also observed the decaying SN on August 3 and 4. The late phase of SN decay was observed by 1.5-m Russian-Turkish telescope (RTT-150) at Tubitak observatory on August 28 (Khorunzhev et al. 2013) and by a 2.5-m Nordic Optical Telescope (NOT) at Roque de los Muchachos Observatory on September 27-28. The raw LC of the GRB 130702A optical counterpart obtained by IKI RAS observational network is presented in Fig. 3a.

2.2.SN 2013dx light curve

All photometric reduction was performed using APPHOT task of NOAO's IRAF package [3] based on nearby SDSS stars. The resulting *BR* magnitudes were transformed to the AB system and compiled with other published data (Fig. 3 D'Elia et al. 2015; Toy et al. 2016).

To extract the LC of the SN 2013dx, the three additional components were subtracted: the line-of-sight absorption, the underlying host galaxy flux and the afterglow component. Firstly, the Galactic extinction of $E(B-V)=0.038$ (Schlafly & Finkbeiner 2011) was taken into account. The host galaxy absorption was modelled with the SED of the galaxy and is suggested to be negligible (Volnova et al. 2017). The flux of the host galaxy was subtracted mathematically using the observational data from Toy et al. (2016).

The contribution from the afterglow was considered based on X-ray data. The standard GRB afterglow model (Sari et al. 1998) suggests that at the late phase the spectrum of the afterglow may be fitted with a single power law in the frequency range from X-ray to optics, and the temporal decay of the LC should be achromatic in the same range, i. e. both in X-rays and in optics. The

X-ray data obtained by *Swift*/XRT from 2 d to 225 d after the GRB trigger (D'Avanzo et al. 2013b) may be fitted by a single power law with the time decay index $\alpha = 1.27$. The optical flux of the afterglow in every filter before 4 d after the trigger (when the SN contribution became non-negligible) was fitted by a single power law with the same decay index and subtracted mathematically from the total flux. The resulting multicolour LCs are presented in Fig. 4a. The LC of SN 2013dx is the second well sampled GRB-SN after SN 1998bw.

2.3. Numerical modelling of the SN light curve

The numerical multicolour light-curve calculations for SN 2013dx were performed with one-dimensional multi-frequency ra- diation hydrodynamics code STELLA (Blinnikov et al. 1998, 2006). In the current calculations we adopted 100 zones for the Lagrangean coordinate and 130 frequency bins. As input parameters, we changed the pre-supernova star mass M and radius R, the energy of the outburst $E_{\rm oburst}$, the mass of synthesized nickel $M_{^{56}\rm Ni}$, the mass of the resulting compact remnant $M_{\rm CR}$, and the initial distribution of chemical elements in the pre-supernova star.

[3] IRAF is the Image Reduction and Analysis Facility, a general purpose software system for the reduction and analysis of astronomical data. IRAF
is written and supported by the National Optical Astronomy Observatories (NOAO) in Tucson, Arizona. NOAO is operated by the Association of Universities for Research in Astronomy (AURA), Inc. under cooperative agreement with the National Science Foundation. http://iraf. noao.edu-

The ejecta of SNe has the same chemical composition as pre- supernova star except for ^{56}Ni, because we do not follow the explosive nucleosynthesis. ^{56}Ni can be put in the centre of SN ejecta in the calculations as well as be spread out within any region.

The mass and radius of pre-supernova star for the model, which offers the best agreement with the observations of SN 2013dx, equal $M = 25\ M_{\odot}$ and $R = 100\ R_{\odot}$, respectively. The resulting energy of explosion is $E_{\text{oburst}} = 3.5 \times 10^{52}$ erg. The $0.2\ M_{\odot}$ of synthesised ^{56}Ni is totally mixed through the ejecta. The central region becomes a black hole with $M_{\text{CR}} = 6M_{\odot}$. The peak

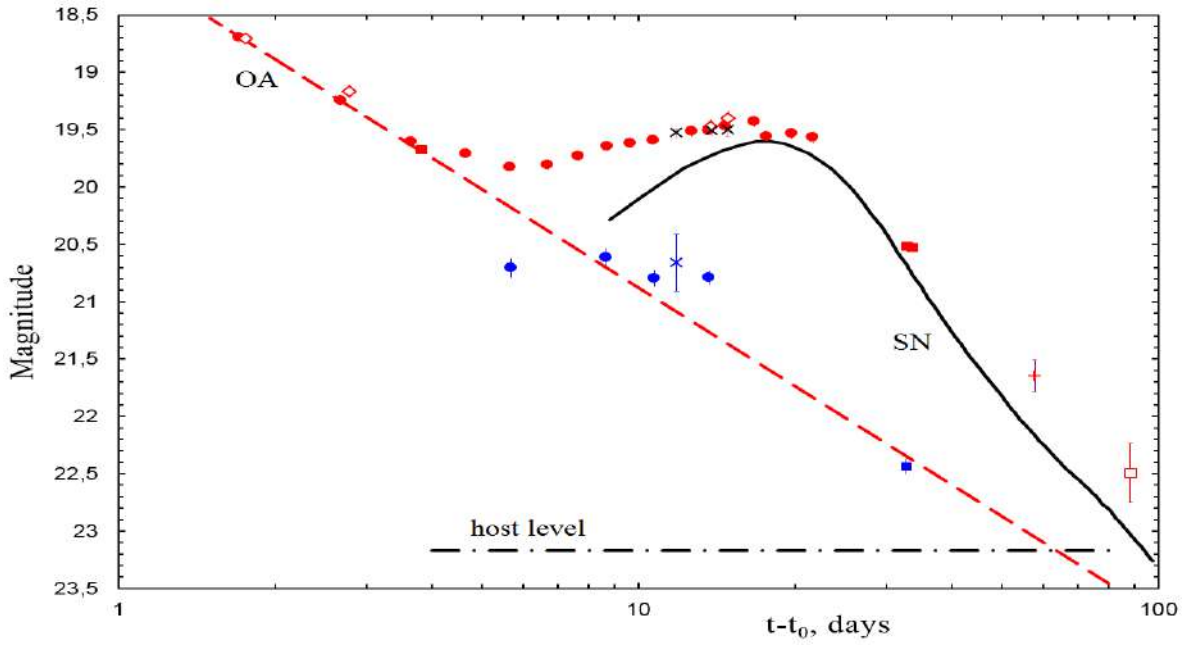

a)

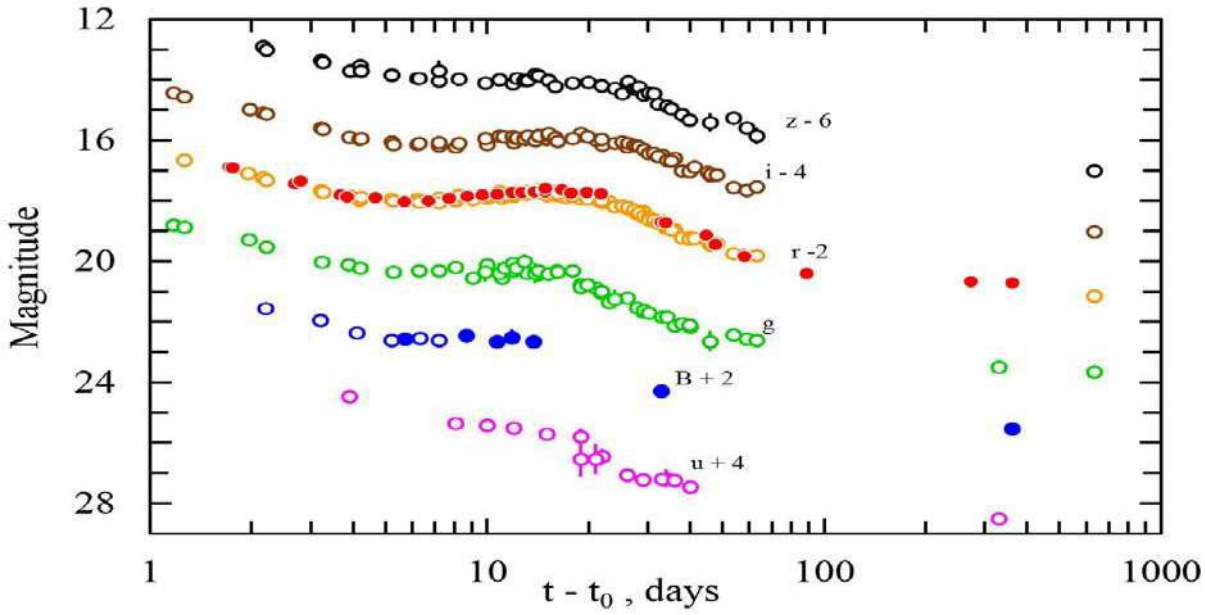

b)

Fig. 3. The observed multicolour LCs of GRB 130702A optical counterpart. (a) Data obtained only by IKI RAS observational collaboration (magnitudes are in Vega system). Dashed dotted line marks the host galaxy level in the filter *R*, the solid straight line and its dashed extension mark the OA trend, and the solid curve is the light curve of the SN feature. (b) All our observational data (solid circles) compiled with those from the literature (open circles; magnitudes in AB system). The Galactic extinction is not considered.

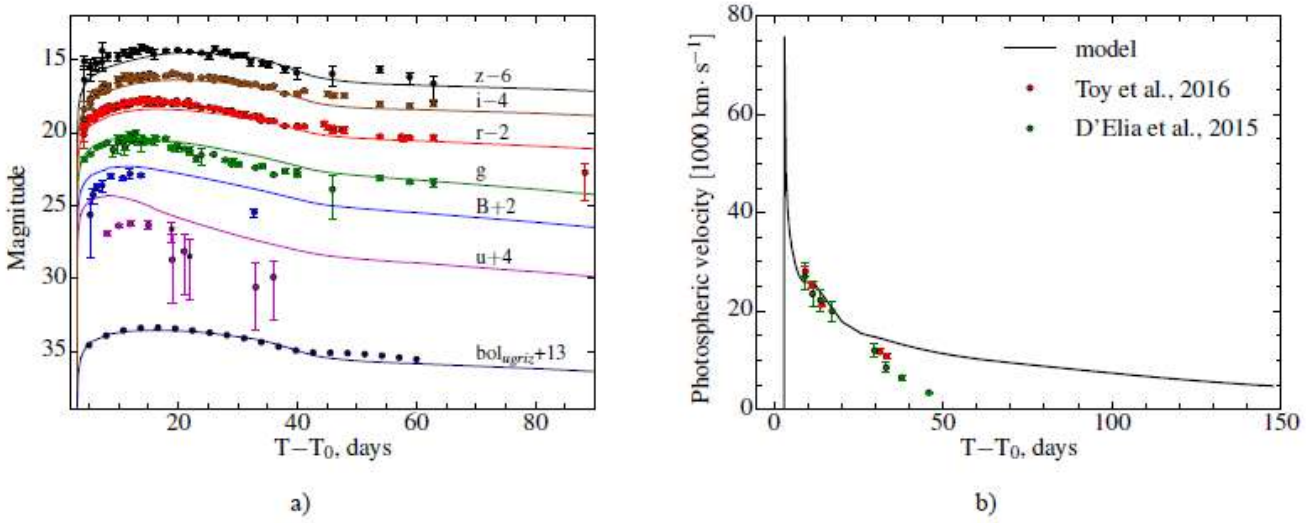

Fig. 4. a) The multicolour LCs of SN 2013dx. The Galactic extinction, the flux from the host galaxy and the optical afterglow contribution are excluded. Solid lines show the best model of the SN LCs obtained by STELLA (see Section 2.3). The quasibolometric LC of the SN in AB photometric system obtained as a sum of the fluxes in *ugriz* filters, is marked as bol*ugriz*. The data and model are in observer frame. b) The evolution of photospheric velocities v_{ph} of SN 2013dx measured via observations (points; adopted from D'Elia et al. 2015; Toy et al. 2016) and calculated from the modelling (solid line). The plot is in observer frame (from Volnova et al. 2017).

bolometric luminosity is $L_p = 5.4 \times 10^{43}$ erg/s, suggesting that SN 2013dx is more luminous at the peak light than the average GRB-SN (see Fig. 2). The bolometric LC of the SN peaks at t_p = 14.35 d according to the model. The parameters E_{oburst} and $M_{^{56}\text{Ni}}$ were adopted from D'Elia et al. (2015), the rest of the parameters were picked up to better match the observed LC by the model. Fig. 4a shows the resulting modelled LCs obtained by STELLA calculations. The quasibolometric LC of the SN in AB photometric system is obtained as a sum of the fluxes in *ugriz* filters. Fig. 4b shows observer-frame photosperic velocities in comparison with observational data obtained via spectroscopy by D'Elia et al. (2015) and Toy et al. (2016). The model evolution of the photospheric velocities is in a good agreement with direct observations during the first ~30 days after the explosion.

We varied the mass *M* and the radius *R* of the pre-supernova star, the mass of synthesized ^{56}Ni, and the energy of the burst E_{oburst} in order to consider their influence on the form of the modelled quasibolometric LC. The ejecta mass affects the descending part of the LC, dependence of radius is stronger on the domes, however, the tail is mainly determined by ^{56}Ni abundance. The models are brighter for higher ejecta or ^{56}Ni mass, and larger radius. The decrease of the compact

remnant mass provides wider maximum of the LC. When ^{56}Ni is not mixed, the light-curve maximum is fainter. Decreasing the outburst energy makes the diffusion time of gamma-photons from radioactive decay longer. This manifests itself as a widening of the LC; moreover, the diminution of decline rate occurs later.

We estimated approximate limits of the main model parameters: the pre-supernova star mass and radius varies in the range of 23–27 $M_\odot$ and 75–125 $R_\odot$, respectively; the ^{56}Ni mass lies between 0. 15 and 0. 25 $M_\odot$; and the explosion energy E_{oburst} — in the range of (30–40) $\times 10^{51}$ erg.

3. Discussion and conclusions

Toy et al. (2016) estimate the bolometric parameters of the SN using the analytical model proposed by Cano et al. (2016). Following their results, we performed the LC modelling adopting $M_{^{56}\text{Ni}} = 0.37\ M_\odot$ (located in the centre of explosion and no mixing), $E_K = 8.2 \times 10^{51}$ erg, and $M_{\text{ej}} = 3.1\ M_\odot$. Following Toy et al. (2016), we assumed that there is no compact object at all, i. e. no gravitational centre that affects the expansion of the innermost layers. Since Toy et al. (2016) reports that the initial radius before explosion is small, we put $R = 10\ R_\odot$. The parameters reported by Toy et al. (2016) do not allow us to reproduce both observed multicolour LC and photospheric velocity evolution. This means that LC of SN 1998bw may be not an universal template to describe SN associated with GRB. In our case of SN 2013dx the template of SN 2003dh, used in D'Elia et al. (2015), gives better initial parameters for the LC modelling. The best parameters of our model are reported in Section 2.

Based on our modelling we may formulate problems that remain to be resolved.

1. There is a problem with simultaneous fitting of observational data in all filters. The time position of the maximum in the modelled and observational LCs does not coincide in every colour, especially in blue ones.
2. Despite the fact that the modelled quasibolometric LC fits well the observational data, the multicolour model does not fit well the peak of the SN in blue filters. The discrepancy between observational points in *B* and *u* filters and resulting modelled LCs may be explained by additional absorption along the line of sight, which is not included in the host extinction.
3. The resulting model does not describe the secondary bump observed during the SN decay phase clearly visible in red filters between 40 and 60 days after the trigger (see Fig. 4a). The bump may not be related to the SN, but to the afterglow. In this case, it may be explained as an interaction of the ejecta with some inhomogeneities in the surrounding interstellar medium, e. g. dense interstellar clouds. For more detailed discussion see Volnova et al. (2017).

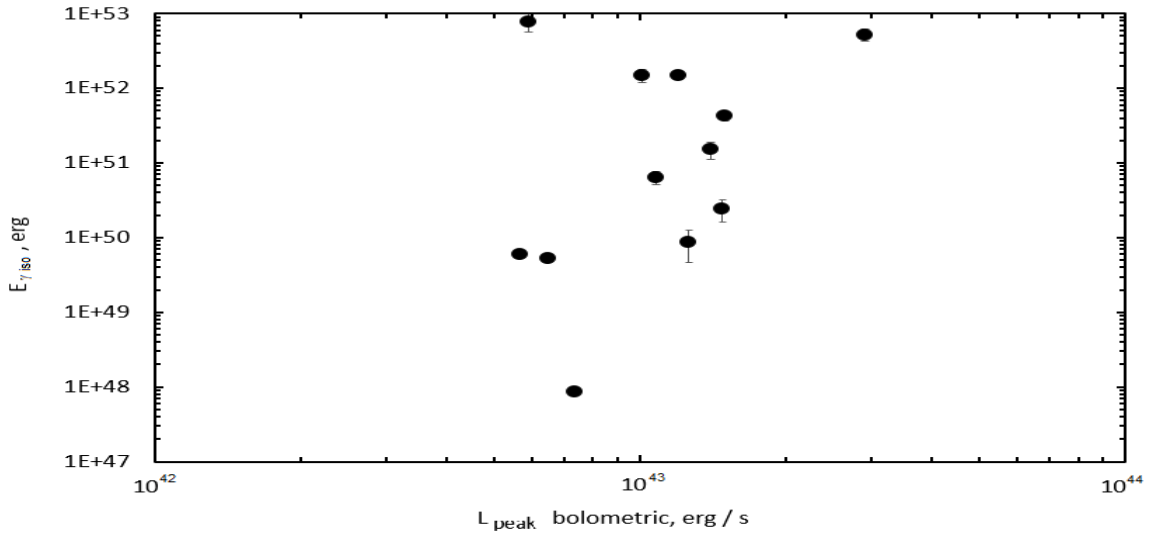

Fig. 5. The plot of the peak bolometric luminosity of the SN L_p vs. the isotropic equivalent energy of the GRB E_{iso}. To present, there is no any reliable correlation between the GRB prompt emission and the SN properties.

4. To present, there is no any reliable correlation between the GRB prompt emission and the SN properties. We attempt to find some statistical correlation between the SN bolometric properties and gamma-ray properties of the associated burst. In this framework we plotted the relation between the peak bolometric luminosity of the SN L_p and the isotropic equivalent energy of the GRB E_{iso} (Fig. 5). We did not find any correlation between these two parameters.

Both analytical and numerical models of the GRB-SNe may estimate physical bolometric properties of the SNe sources and explosions. Though their results are in reasonable agreement, the numerical model is more physically accurate and allows changing many different parameters. The development of the numerical hydrodynamical radiation-transfer codes to 2D and 3D will help to consider asymmetrical explosions and improve our knowledge about GRB-SNe physics.

4. Acknowledgments

A.V., A.P., and E.M. are grateful to the grant RFBR 17-02-01388 for a partial support. R.Ya.I. is grateful to the grant RUSTAVELI FR/379/6-300/14 for a partial support.

References

Arnett W. D. 1982, Astroph. J., 253, 785
Baklanov P. V., Blinnikov S. I., Pavlyuk N. N., 2005, Astron. Lett., 31, 429
Bersten M. C., Benvenuto O. G., Orellana M., Nomoto K., 2016, Astroph. J. Lett., 817, L8
Blinnikov S. I., Eastman R., Bartunov O. S., et al., 1998, Astroph. J., 496, 454
Blinnikov S. I., Röpke F. K., Sorokina E. I., et al., 2006, Astron. Astroph., 453, 229

Bufano F., Benetti S., Sollerman J., Pian E., Cupani G., 2011, Astronomische Nachrichten, 3, 262
Bufano F., Pian E., Sollerman J., et al., 2012, Astron. J., 753, 67
Burrows D. N., Hill J. E., Nousek J. A., et al., 2005, Sp. Sci. Rev., 120, 165
D'Elia V., D'Avanzo P., Melandri A., et al., 2013, GCN Circ. No 15000
D'Elia V., Pian E., Melandri A., et al., 2015, Astron. Astroph., 577, A116
Deng J., Tominaga N., Mazzali P. A., et al., 2005, Astroph. J., 624, 898
Cano Z., 2013, Mon. Not. Roy. Astron. Soc., 434, 1098
Cano Z., de Ugarte Postigo A., Pozanenko A., et al., 2014, Astron. Astroph., 568, id. A19
Cano Z.,Wang S. -Q., Dai Z. -G.,Wu X. -F., 2016, Xiv:1604. 03549
Cheung T., Vianello G., Zhu S., et al., 2013, GCN Circ. No 14971
Chugai N. N., Blinnikov S. I., Cumming R. J., et al., 2004, Mon. Not. Roy. Astron. Soc., 352, 1213
Cenko S. B., A. Gal-Yam M. M., Kasliwal D., et al., 2013. GCN Circ. No 14998
Clocchiatti A., Suntzeff N. B., Covarrubias R., Candia P., 2011, Astron. J., 141, id. 163
Collazzi A. C., Connaughton V., 2013, GCN Circ. No 14972
Corsi A., Perley D. A., & Cenko S. B., 2013, GCN Circ. No 14990
D'Avanzo. P., D'Elia. V., Tagliaferri. G., et al., 2013a. GCN Circ. No 14984
D'Avanzo P., Porterfield B., Burrows D. N., et al., 2013b, GCN Circ. No 14973
Ferrero P., Kann D. A., Zeh A., et al., 2006, Astron. Astroph., 457, 857
Ferrero P., Palazzi E., Pian E., Savaglio S., 2007, AIP Conf. Proc., 924, 120
Folatelli G., Contreras C., Phillips M., et al., 2006, Astroph. J., 641, 1039
Galama T. J., Vreeswijk P. M., van Paradijs J., et al., 1998, Nature, 395, 670
Gehrels N., Chincarini G., Giommi P. et al., 2004, Astroph. J., 611, 1005
Golenetskii S., R. Aptekar V., Pal'shin D., et al., 2013, GCN Circ. No 14986
Greiner J., Mazzali P. A., Kann D. A. et al., 2015, Nature, 523, 189
Hjorth J., Sollerman J., Møller P. et al., 2003, Nature, 423, 847
Hurley K., Goldsten J., Connaughton V., et al., 2013, GCN Circ. No 14974
Iwamoto K., Mazzali P. A., Nomoto K., et al., 1998, Nature, 395, 672
Kelly P. L., Filippenko A. V., Fox O. D., Zheng W., Clubb K. I. 2013, Astroph. J. Lett., 775, L5
Khorunzhev G., Volnova A., Pozanenko A., et al., 2013, GCN Circ. No 15243
Kouveliotou C., Meegan C. A., Fishman G. J., et al., 1993, Astroph. J. Lett., 413, L101
Kulkarni S. R., Frail D. A., Wieringa M. H., et al., 1998, Nature, 395, 663
Law N. M., Kulkarni S. R., Dekany R. G., et al., 2009, Publ. Astron. Soc. Pacific, 121, 1395
Maeda K., 2006, Astroph. J., 644, 385
Maeda K., Nakamura T., Nomoto K., et al., 2002, Astroph. J., 565, 405
Maeda K., Kawabata K., Tanaka M., et al., 2007, Astroph. J. Lett., 658, L5
Matheson T., Garnavich P. M., Stanek K. Z. et al., 2003, Astroph. J., 599, 394
Mazzali P. A., Nomoto K., Patat F., Maeda, K., 2001, Astroph. J., 559, 1047
Mazzali P. A., Deng J., Tominaga N., et al., 2003, Astroph. J., 599, 95
Meegan C., Lichti G., Bhat P. N., et al., 2009, Astroph. J., 702, 791
Mulchaey J., Kasliwal M. M., Arcavi. I., et al., 2013a, GCN Circ. No 14985
Mulchaey J., Kasliwal M. M., Arcavi I., et al., 2013b, Astron. Tel., 5191
Nagataki S., Mizuta A., Sato K., 2006, Astroph. J., 647, 1255
Nakamura T., Mazzali P. A., Nomoto K., Iwamoto K., 2001, Astroph. J., 550, 991
Paczy´nski B., 1998, Astroph. J., 494, L45
Perley D. A., Cenko S. B., Corsi A., et al., 2014, Astroph. J., 781, id. 37
Perley D., & Kasliwal M., 2013, GCN Circ. No 14979
Pozanenko A., Volnova A., Burhonov O., Molotov I., 2013, GCN Circ. No 14988
Rau A., Kulkarni S. R., Law N. M., et al., 2009, Publ. Astron. Soc. Pacific, 121, 1334

Sari R., Piran T., Narayan R., 1998, Astroph. J., 497, L17
Schlafly E. F., & Finkbeiner D. P., 2011, Astroph. J., 737, id. 103
Schulze S., Leloudas G., Xu D., et al., 2013, GCN Circ. No 14994
Singer L. P., Cenko S. B., Kasliwal M. M., et al., 2013a, GCN Circ. No 14967
Singer L. P., Cenko S. B., Kasliwal M. M., et al., 2013b, Astroph. J. Lett., 776, L34
Sollerman J., Fynbo J. P. U., Gorosabel J. et al., 2007, Astron. Astroph., 466, 839
Stanek K. Z., Matheson T., Garnavich P. M. et al., 2003, Astroph. J. Lett., 591, L17
Tauris T. M., Langer N., Moriya T. J., et al., 2013, Astroph. J., 778, 23
Thöne C. C., de Ugarte Postigo A., Fryer C. L. et al., 2011, Nature, 480, 72
Tominaga N., Blinnikov S., Baklanov P., et al., 2009, Astroph. J., 705, 10
Toy V. L., Cenko S. B., Silverman J. M., et al., 2016, Astroph. J., 818, id. 79
de Ugarte Postigo A., Cano Z., Izzo L., et la., 2016, GCN Circ. No 20342
van der Horst A. J., 2013, GCN Circ. No 14987
Volnova A. A., Pruzhinskaya M. V., Pozanenko A. S., et al., 2017, Mon. Not. Roy. Astron. Soc., 467, 3500

Astronomy & Astrophysics (Caucasus) 3, (2018)

New observations of variable stars at the Astronomical Institute of Karazin Kharkiv National University

V. G. Shevchenko[1,2], O. I. Mikhalchenko[1,2], I. G. Slyusarev[1,2], V. P. Khramtsov[2], R. A. Chigladze[3]

[1]Institute of Astronomy of V. N. Karazin Kharkiv National University, Kharkiv, Ukraine
[2]Department of Astronomy and Space Informatics of V. N. Karazin Kharkiv National University, Kharkiv, Ukraine
[3]Samtskhe-Javakheti State University, Kharadze Abastumani Astrophysical Observatory, Georgia

E-mail: shevchenko@astron.kharkov.ua

Abstract

New observations of nine variable stars of different types (six binary stars and three pulsating stars) were done to study their physical properties at the Astronomical Institute of Karazin Kharkiv National University. Two rotational periods of EW binary stars and one of shadowing star have been determined for the first time. More precise values of rotational periods for other binary stars and the pulsation periods for the pulsating stars have been obtained. The absolute magnitudes, distances, effective temperatures, radii and luminosities for two DSCT pulsating stars have been determined using the relations connecting the pulsation period with the radius and the absolute magnitude. The absolute magnitudes and distances for four EW binary stars have been calculated.

Key words: pulsating stars, binary stars, CCD-observations, lightcurves, periods

1. Introduction

Presently, a very large number of variable stars of the different types in the Milky Way and other galaxies are known (Rodríguez et al. 2002), and the rate of their discoveries is growing rapidly due to special survey programs with 1-2 m telescopes (Catalina Sky Survey, Pan-STARRS, Palomar Transient Factory), allowing studying faint stars with smaller amplitude of brightness. Of a particular interest are pulsating stars of different types, since the analysis of their pulsations and the determination of main and other modes of period make it possible to build more accurate models of their internal structure (Lenz et al. 2008). Moreover, the correlation relations of the pulsation period with the absolute magnitude and with the radius (Fernie 1992, McNamara 2000, Laney et al. 2002, etc.) allow determining other physical characteristics (temperature, mass, radius, spectral type), estimating the distances to the stars and using these data to study the kinematics of the Galaxy (McNamara et al. 2000, Collinge et al. 2006). Often, variable stars are discovered during the observations of another space objects such as asteroids. Several variable stars were discovered in this way within the asteroid photometric observation program carried out at the Institute of Astronomy of Karazin Kharkiv National University (Shevchenko et al. 2013, Zheleznyak et al. 2015). In the present paper, we present the new results of observations of some variable stars of different types that were discovered recently or earlier.

2. Observations and Results

The CCD-observations of variable stars were carried out from 2010 to 2016 for 26 nights with the 0.7-m reflector at the Chuguev Observational Station of the Astronomical Institute of Karazin Kharkiv National University as a part of a student astrophysical practice (Shevchenko et al. 2013, Zheleznyak et al. 2015) and program of an investigation of the asteroid magnitude-phase relations (Shevchenko et al. 2012, 2016). The telescope is equipped with a ML4710 Peltier-cooled CCD camera (1027×1056 pixels, pixel size 13×13 μm). Images were taken using *V* and *R* bands of the Johnson–Cousins photometric system. Original CCD-frames were calibrated for dark current and flat field in the standard manner. The CCD-observations and data reduction methods were explained by Krugly et al. (2002) and by Shevchenko et al. (2012). The brightness measurements of stars on CCD-images were done using the aperture photometry package (ASTPHOT) developed by Mottola et al.

(1995). The absolute calibrations of the magnitudes were performed with standard star sequences from Landolt (1992) and Skiff (2007). The accuracy of the resultant absolute photometry is within 0.01-0.03 mag. The number of the star in according to the catalog USNO-B1.0, the equatorial coordinates at the epoch J2000.0, the variable type, the average value of apparent magnitude in *R* band, the period (in days), and the epoch of the composite lightcurve initial time moment are listed in Table 1. In section 2.1, we present composite lightcurves, short characteristics and some physical parameters for the observed pulsating stars of delta Sct (DSCT) and RR Lyr stars. The results of observations of four close binary stars of W UMa systems (EW type) and their physical characteristics are given in section 2.2, while section 2.3 presents the results of observations of two wide binary stars.

Table 1. Coordinates, types, magnitudes, colors, periods and epoch of the lightcurve initial time moment of the observed variable stars

USNO-B1.0	α_{2000}	δ_{2000}	Type	*R*	*V-R*	Period	Epoch
1214-0488288	20 32 08.80	+31 24 17.1	DSCT	15.98 ± 0.02	0.62 ± 0.02	0.1300405	2455414.27996
1464-0465888	23 38 17.17	+56 28 33.7	DSCT	13.88 ± 0.01	0.31 ± 0.02	0.13100	2456500.35140
0717-0911392	20 40 42.10	-18 12 49.2	RR	13.92 ± 0.01	0.50 ± 0.03	0.518702	2456129.434606
0982-0239035	11 30 59.62	+08 13 11.0	EW	12.31 ± 0.01	0.52 ± 0.01	0.293875	2457494.28256
1211-0481170	20 32 39.16	+31 11 57.5	EW	15.67 ± 0.02	0.76 ± 0.02	0.3239274	2455753.29085
1465-0461237	23 37 03.66	+56 31 59.8	EW	15.13 ± 0.01	0.64 ± 0.02	0.3630479	2456493.50205
1466-0470221	23 37 21.08	+56 37 58.0	EW	15.35 ± 0.01	0.52 ± 0.02	0.3425703	2456493.42361
1212-0480463	20 32 05.88	+31 17 58.7	EB	16.20 ± 0.02	0.55 ± 0.02	0.6817768	2455751.30123
1213-0486686	20 32 29.67	+31 21 45.9	EB	16.36 ± 0.02	0.67 ± 0.02	0.9831827	2456119.34881

2.1. Pulsating stars

1214-0488288, 1464-0465888. These stars are classified as DSCT pulsating stars with radial periods of 0.1300405 0.0000002 and 0.13100 0.00015 days, respectively (see fig. 1 *a,b*). For the first star (1214-0488288), the observations were carried out from 2010 to 2013 years to detect the Blazhko-effect, but no changes were found in pulsating period during observational time. Another star (1464-0465888) was observed during one night only, and this star has the amplitude less than the first one (see Table 2). The amplitudes of pulsations in *V*-band are large with comparison to *R*-band for both stars: 0.09 and 0.03 mag, respectively. Asymmetry of lightcurves is close to 0.35 *P* for both stars.

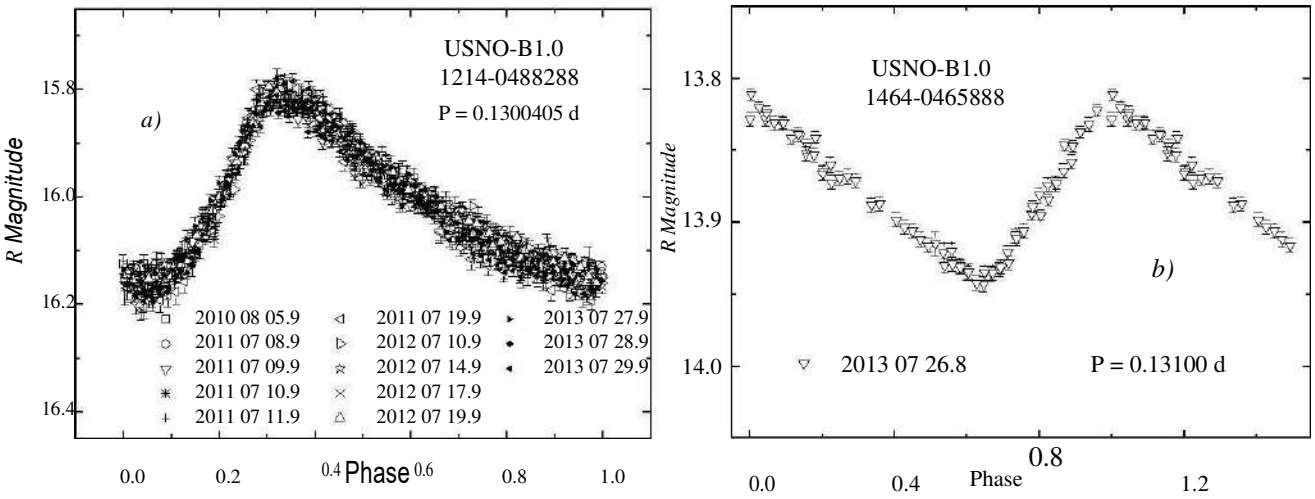

Fig. 1. Composite lightcurves of DSCT pulsating stars

Table 2. Physical characteristics of pulsating stars

USNO-B1.0	*P* (day)	Ampl. (mag)	M_V (mag)	M_{bol} (mag)	*r* kpc	$R_\odot$	$L_\odot$	T_{ef} K	Sp
1214-0488288	0.1300405	0.35 ± 0.01	1.30 ± 0.03	1.22 ± 0.03	1.62 ± 0.02	3.11 ± 0.05	26.1 ± 0.5	7400 ± 100	A9
1464-0465888	0.13100	0.13 ± 0.01	1.29 ± 0.03	1.21 ± 0.03	1.30 ± 0.02	3.13 ± 0.05	26.4 ± 0.5	7400 ± 100	A9

By using the "period-radius" and the "period-absolute magnitude" relations for DSCT stars (Lany et al. 2002, 2003), we have estimated the values of the radii, the absolute magnitudes, the luminosities, the effective temperatures and spectral types of observed stars. These data are presented in Table 2. To obtain the distances to the stars, we used a three-dimensional map of Milky Way dust (Green et al. 2015) for taking into account the interstellar extinction that turned to be A_V = 2.491 mag/kpc and A_V = 1.788 mag/kpc, respectively. In the future, the scale of the absolute magnitudes can be checked using the distance values from next Gaia data release. By now, we have not found the parallaxes of our stars in Gaia data release 1 (Lindegren et al. 2016).

0717-0911392. The star is classified by Miceli et al. (2008) as RR Lyr. Their determined pulsation period is P = 0.518702 day with the amplitude of 0.94 mag and their average brightness in V-band equals 14.22 mag. Our observations were performed in the R-band and the amplitude equals 0.84 mag (fig. 2), it is 0.1 mag less compared to Miceli et al. (2008). By using our data in R-band and Miceli et al. (2008) in V-band, we determined the value of the color index V-R = 0.50 0.03 mag. The asymmetry of the lightcurve is 0.12 P.

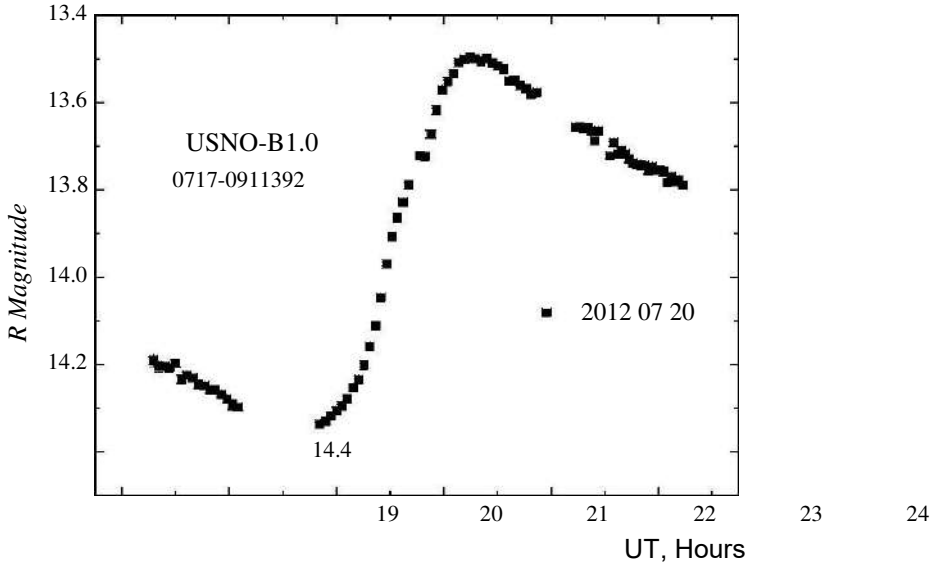

Fig. 2. Lightcurve of 0717-0911392 RR Lyr pulsating star

2.2. EW binary stars

0982-0239035. The star was observed for four nights in April of 2016. The composite lightcurve obtained with the period of 0.293875 0.000015 days is shown in fig. 3 *a*. The value of the period was obtained for the first time. The amplitude of lightcurve equals 0.22 mag. The value of V-R color index is 0.52 mag and it has no variations with the rotational phase.

1211-0481170. The observations of this star were done by Shevchenko et al. (2013) in the past. In 2013, we obtained the new observational data and did not detect any changes in the lightcurve of this star. By using a more observational interval, we obtained a more accurate rotational period that is equal to 0.3239274 0.0000005 days. A composite lightcurve with this period is presented in fig. 3 *b*. The value of V-R color index is 0.76 mag and it has no variations with the rotational phase.

1465-0461237. The star was observed for eight nights in 2013 and 2016. We determined the rotational period that equals 0.3630479 0.0000015 days. The composite lightcurve (fig. 3 *c*) has a maximum amplitude of 0.44 0.02 mag with small differences in the neighboring minima (about 0.4 0.01 mag). The values of the color index V-R are different for the minimum and the maximum of the lightcurve and are equal to 0.68 0.02 mag and 0.60 0.02 mag, respectively.

1466-0470221. The observations of this star were earlier carried out by Zheleznyak et al. (2015), but because of the small number of observational data, the rotational period determined by them was not correct. The new observations in 2015 allowed us to determine the rotational period that is equal to 0.3425703 0.0000015 days. The composite lightcurve (fig. 3 *d*) has th

maximum amplitude of 0.27 0.02 mag and the neighboring minima differ on 0.07 0.01 mag. The value of the color index *V-R* is equal to 0.52 0.02 mag. There are no differences in the color index with the rotational phase.

Rucinski (2006) has performed a calibration by using the maximum brightness of 21 contact EW binary systems with P < 0.56 days using Hipparcos data. He has obtained the next relation between the period and the absolute magnitude: $M_V = -1.5 - 12.0 \log(P)$. By using this relation and three-dimensional map of Milky Way dust (Green et al. 2015) to take the interstellar extinction into account, we determined the absolute magnitudes and the distances to the stars. Our results are presented in Table 3. In the future, these distances can be checked from Gaia data release 2. At present, we have not found the parallaxes of our stars in Gaia data release 1 (Lindegren et al. 2016).

Table 3. Physical characteristics of contact binary stars

USNO-B1.0	*P* (day)	Ampl. (mag)	*V* (mag)	M_V (mag)	A_V (mag/kpc)	*r* kpc
0982-0239035	0.293875	0.35 ±0.01	12.72 ±0.01	4.88 ±0.26	0.18	0.36 ±0.05
1211-0481170	0.3239274	0.24 ±0.01	16.32 ±0.02	4.35 ±0.18	2.56	0.87 ±0.03
1465-0461237	0.3630479	0.44 ±0.02	15.56 ±0.02	3.78 ±0.08	2.01	0.95 ±0.02
1466-0470221	0.3425703	0.27 ±0.02	15.76 ±0.02	4.08 ±0.13	2.01	0.92 ±0.03

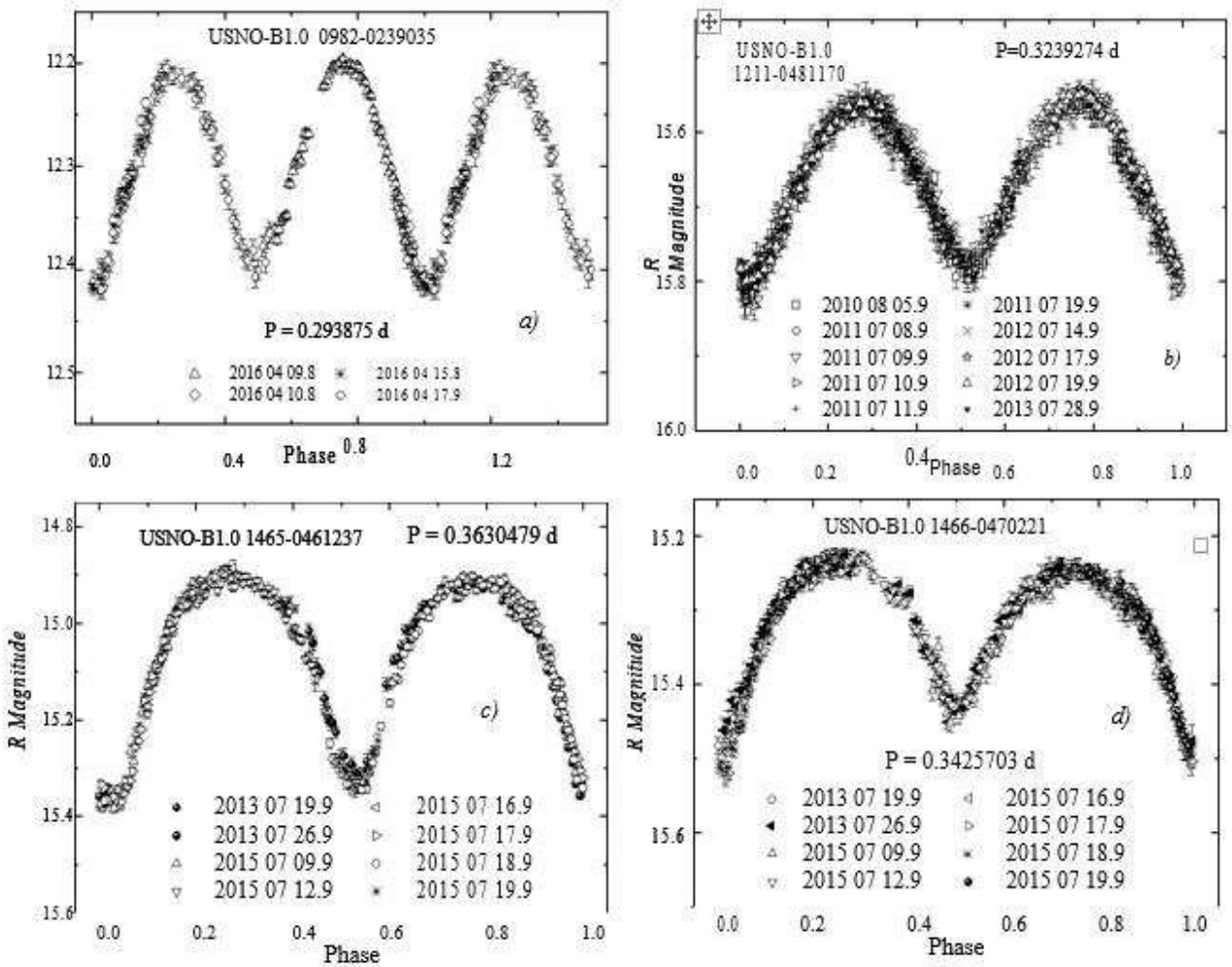

Fig. 3. Composite lightcurves of contact binary stars

2.3. Shadowing binary stars

1212-0480463. This star was observed from 2010 to 2013 for eleven nights. We have determined rotational period of components, which equals 0.6817768 0.0000005 days. The composite lightcurve (fig. 4 *a*) has a maximum amplitude of 0.28 0.02 mag, the levels of neighbor ightcurve minima differ on 0.08 0.02 mag, and small flat place of a duration about 1.6 hour is in the minima. The value of the color index *V-R* equals 0.55 0.02 mag. There are no differences in the color index with phase of rotation.

1213-0486686. This star was also observed from 2010 to 2013 for thirteen nights in July and August. We could not get the complete composite lightcurve (fig. 4 *b*) because the value of the rotational period of the components is close to one day. The obtained data allowed us to determine the rotational period for the first time that equals 0.9831827 0.0000015 days. The composite lightcurve has the maximum amplitude of 0.24 0.02 mag and small flat parts at the minima, about 3.6 hours duration. The value of the color index *V-R* is 0.67 0.02 mag, and we have not found any differences in the color index with the phase of rotation.

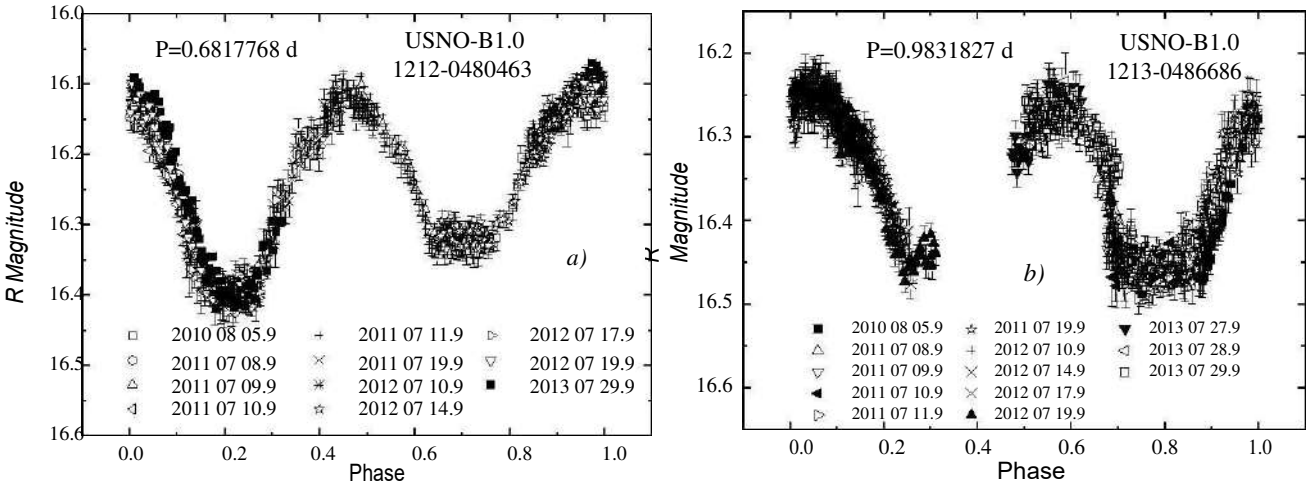

Fig. 4. Composite lightcurves of shadowing binary stars

3. Conclusions

As a result of the new photometric observations for 26 nights, two new contact binary stars were detected and their rotational periods were determined for the first time. The rotational period of the shadowing star has been also determined for the first time. More precise values of periods for the other six stars have been obtained and the composite lightcurves have been built for all stars. The absolute magnitudes, the effective temperatures, the radii, the luminosities and the distances for DSCT stars have been calculated using the relations connecting the pulsation period of the star with its radius and with the absolute magnitude. We have also determined the absolute magnitudes of the four EW binary stars and distances for them using the relation connecting the rotational period with the absolute magnitude. The obtained data will be used for modeling kinematical and dynamical properties of the observed stars.

Acknowledgments

Shevchenko V. G. is grateful to the Samtskhe-Javakheti State University for the support allowing him to participate at the International Scientific Conference "Problems of modern astrophysics". This research was partly supported by the Ministry of Education and Science of Ukraine. The present work has used the data from the European Space Agency (ESA) mission Gaia (http://www.cosmos.esa.int/gaia) processed by the Gaia Data Processing and Analysis Consortium (DPAC, http://www.cosmos.esa.int/web/gaia/dpac/consortium). Funding for the DPAC has been provided by national institutions, in particular the institutions participating in the Gaia Multilateral Agreement.

References

Collinge, M. J., Sumi, T., Fabrycky, D. 2006, Astrophys. J., 651, 197.
Fernie, J. D. 1992, Astron. J. 103, 1647.
Green, G. M., Schlafly, E. F., Finkbeiner, D. P., et al. 2015, Astrophys. J., 810,
25. Krugly, Yu. N., Belskaya, I. N., Shevchenko, V. G., et al. 2002, Icarus, 158,
294. Landolt, A. U. 1992, Astron. J., 104, 340.
Laney, C. D., Joner, M., Schvendiman, L. 2002, ASP Conference series 259, 112.
Laney, C. D., Joner, M., Rodriguez, E. 2003, ASP Conference series 292, 203.
Lenz, T., Pamyatnykh, A. A., Breger, M., Antoci V. 2008, Astron. Astrophys., 478,
855. Lindegren, L., Lammers, U., Bastian, U., et al. 2008, Astron. Astrophys., 595, A4.
McNamara, D. H. 2000, ASP Conference series 210, 373.
McNamara, D. H., Madsen, J. B., Barnes, J., Ericksen, B. F. 2000, PASP, 112,
202. Miceli, A., Rest, A., Stubbs, C.W., et al. 2008, Astrophys. J., 678, 865.
Mottola, S., de Angelis, G., di Martino, M., et al. 1995, Icarus, 117, 62.
Rodríguez, E., López-González, M. J., López de Coca, P. 2002, ESA SP-485, 317.
Rucinski, S. M. 2006, Monthly Notices of the Royal Astronomical Society, 368, 1319.
Shevchenko, V. G., Belskaya, I. N., Slyusarev, I. G., et al. 2012, Icarus, 217, 202.
Shevchenko, V., Drobjazko, N., Slyusarev, I., et al. 2013, PZP, 13, No. 7.
Shevchenko, V. G., Belskaya, I. N., Muinonen, K., et al. 2016, Planet. Space Sci., 123, 101.
Skiff, B. A. 2007. VizieR on-line data catalog: II/ 277. Originally published in Lowell
Observatory. Zheleznyak, A. P., Shevchenko, V. G., Slyusarev, I., et al. 2015, PZP, 15, No.

Ca II INFRARED TRIPLET LINE PROFILES IN THE SOLAR SPECTRUM

R. Sartibzade, D.M. Kuli-Zade, Z.F. Aliyeva

Baku State University

ckulizade@mail.ru

Abstract

The profiles of Ca II infrared triplet lines are constructed in solar disk center spectrum. High dispersion and high spectral resolution digital spectral materials obtained by Delbouille and others were used with a double monochromator. The main spectrophotometric characteristics of profiles (equivalent widths, half-widths, quarter of width and central depths) were determined with a high accuracy. Theoretical relative intensities of lines are determined.

1.Introduction

Quasi-resonant Ca II infrared triplet lines $4^2P^0_{1/2,3/2} \rightarrow 3^2D_{3/2,5/2}$ are the strongest in the infrared spectral region of the Sun. However, their profiles have not been studied to date due to the fact that it was impossible to obtain high dispersion and high spectral resolution solar spectrum in the given spectrum region.

Only after using new spectral devices – high resolution double monochromators it was made possible to obtain a high-quality solar spectrum, which allows studying Fraunhofer line profiles in the infrared spectral region of the Sun.

The present work explores the profiles of Ca II infrared triplet lines occurring during the transition from odd term $4^2P_{1/2,3/2}$ to even term $3^2D_{3/2,5/2}$ [1]. Figure 1 shows the transitions corresponding to lines λ8542.089Å ($^2P_{3/2} \rightarrow ^2D_{5/2}$), λ8498.144 Å ($^2P_{3/2} \rightarrow ^2D_{3/2}$), λ8662.170 Å ($^2P_{1/2} \rightarrow ^2D_{3/2}$).

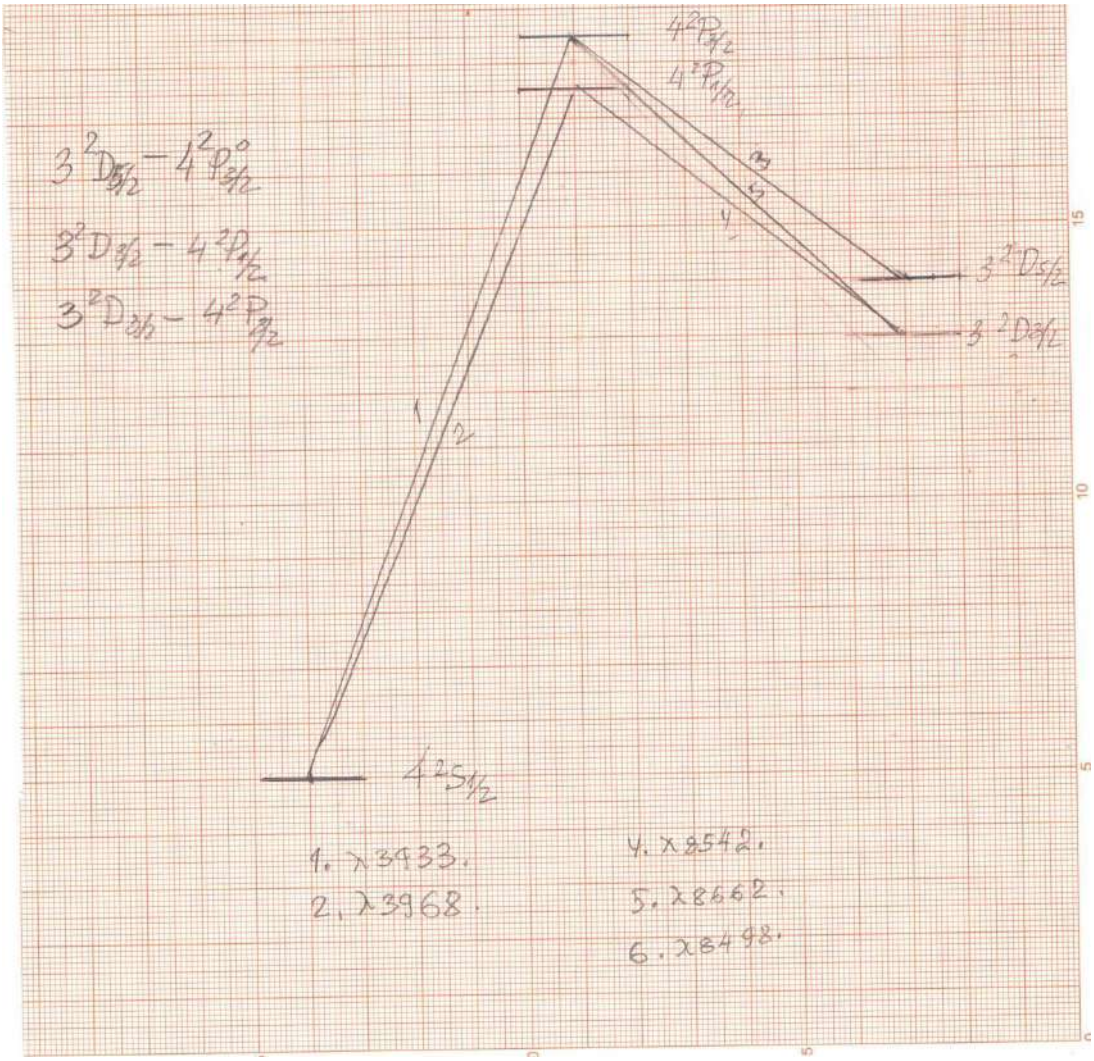

Figure 1. Ca II infrared triplet

2. Observed profile lines

Line profiles were constructed by high dispersion digital spectral materials [2]. Residual intensities in this material are given through 2 mÅ, which allows constructing the most reliable line profiles and determining their spectrophotometric characteristics with a high accuracy.

The method of constructing line profiles and determining spectrophotometric characteristics are described in [4]. The analysis of line profiles was performed according to [5, 6, 7].

Table 1

Observed line profile λ8498.062 Å

Δλ, Å	$R_v(\Delta\lambda)$	$R_r(\Delta\lambda)$	$R_{cp} = \frac{R_v + R_r}{2}$	$\Delta R = R_v - R_r$
0.00	0.722	0.722	0.722	0.00
05	713	714	713	-0,001
10	675	687	681	-0,012
15	604	650	627	-0,046
20	550	592	571	-0,042
25	507	508	507	-0,001
30	470	450	460	0,02
35	433	420	426	0,013
40	413	390	401	0,023
45	392	368	380	0,024
50	369	345	357	0,024
55	348	327	337	0,021
60	325	308	316	0,017
65	305	287	296	0,018
70	285	265	275	0,02
75	267	250	258	0,017
80	253	236	244	0,017
1.20	143	150	146	-0,007
60	097	087	092	0,01
2.00	084	067	075	0,017
40	048	050	049	-0,002
80	035	037	036	-0,002
3.20	027	030	028	-0,003
60	019	030	024	-0,011
4.00	018	028	023	-0,01
40	016	027	021	-0,011
80	012	026	019	-0,014
5.20	010	025	017	-0,015
60	009	022	015	-0,013
6.00	006	017	011	-0,011
7.00	002	010	006	-0,008
8.00	000	005	002	-0,005
9.00	000	000	000	0.000

Table 2

Observed line profile λ8542.144 Å

Δλ, Å	$R_v(\Delta\lambda)$	$R_r(\Delta\lambda)$	$R_{cp} = \frac{R_v + R_r}{2}$	$\Delta R = R_v - R_r$
0.00	0.812	0.812	0.812	0.000
20	670	695	682	-0.025
40	530	520	525	0.010
60	465	460	462	0.005
80	420	415	417	0.005
1.00	380	373	376	0.007
20	345	332	338	0.013
40	312	300	306	0.012
60	275	273	274	0.002
80	247	243	245	0.004
2.00	220	215	217	0.005
20	197	196	196	0.001
40	177	175	176	0.002
60	157	162	159	-0.005
80	142	148	145	-0.006
3.00	130	137	133	-0.007
20	120	125	122	-0.005
40	108	115	111	-0.007
60	102	105	103	-0.003
80	091	097	094	-0.006
4.00	082	089	085	-0.007
20	067	084	075	-0.017
40	056	077	066	-0.021
60	062	070	066	-0.008
80	057	063	060	-0.006
5.80	040	050	045	-0.010
6.80	030	032	031	-0.002
7.80	020	023	022	-0.003
8.80	010	010	010	0.000
9.80	005	004	005	0.001
10.60	000	000	000	0.000

The main characteristics of line profiles (equivalent widths W, half-widths $\Delta\lambda_{1/2}$, quarter-widths $\Delta\lambda_{1/4}$ and central depths R_o) given in Table 4 were determined using standard method of spectrophotometry.

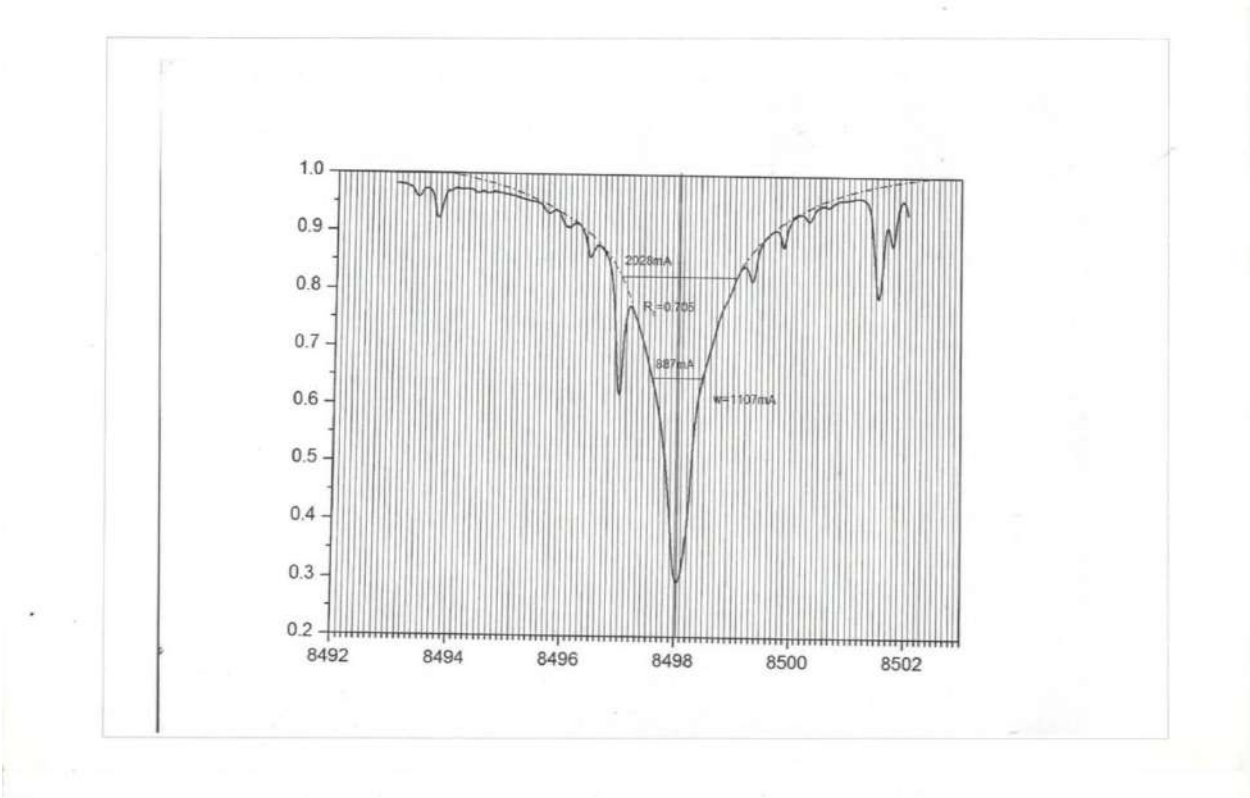

Line profile λ 8498.062Å

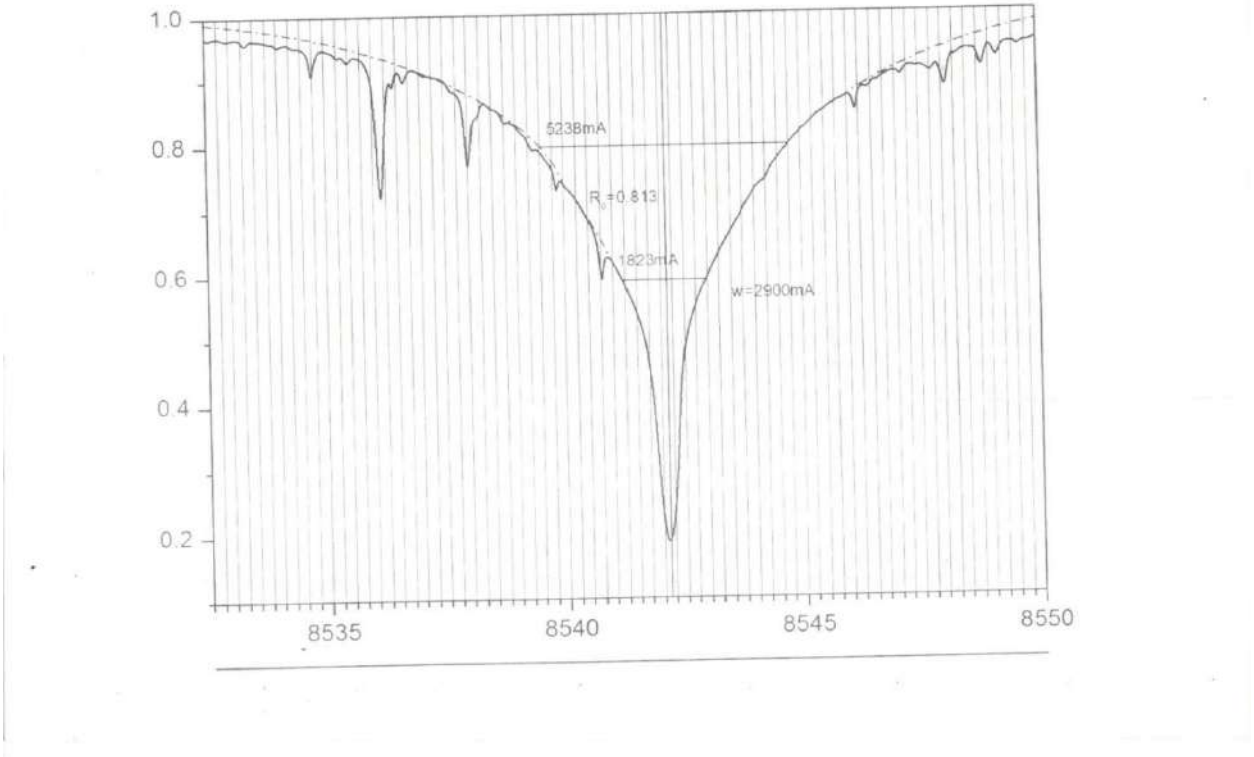

Line profile λ8542.144Å

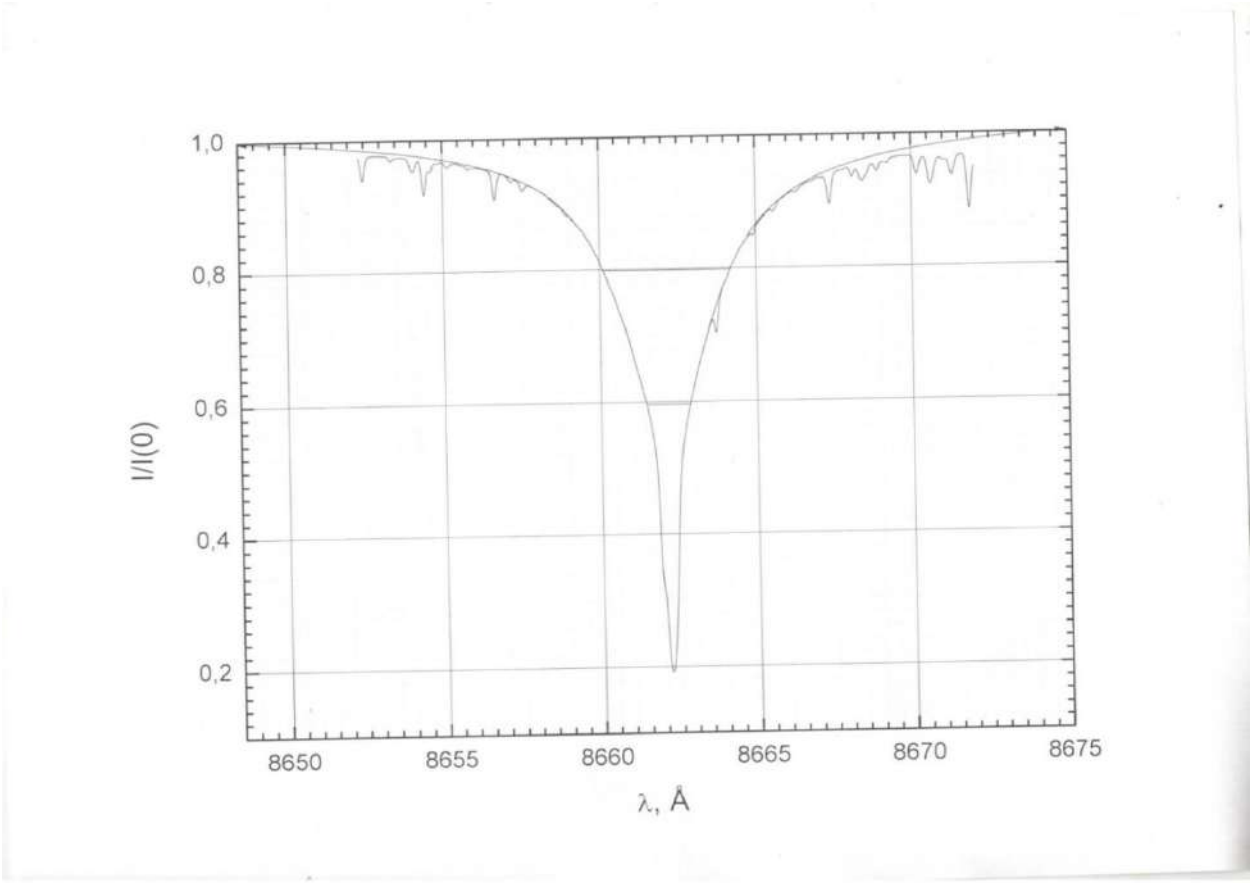

Line profile λ 8662.170

Table 4

The main spectrophotometric characteristics of Ca II infrared triplet lines in solar disk center spectrum

Values / Lines	ε, eV	W, Å	$\Delta\lambda_{1/2}$,Å	$\Delta\lambda_{1/4}$,Å	R_0
λ8498.062	1.69-3.14	1.26	0.99	2.07	0.726
λ8542.144	1.69-3.14	2.96	2.10	5.37	0.818
λ8662.170	1.69-3.14	2.52	1.72	4.24	0.812

3. Discussion

According to the photometric catalogue of Moore, Minnaert and Houtgast [2], equivalent width of line λ8542.144 Å makes 3.7 Å, which is twice as more as lines λ8498.062 Å and λ8662.170 Å.

According to our data, the equivalent width of line λ8542.144 Å is nearly 0.7 Å less than [3] requiring a separate study. The conformity is satisfactory for other two lines.

According to the sum rule for intensity ratios of Ca II infrared triplet lines, we obtain:

$$I(^2P_{3/2}\rightarrow{}^2D_{5/2}):I(^2P_{3/2}\rightarrow{}^2D_{3/2}):I(^2P_{1/2}\rightarrow{}^2D_{3/2})=9:1:5$$

Under the conditions of solar photosphere, this ratio is not justified because of self-absorption. Since self-absorption in strong lines is more, the alignment of intensities takes place.

Relative intensities of lines of this triplet can be determined according to quantum mechanical formulas:

$$I(^2P_{3/2}\rightarrow{}^2D_{5/2})=\frac{F(J+1)F(J)}{J+1}$$

$$I(^2P_{3/2}\rightarrow{}^2D_{3/2})=\frac{(2J+1)R(J)F(J)}{J(J+1)}$$

$$I(^2P_{1/2}\rightarrow{}^2D_{3/2})=\frac{P(J)P(J-1)}{J}$$

where

$$P(J)=\left[(J+L+1)(J+L)-S(S+1)\right]$$

$$F(J)=\left[S(S+1)-(J-L+1)(J-L)\right]$$

$$R(J)=\left[J(J+1)+L(L+1)-S(S+1)\right]$$

From these formulas we obtain:

$$I(^2P_{3/2}\rightarrow{}^2D_{5/2}):I(^2P_{3/2}\rightarrow{}^2D_{3/2}):I(^2P_{1/2}\rightarrow{}^2D_{3/2})=100:11.1:55.6=10:1.1:5.6$$

As it can be seen, quantum mechanical calculations are in good conformity with the results of Burger-Dorgelo sum rule.

REFERENCES

1. Moore C.E., A Multiplet Table of Astrophysical Interest, Nat. Berean of St., Washington, 1959, 206 p.
2. Moore C.E., Minnaert M.G.J., Houtgast, The Solar Spectrum 2935 Å to 8770 Å, Nat. Berean of St., Monograph 61, Washington, 1966, 249 p.
3. Delbouille L., Neven L., Roland G. Photometric Atlas of the solar spectrum from Å 3000 to 10 000Å; Lige, 1973, 241 p.
4. Kuli-Zade D.M. Fraunhofers of the solar spectrum, Baku, Elm, 2006, 346 p.
5. Kuli-Zade D.M. Herald of BSU, 2002, №2, pp.72-100.
6. Kostik R.I., Shukina N.G. Astron. journal, 2004, 79, №11, pp. 1027-1033.
7. Kuli-Zade D.M. Kinematics and physics of celestial bodies, 2009, №6, pp. 369-371.

Astronomy & Astrophysics (Caucasus) 3, (2018), pp.74-90

THE CONTRACTION OF THE REPRESENTATIONS OF THE GROUP $SO(4,1)$ AND COSMOLOGICAL INTERPRETATION

B.A. RAJABOV[1]

Abstract. We consider the operation of contraction of unitary irreducible representations of the de Sitter group $SO(4,1)$. It is shown that a direct sum of unitary irreducible representations of the Poincaré group with different signs of the rest mass is obtained as a result of contraction. The results obtained are used to interpret the phenomena of "dark matter" and "dark energy" in terms of the elementary quantum systems of de Sitter's world.

Keywords: de Sitter world, $SO(4,1)$ group, Wigner-Inönü limit, "dark matter", "dark energy", unitary irreducible representations, contraction, elementary systems.

AMS Subject Classification: 20-20C, 83-83C, 83-83F, 81-81G

1. Introduction

In this article, we will consider the application of the operation of contraction for representations of the group of movements of the de Sitter world. The operation of contraction was introduced in the paper of Wigner-Inönü for the Lie algebra of the relativistic Poincaré group, and the speed of light was used as the contraction parameter, [1]. As a result, a transition to the non-relativistic Galilean group was obtained. Subsequently, this operation was generalized to all Lie algebras, [2].

The contraction of the representations of the de Sitter group $SO(4,1)$ from the points of Lie algebra was considered in [3]-[4]. In the article [5], the contraction operation is extended to representations of the continuous basic series of groups $SO(p,1)$, and two types of contraction are considered: to representations of the non-homogeneous Lorentz group $ISO(3,1)$ and to the representations of the group of Euclidean motions $M(p)$. Drechsler considered contraction in a fiber bundle with Cartan connection, in particular, with the de Sitter group bundle, [6].

In [7], explicit expressions for the matrix elements of non-degenerate irreducible representations of the group $M(4)$ are found using the operation of contraction of the matrix elements of unitary irreducible representations of the continuous fundamental series of $SO(4,1)$ group.

The monograph [8] is devoted to multidimensional generalizations of contraction for classical and quantum groups.

[1] N.Tusi Shamakhi Astrophysics Observatory, National Academy of Sciences of Azerbaijan; e-mail: balaali.rajabov@mail.ru.

The papers [9]-[11] consider the quantum field theory in the de Sitter world. The monograph [12] presents the results of quantum field theory in curved space-time, in particular, in the world of De Sitter. The problems of dark matter and dark energy are reviewed [13]-[17].

The present paper is devoted to the contraction of unitary irreducible representations of the de Sitter group $SO(4,1)$. The scalar radius of curvature of space-time is chosen as the contraction parameter. Using the of Wigner-Inönü limit, a direct sum of unitary irreducible representations of the Poincaré group with different energy signs is obtained. Results obtained are used to interpret "dark matter" and "dark energy" using the elementary systems of de Sitter's world.

The main results of this work were reported in the 3rd international Scientific Conference "Modern Problems of Astrophysics-III", September 25-27, 2017, Georgia.

2. Background ... Spin is a purely quantum phenomenon

The Stern-Gerlach experiment proved the existence of an intrinsic orbital angular momentum and the magnetic moment of the electron, which assume discrete values (1922), [18].

The works of Goudsmit and Uhlenbeck showed that an attempt to explain the spin in the representations of classical physics leads to insuperable difficulties (appear speeds greater than the speed of light, 1925), [19]-[20].

V. Pauli proposed a non-relativistic Schrödinger equation for an electron with allowance for the spin variable (Pauli equation for a 2-component electron, 1927), [21].

P. Dirac developed the relativistic theory of the electron and introduced 4-component wave functions (Dirac equation, 1928), [22].

The main conclusion was that the electron spin is a purely quantum phenomenon. The peak of these theories was the connection of spin with statistics and the prediction of the positron.

Since then, in all reviews, monographs, and courses, this story is given to explain the quantum nature of spin...

3. Wigner's theory of elementary systems

A real understanding of the nature of the spin appeared after the classical work of E. Wigner on the representations of the inhomogeneous Lorentz group (that is, the Poincaré group, 1937), [23]. He established that projective representation of this group acts in the Hilbert space of states. Wigner introduced the concept of an elementary system and showed that such systems correspond to irreducible representations, that is, the space of these representations does not have invariant subspaces.

Most importantly. Wigner proved that the rest mass and the spin of an elementary particle (!) are:

- invariants that uniquely characterize irreducible representations of the Poincaré group;

- consequences of the space-time symmetries and are not consequences of the equations of dynamics.[1]

Invariants of the inhomogeneous Poincaré group (Casimir operators) are constructed using translation generators P_μ and 4-dimensional rotations $M_{\mu\nu}$ as follows:

$$m^2 = P^\mu P_\mu; \qquad w^2 = w^\mu w_\mu = m^2 s(s+1); \qquad w_\varrho = \frac{1}{2}\epsilon_{\lambda\mu\nu\varrho} P^\lambda M^{\mu\nu}, \qquad (1)$$

where

m – mass, s – spin of the particle, and w_ϱ is the Pauli-Lubansky-Bargmann vector.

Important! In the case $m^2 \geq 0$, there is a third invariant - the sign of energy:

$$\varepsilon = \frac{P_0}{|P_0|} = \pm 1$$

So, spin is a purely quantum phenomenon, but it is associated with groups of space-time movements ...[2]

4. Einstein's equations and de Sitter's solutions

According to Einstein's general relativity, the metric properties of space-time are determined by the distribution and motion of matter, [25]:

$$R_{\mu\nu} - \frac{1}{2} g_{\mu\nu} R^\lambda_\lambda + \Lambda g_{\mu\nu} = -\frac{8\pi G}{c^4} T_{\mu\nu}; \qquad (2)$$

where

$R_{\mu\nu}$ – Ricci tensor, $g_{\mu\nu}$ – metric tensor, Λ – cosmological constant, G – the gravitational constant of Newton, $T_{\mu\nu}$ – energy-momentum tensor and $\lambda, \mu, \nu = 0, 1, 2, 3..$

This equation can be rewritten in an equivalent form:

$$R_{\mu\nu} = \Lambda g_{\mu\nu} - \frac{8\pi G}{c^4}(T_{\mu\nu} - \frac{1}{2} g_{\mu\nu} T^\lambda_\lambda); \qquad (3)$$

It is clear from (2) that the Λ-term, even in the absence of matter ($T_{\mu\nu} = 0$), changes the space-time geometry and $g_{kl}\Lambda$ is the energy-momentum tensor of the vacuum.[3]

In the vacuum, the Einstein equations take the form:

$$R_{\mu\nu} = \Lambda g_{\mu\nu}. \qquad (4)$$

For $\Lambda = 0$, the solution of (3) is the Minkowski manifold with a group of Poincaré motions.

The histories of the cosmological constant are reviewed in [26]-[27].

---

[1] Thus, the justification of the spin by the Pauli and Dirac equations is of historical significance. Rephrasing Oscar Wilde, we can say that if Wigner's work had appeared earlier, the history of quantum electrodynamics would have evolved differently.

[2] In 1947, Wigner and Bargmann, on the basis of the theory of representations of the Poincaré group, classified the relativistic equations for spin particles, [24]. That is, first the spin, and then the equations ...

[3] The values of G and Λ are constantly refined with the accumulation of observations:
$G = 6,67545 \frac{sm^3}{g \cdot sec^2}$, (2013); $\Lambda \sim 10^{-53} m^{-2}$, (1998).

In the general case, the solutions of the Einstein (1)-(2) equations do not have a group of motions. But in 1917 Willem de Sitter found two solutions of (3) for $\Lambda \neq 0$ with different global groups of movements, [28]–[30]:

$$ds^2 = \frac{dr^2}{1 - r^2/R^2} + r^2(d\vartheta^2 + \sin^2\vartheta d\varphi^2) - \left(1 - \frac{r^2}{R^2}\right) c^2 dt^2, \qquad if\ \Lambda > 0; \tag{5}$$

$$ds^2 = \frac{dr^2}{1 + r^2/R^2} + r^2(d\vartheta^2 + \sin^2\vartheta d\varphi^2) - \left(1 + \frac{r^2}{R^2}\right) c^2 dt^2, \qquad if\ \Lambda < 0. \tag{6}$$

Here the radius of space R and the cosmological constant Λ are related by the following formula:[4]

$$\Lambda = \pm\frac{3}{R^2}$$

Using stereographic projections:

$$\xi_1 = r\cos\varphi; \quad \xi_2 = r\sin\vartheta\cos\varphi; \quad \xi_3 = r\sin\vartheta\sin\varphi;$$
$$\xi_4 = R\sqrt{1 - \frac{r^2}{R^2}}\cosh\left(\frac{ct}{R}\right); \quad \xi_0 = R\sqrt{1 - \frac{r^2}{R^2}}\sinh\left(\frac{ct}{R}\right)$$

and

$$\eta_1 = r\cos\varphi; \quad \eta_2 = r\sin\vartheta\cos\varphi; \quad \eta_3 = r\sin\vartheta\sin\varphi;$$
$$\eta_4 = R\sqrt{1 + \frac{r^2}{R^2}}\cosh\left(\frac{ct}{R}\right); \quad \eta_5 = R\sqrt{1 + \frac{r^2}{R^2}}\sinh\left(\frac{ct}{R}\right)$$

de Sitter solutions can be isometrically embedded as sub-manifolds in 5-dimensional pseudo-Euclidean spaces:

$$\xi_0^2 - \xi_1^2 - \xi_2^2 - \xi_3^2 - \xi_4^2 = -R^2 \tag{7}$$

and

$$\eta_1^2 + \eta_2^2 + \eta_3^2 - \eta_4^2 - \eta_5^2 = -R^2, \tag{8}$$

respectively.

These spaces have global symmetry groups $SO(4,1)$ and $SO(3,2)$ that leave the metrics (6)-(7) invariant. Groups $SO(4,1)$ and $SO(3,2)$ are called de Sitter groups. Spaces (4),(6) and (5),(7) are called de Sitter worlds of the 1st and 2nd kind or according to the modern terminology, de Sitter worlds dS and anti–de Sitter AdS.

We restrict ourselves to the de Sitter world (5),(7) and the $SO(4,1)$ group. The case of the anti-de Sitter world will be considered in a separate paper, because of the difficulties in interpreting the space-time measurements.

The commutation relations for the generators of the group $SO(4,1)$ have the form:

$$[M_{\mu\nu}, M_{\varrho\sigma}] = i\left(g_{\mu\varrho}M_{\nu\sigma} - g_{\mu\sigma}M_{\nu\varrho} - g_{\nu\varrho}M_{\mu\sigma} + g_{\nu\sigma}M_{\mu\varrho}\right);$$
$$[M_{\mu\nu}, P_\varrho] = i\left(g_{\mu\varrho}P_\nu - g_{\nu\varrho}P_\mu\right); \qquad [P_\mu, P_\nu] = \frac{i}{R^2}M_{\mu\nu};$$

where $P_\mu = (1/R)M_{4\mu}$.

[4]It is easy to see that for $\Lambda \to 0$, i.e. $R \to \infty$ both solutions (4)-(5) are transferred to the flat world of Minkowski.

The Casimir operators of the Lie algebra of the group $SO(4,1)$ have the following form, [31]:

$$C_1 = -\frac{1}{2R^2}M_{ab}M^{ab} = -P_\lambda P^\lambda - \frac{1}{2R^2}M_{\mu\nu}M^{\mu\nu} = M^2, \tag{9}$$

and

$$C_2 = -W_aW^a, \quad W_a = \frac{1}{8R}\varepsilon_{abcde}M^{bc}M^{de}. \tag{10}$$

Here, the lifting and lowering of the indexes are carried out using the 5-dimensional metric tensor (43).

To consider the result contraction $R \to \infty$, it is convenient to represent the operator C_2 in the following form:

$$C_2 = -V_\lambda V^\lambda - \frac{1}{R^2}W_4^2, \tag{11}$$

where

$$W_\lambda = -\frac{1}{2}\varepsilon_{\lambda\varrho\mu\nu 4}P^\varrho M^{\mu\nu}, \tag{12}$$

$$W_5 = \frac{1}{8}\varepsilon_{\lambda\mu\nu\varrho}M^{\lambda\mu}M^{\nu\varrho}. \tag{13}$$

From the last expressions, it is clear that when $R \to \infty$ the Lie algebra of the group $SO(4,1)$ becomes over to the Lie algebra of the Poincaré group, and the Casimir operators become:

$$C_1 \to -P_\lambda P^\lambda = m^2, \tag{14}$$

$$C_2 \to -V_\lambda V^\lambda = m^2 s(s+1). \tag{15}$$

where s, m – spin and rest mass, respectively.

From the limiting transition of the Casimir operators C_1, C_2 it follows that unlike the Minkowski world in the de Sitter world, elementary systems are identified not by mass and spin, but by some functions of spin and mass.

Important! It is obvious that any function of invariants is invariant. Therefore, as invariants characterizing unitary irreducible representations of the group $SO(4,1)$, any pair of functionally independent invariants can be chosen.

In particular, non-degenerate representations of the group $SO(4,1)$ can be realized in the space of $(2s+1)$-component vector-functions and the degree of homogeneity of σ on the upper field of the cone, [7, 32, 33]. Then the parameters s and σ will play the role of invariants characterizing the irreducible representations of the group $SO(4,1)$.

In addition, as will be shown in the next section, after the operation of contraction, the parameter s becomes into spin and the σ to the function of mass m.

5. The contraction of the representations of the group $SO(4,1)$

Representations of the group $SO(4,1)$ will be constructed in the space of measurable vector-valued functions $\Phi : SO(4,1) \longrightarrow C^{2s+1}$ that satisfies the following conditions:

$$\Phi_\lambda(gp) = \sum_{\lambda'=-s}^{s} \Delta^{(\sigma,s)}_{\lambda\lambda'}(p^{-1})\Phi_{\lambda'}(g), \qquad Re\,\sigma = -3/2; \tag{16}$$

$$\sum_{\lambda=-s}^{s} \int |\Phi_\lambda(p)|^2 \varrho(g) dg < \infty.$$

Here, $\rho(\cdot)$ is a continuous non-negative function on the group $SO(4,1)$ such that

$$\int \varrho(gp) d_l(p) = 1 \tag{17}$$

and $\operatorname{supp} \rho$ has a compact intersection with each class of the contiguity gP. Such a function exists for any locally compact group [34]. We introduce in this space a scalar product:

$$\left(\Phi^{(1)}, \Phi^{(2)}\right) = \sum_{\lambda=-s}^{s} \overline{\Phi_\lambda^{(1)}(g)} \Phi_\lambda^{(2)}(g) \varrho(g) dg. \tag{18}$$

The Hilbert space obtained in this way will be denoted by $\mathfrak{L}^2\left(SO(4,1); \Delta^{(\sigma,S)}\right)$ and consider the representation of the group $SO(4,1)$ acting in this space along formula:

$$T^{(\sigma,s)}(g)\Phi_\lambda(g_1) = \Phi_\lambda(g^{-1}g_1). \tag{19}$$

This is the induced representation in the Mackey sense of the group $SO(4,1)$, [35].

We now construct another realization of the space used for studying problems of contraction of representations. For this, we consider on the cone:

$$[k,k] = k_0^2 - k_1^2 + k_2^2 + k_3^2 + k_4^2 = 0, \quad k_0 > 0,$$

the new coordinate system:

$$\begin{aligned} k &= |k_4|\,(\zeta, \varepsilon), \\ \zeta_0 &= \cosh\beta, \\ \zeta_1 &= \sinh\beta \sin\vartheta \sin\varphi, \\ \zeta_2 &= \sinh\beta \sin\vartheta \cos\varphi, \\ \zeta_3 &= \cos\vartheta \sinh\beta; \end{aligned} \tag{20}$$

$$|k_4| \neq 0, \quad \varepsilon = \pm 1, \quad 0 \leq \beta < \infty, \quad 0 \leq \vartheta \leq \pi, \quad 0 \leq \varphi < 2\pi.$$

$$\zeta_0^2 - \zeta_1^2 - \zeta_2^2 - \zeta_3^2 = 1. \tag{21}$$

The set of points of the upper half of the cone that is not covered by this coordinate system forms a manifold of lower dimension. Since the upper half of the cone is a transitive surface, one can obtain parametrization of the elements of the group starting from this coordinate system.

First, we fix one of the points of the cone, namely, the point $\mathring{k}$:

$$|k_4| = 1, \quad \varepsilon = 1, \quad \beta = \vartheta = \varphi = 0. \tag{22}$$

Next we note that the stationary group $\mathfrak{W}$ of the point $\mathring{k}$ is isomorphic to the group motions $M(3)$ of 3-dimensional Euclidean space E_3. Each element $w \in \mathfrak{W}$ can be uniquely represented as:

$$w = R(\rho)B(\vec{z}), \tag{23}$$

where $\vec{z}$ is a 3-dimensional vector, and ρ is an orthogonal matrix 3×3. The matrices $R(\rho)$ and $B(z)$ have the following form:

$$R(\rho)=\begin{pmatrix}1 & \vec{0}^{\intercal} & 0\\ \vec{0} & \rho & \vec{0}\\ 0 & \vec{0}^{\intercal} & 1\end{pmatrix}, \quad R(\rho)\in SO(3)\subset SO(4,1), \tag{24}$$

$$B(\vec{z})=\begin{pmatrix}1+z^2/2 & \vec{z}^{\intercal} & -z^2/2\\ \vec{z} & I_3 & -\vec{z}\\ z^2/2 & \vec{z}^{\intercal} & 1-z^2/2\end{pmatrix}, \quad z^2=\vec{z}^{\,2} \tag{25}$$

The matrices $B(\vec{z})$ form an abelian subgroup that is normal division subgroup of the stationary subgroup $\mathfrak{W}$.

The transitivity property allows an almost element $g\in SO(4,1)$ to represent an expansion:

$$g=h_\varepsilon(k)w, \quad \varepsilon=\pm 1, \quad w\in\mathfrak{W}, \tag{26}$$

where $h_\varepsilon(k)$ is the so-called Wigner operator ("boost") having the property:

$$k=h_\varepsilon(k)\mathring{k}.$$

The Wigner operator is defined by the following formulas:

$$h_1(k)=g_{12}(\varphi)g_{23}(\vartheta)g_{03}(\beta)g_{04}(\tau), \qquad \tau=\ln|k_4|, \tag{27}$$

for the subset $\varepsilon=1$, and

$$h_{-1}(k)=g_{12}(\varphi)g_{23}(\vartheta)g_{03}(\beta)\eta g_{04}(\tau), \qquad \tau=\ln|k_4|, \tag{28}$$

for the subset $\varepsilon=-1$.

Here η is the diagonal 5×5 matrix: $\eta=\mathrm{diag}(1,-1,-1,-1,-1)$.

We now note that the action of $g\in SO(4,1)$ on a cone induces nonlinear transformation of this element on the sections $|k_4|=1$, which are the uppers of a two-sheeted hyperboloid.

It follows from (27)-(26) that the stationary subgroup of this variety is the minimal parabolic subgroup P, (61) and for almost all $g\in SO(4,1)$ the expansion is valid:

$$g=h_\varepsilon(\zeta)p, \tag{29}$$

where

$$h_\varepsilon(\zeta)=h_\varepsilon(k)|_{\tau=0}, \quad \varepsilon=\pm 1.$$

Let $\mathfrak{H}_i$, $i=1,2$ be the Hilbert spaces of vector functions on the hyperboloid (21) with the scalar product:

$$(F^{(1)},F^{(2)})=\int\overline{F^{(1)}(\zeta)}F^{(2)}(\zeta)d\mu(\zeta), \tag{30}$$

where

$$\begin{aligned} d\mu &= \frac{\left(d\vec{\zeta}\right)}{2\sqrt{1+\zeta^2}},\\ \left(d\vec{\zeta}\right) &= d\zeta_1 d\zeta_2 d\zeta_2, \end{aligned} \tag{31}$$

is the usual Lorentz-invariant measure on the field of a two-sheeted hyperboloid.

We define an isometric mapping:

$$\mathfrak{L}^2\left(SO(4,1);\Delta^{(\sigma,s)}\right)\longrightarrow\mathfrak{H}_1\oplus\mathfrak{H}_2$$

in the following way:

$$F_\lambda(\zeta;\varepsilon)=\Phi_\lambda(h_\varepsilon(\zeta)). \tag{32}$$

The inverse mapping is found with the help of (16) and (26):

$$\Phi_\lambda(g)=\sum_{\lambda'=-s}^{s}\Delta^{(\sigma,s)}_{\lambda\lambda'}(p^{-1})F_{\lambda'}(\zeta;\varepsilon). \tag{33}$$

These mapping properties are easily verified. It follows from (16), that under the mapping (32)-(33) the representation of the group $SO(4,1)$ in the space $\mathfrak{L}^2\left(SO(4,1);\Delta^{(\sigma,s)}\right)$ becomes a unitary representation of this group in $\mathfrak{H}_1\oplus\mathfrak{H}_2$:

$$T^{(\sigma,s)}(g)F_\lambda(\zeta;\varepsilon)=\sum_{\lambda'=-s}^{s}\Delta^{(\sigma,s)}_{\lambda\lambda'}(p_g^{-1})F_{\lambda'}(\zeta_g;\varepsilon_g), \tag{34}$$

where $\zeta_g,\varepsilon_g,p_g$ - are determined by the equation:

$$g^{-1}h_\varepsilon(\zeta)=h_{\varepsilon_g}(\zeta_g)p_g. \tag{35}$$

Thus, we have found the realization of the UIR's of the continuous main series of the group $SO(4,1)$ in the space $\mathfrak{H}_1\oplus\mathfrak{H}_2$.

Consider now the Wigner-Inönü limit at which the UIR's of the group $SO(4,1)$ goes into the UIR's of the group $ISO(3,1)$. For this, it is necessary to know the limit of the parameters of the group $SO(4,1)$, under which the de Sitter group passes to the Poincaré group $ISO(3,1)$.

Since the $SO(4,1)$ is a group of motions leaving an invariant quadratic form (7) It is clear that to find the required limit it is sufficient to consider only transformations in the planes $(\xi_0,\xi_j),\ j=1,2,3,4$. For example, consider the transformation:

$$\xi_0^{'}=\xi_0\cosh\alpha+\xi_4\sinh\alpha,\qquad \xi_4^{'}=\xi_0\sinh\alpha+\xi_4\cosh\alpha.$$

Since the de Sitter space (7) when $R\to\infty$ transforms to Minkowski space, we redefine parameter α, putting $\alpha=a_0/R$. Since

$$\xi_4=\sqrt{\xi_0^2-\xi_1^2-\xi_2^2-\xi_3^2+R^2}, \tag{36}$$

we obtain:

$$\begin{aligned}\xi_0' &= \xi_0\cosh\left(\frac{a_0}{R}\right)+\sqrt{\xi_0^2-\xi_1^2-\xi_2^2-\xi_3^2+R^2}\sinh\left(\frac{a_0}{R}\right)\xrightarrow{R\to\infty}\xi_0+a_0,\\ \xi_4' &\to \xi_4.\end{aligned}$$

Thus, we see that the transformations $g_{04}(\alpha)$, $g_{i4}(a_i)$, $i=1,2,3$ in the planes $(\xi_n,\,\xi_4)$, $n=0,1,2,3$ go to the translation group if we assume:

$$\alpha=a_0/R,\ \varphi_i=a_i/R,\ i=1,2,3\qquad\text{if}\quad R\to\infty.$$

Thus we have the statement: the transformations of the subgroup $SO(3,1)\subset SO(4,1)$, leaving the vertex of the one-sheeted hyperboloid $[k,k]=-R^2$ (i.e. the de Sitter world) transform into homogeneous Lorentz transformations of the Minkowski world, and the rotation $g_{n4}(\alpha_n)$ on the planes $(k_4,k_n),\ n=0,1,2,3$ translate into

translations along the corresponding axes of a Cartesian coordinate system on the quantities: $a_n = \alpha_n R$.

The result of contraction of the representation (34)-(35) of the group $SO(4,1)$ is formulated as a theorem:

Theorem 5.1. *The result of the contraction of the UIR's, $T^{(\sigma,s)}(g), g \in SO(4,1), \sigma = -3/2 + imR$, for $R \to \infty$ is the direct sum of UIR, $U^{(m,s;\varepsilon)}(g)$, $g \in ISO(3,1)$, with mass m, spin s and differing in energy sign ε.*

Proof. It is easy to see that the reduction of the representation (34)-(35) to the subgroup $SO(3,1) \subset SO(4,1)$ has the following form:

$$T^{(\sigma,s)}(L)F_\lambda(\zeta;\varepsilon) = \sum_{\lambda'=-s}^{s} t^s_{\lambda\lambda'} \left(R^{-1}_\varepsilon(\zeta)\right) F_{\lambda'}(L^{-1}\zeta_g;\varepsilon_g). \tag{37}$$

Here $R^{-1}_\varepsilon(g,\zeta)$ is the Wigner rotation:

$$R_\varepsilon(\zeta,L) = h^{-1}_\varepsilon \left(L^{-1}\zeta\right) L^{-1} h_\varepsilon(\zeta), \qquad L \in SO(3,1). \tag{38}$$

Since the parameter $\sigma = -3/2 + i\rho, \quad -\infty < \rho < +\infty$ is not included in the formula (37) explicitly, limit σ is not defined , if UIR of the group $SO(4,1)$ becomes to UIR of the group $ISO(3,1)$. In order to find this limit, we consider transformations in the planes $(k_4, k_n),\ n = 0,1,2,3$. For example, from (20) and (35) for the transformation $g_{04}(\alpha_0),\ \alpha_0 = a_0/R$:

$$\begin{aligned}
(\zeta_g)_n &= \frac{\zeta_n}{|\varepsilon\cosh\alpha_0 + \zeta_0 \sinh\alpha_0|}, \quad n = 1,2,3; \\
(\zeta_g)_0 &= \frac{\zeta_0\cosh\alpha_0 + \varepsilon\sinh\alpha_0}{|\varepsilon\cosh\alpha_0 + \zeta_0\sinh\alpha_0|}, \\
\varepsilon_g &= \frac{\varepsilon\cosh\alpha_0 - \zeta_0\sinh\alpha_0}{|\varepsilon\cosh\alpha_0 + \zeta_0\sinh\alpha_0|}, \quad \alpha_0 = \frac{a_0}{R}.
\end{aligned} \tag{39}$$

From this, in particular, it is clear that for sufficiently large R, (i.e. for sufficiently small α_0): $\varepsilon_g = \varepsilon$.

Thus (34) for $g = g_{04}\,(a_0/R)$ becomes:

$$T^{(\sigma,s)}(g_{04})F_\lambda(\zeta;\varepsilon) = \sum_{\lambda'=-s}^{s} \tau_g^\sigma t^s_{\lambda\lambda'} \left(R^{-1}_g\right) F_{\lambda'}(\zeta;\varepsilon). \tag{40}$$

Here, the element $p_g = D(\tau_g)R_g B(\vec{b}_g)$ is found from of the equation (35). In particular, for τ_g we have:

$$\tau_g = |\varepsilon\cosh\alpha_0 - \zeta_0\sinh\alpha_0| \tag{41}$$

On the other hand, it follows from (35) and (39) that for $R \to \infty$ we have:

$$\zeta_g \to \zeta, \qquad p_g \to I,$$

including $R_g \to I, \quad B(\vec{b}_g) \to I$, since $\alpha_0 \to 0$.

Then from (40)-(41) we get that the representation (40) goes into the translation representation $U^{(m,s;\varepsilon)}(a_0)$:

$$U^{(m,s;\varepsilon)}(a_0)\tilde{F}_\lambda(q;\varepsilon) = e^{iq_0a_0}\tilde{F}_\lambda(q;\varepsilon),$$

if we consider a one-parameter family of UIR's $g \in SO(4,1)$, $\sigma = -3/2 + imR$, where m is a constant and put:

$$\tilde{F}_\lambda(q;\varepsilon) = F_\lambda(\zeta;\varepsilon), \qquad q_0 = \varepsilon m \zeta_0.$$

Here we used the following limit:

$$|\varepsilon \cosh \alpha_0 - \zeta_0 \sinh \alpha_0|^{-3/2+imR} \xrightarrow{R\to\infty} e^{i\varepsilon m \zeta_0 a_0} = e^{iq_0 a_0}.$$

Similarly, limit transitions are considered for transformations on planes (k_4, k_n), $n = 1, 2, 3$.

□

This conclusion is the same as the result of [4], obtained using infinitesimal transformations. Moreover, it is proposed in [37] to construct an unitary representation of the de Sitter group $SO(4,1)$ on the direct sum of irreducible representation spaces of the Poincaré group.

6. Conclusion

So let's sum up ...

In the flat world of Minkowski, Wigner's elementary systems are determined by the rest mass, the spin and the sign of their energy can be identified with elementary particles. Considerations of the stability of physical systems force us to limit the spectrum of energy from below and to exclude negative energies.

In the de Sitter world, elementary Wigner systems are identified by spin and by a parameter, which is the flat limit of a function of spin and mass, with different energy signs. But unlike the Minkowski world, we can not exclude negative energies from consideration.

That is, elementary systems on a cosmological scale can be in states with positive and negative energies. Elementary systems in a state with positive energy behave like a gravitating mass, and in a negative energy state as an anti-gravity mass.

Thus, we arrive at the following conclusions:

(1) Mysterious "dark matter" and "dark energy" consist of such elementary systems.
(2) "Dark matter" and "dark energy" are the first manifestations of quantum properties on the scale of the universe. Until now, quantum phenomena have been encountered in the micro-world, and also as macroscopic quantum effects in the theory of condensed matter.
(3) "Dark matter" and "dark energy" are carriers of information about the first moments of the universe after the Big Bang.

The last conclusion follows from the fact that according to the standard cosmological model, the de Sitter world is a necessary phase of the evolution of the universe in the first instants ($10^{-34} - 10^{-32}$ seconds) after the Big Bang.

Of course, our universe is not de Sitter's world, although according to some data it is developing in the direction of this model. Considering the given phenomena of dark matter and dark energy in the general case is a difficult task because today there is no quantum theory of gravity. The solution of this problem in general

for the gravitational field requires not only new physical concepts but also new mathematics.

The main results are in the arXiv.org, [38].

Appendix: Parametrization of elements of the group $SO(4,1)$

The group $SO(4,1)$ is a connected component of the unit group of motions 5-dimensional pseudo-Euclidean space that leaves invariant quadratic form, [31]:

$$[k,k] = k_0^2 - k_1^2 - k_2^2 - k_3^2 - k_4^2.$$

It is a 10-parametric, as well as the Poincaré group, which describes symmetry of Minkowski space.

Elements of $g \in SO(4,1)$ are represented by 5×5 by matrices that linear transformation in the space of points $k = (k_0, k_1, k_2, k_3, k_4)$. It follows from the definition that they satisfy the following relations:

$$g^{\intercal}\eta g = \eta, \quad \det g = 1, \quad g_{00} \geqslant 1, \tag{42}$$

where the symbol $\intercal$ denotes transposition and η is the diagonal 5×5 matrix:

$$\eta = \mathrm{diag}(1, -1, -1, -1, -1). \tag{43}$$

The matrix elements will be indexed:

$$\begin{aligned} a, b, c &= 0, 1, 2, 3, 4; \\ i, j, k &= 0, 1, 2, 3; \\ \alpha, \beta, \gamma &= 1, 2, 3. \end{aligned}$$

In the latter case, vector notation will also be used:

$$\vec{a} = \{a^\alpha : \ \alpha = 1, 2, 3\}.$$

Elements of the Lie algebra $SO(4,1)$ of the de Sitter group Γ_{ab} are five-row matrices with elements of the form:

$$(\Gamma_{ab})^c_d = \delta^c_a \eta_{bd} - \delta^c_b \eta_{ad}$$

and satisfy the commutation relations:

$$[\Gamma_{ab}, \Gamma_{cd}] = \eta_{ac}\Gamma_{bd} - \eta_{bc}\Gamma_{ad} - \eta_{ad}\Gamma_{bc} + \eta_{bd}\Gamma_{ac}$$

Here δ^b_a is the Kronecker symbol:

$$\delta^b_a = \begin{cases} 1, & \text{if} \quad a = b; \\ 0, & \text{if} \quad a \neq b. \end{cases}$$

Since the transformations $g \in SO(4,1)$ preserve the form $[k,k] = k_0^2 - k_1^2 - k_2^2 - k_3^2 - k_4^2$, then the surfaces are:

$$k_0^2 - k_1^2 - k_2^2 - k_3^3 - k_4^2 = const$$

transform into themselves under transformations from the de Sitter group.

There are three types of such surfaces, namely the upper (or lower) floor of the two-cavity hyperboloid $[k,k] = c > 0$, the one-sheeted hyperboloid $[k,k] = c < 0$, and finally the upper (or lower) floor of the cone $[k,k] = 0$ without a vertex, since the point $k_0 = k_1 = k_2 = k_3 = k_4 = 0$ itself forms a homogeneous space.

The action of the group on each of these surfaces is transitive. As is known, transitivity surfaces are characterized by their stationary subgroup, i.e. closed subgroup leaving the selected point fixed. Used on the different coordinate systems given on these surfaces, one can obtain different parameterizations of the elements of the group.

We will consider a spherical coordinate system on a cone $[k,k]=0,\ k_0>0$:

$$k=\omega(1,\upsilon),$$

where υ is the point of a 3-dimensional unit sphere:

$$\upsilon^2=\upsilon_1^2+\upsilon_2^2+\upsilon_3^2+\upsilon_4^2=1, \tag{44}$$

$$\upsilon=(\sin\chi\sin\vartheta\sin\varphi,\sin\chi\sin\vartheta\cos\varphi,\sin\chi\cos\vartheta,\cos\chi),$$

where $0<\omega<\infty,\quad 0\le\chi\le\pi,\quad \underset{0}{0}\le\vartheta\le\pi,\quad 0\le\varphi<2\pi.$

Coordinates of the selected point $\overset{\circ}{k}=(1,0,0,0,1):\qquad \omega=1,\ \chi=\vartheta=\varphi=0.$

Wigner's operator:

$$h(k)=g_{12}(\varphi)g_{23}(\vartheta)g_{34}(\chi)g_{04}(\beta),\quad \beta=\ln\omega \tag{45}$$

The stationary group W of the point $\overset{\circ}{k}$ is isomorphic to the group motions of $M(3)$, 3-dimensional Euclidean space E_3. Each element $w\in\mathfrak{W}$ can be uniquely represented as:

$$w=R(\rho)B(\vec{z}), \tag{46}$$

where $\vec{z}$ is a 3-dimensional vector, and ρ is an orthogonal matrix 3×3 :

$$\rho^{\intercal}\rho=I.$$

The matrices $R(\rho)$ and $B(\vec{z})$ have the following forms:

$$R(\rho)=\begin{pmatrix}1&\vec{0}^{\intercal}&0\\ \vec{0}&\rho&\vec{0}\\ 0&\vec{0}^{\intercal}&1\end{pmatrix},\quad R(\rho)\in SO(3)\subset SO(4,1), \tag{47}$$

$$B(\vec{z})=\begin{pmatrix}1+z^2/2&\vec{z}^{\intercal}&-z^2/2\\ \vec{z}&I_3&-\vec{z}\\ z^2/2&\vec{z}^{\intercal}&1-z^2/2\end{pmatrix},\quad z^2=\vec{z}^{\,2}. \tag{48}$$

The matrices $B(\vec{z})$ form an abelian subgroup that is the normal subgroup of the stationary subgroup $\mathfrak{W}$.

For $g\in SO(4,1)$ we have:

$$g=h(k)w. \tag{49}$$

Hence, using the formulas (45)-(46), we obtain the Iwasawa expansion for the elements of the group $SO(4,1)$:

$$g=ug_{04}(\beta)B(\vec{z}),\quad u\in SO(4). \tag{50}$$

In doing so, we used the commutativity of the transformations $g_{04}(\beta)$ and $R(\rho)$, and the fact that the group is locally $SO(4)\simeq SO(3)\otimes SO(3)$.

Here it is necessary to make two comments:

(1) The action of the group $SO(4,1)$ on the cone induces a nonlinear mapping section of the cone $\omega = 1$, i.e. 3-dimensional unit sphere (44) to itself. It is easy to verify that this mapping is a homeomorphism. Thus, the 3-sphere is a homogeneous space, where the group $SO(4,1)$ acts nonlinearly. For this space Wigner operator $h(\upsilon)$ can be defined as follows:

$$h(\upsilon) = h(k)|_{\omega=1}. \tag{51}$$

(2) The mappings (45) and (51) are Borel. Moreover, they are differentiable almost everywhere.

On the cone $[k,k] = 0,\ k_0 > 0$ we can introduce one more coordinate system:

$$\begin{aligned} k_0 &= \tau\frac{1+a^2}{2}, \\ \vec{k} &= \tau\vec{a}, \\ k_4 &= \tau\frac{1-a^2}{2}, \end{aligned} \tag{52}$$

where $a = \vec{a}^2, \quad \tau > 0$.

Since $k_0 + k_4 > 0$, this coordinate system does not cover the whole cone, namely, outside the coordinate system there remains the intersection of the cone by a hyperplane $k_0 + k_4 = 0$, which forms a set of smaller dimension. It is obvious that the corresponding parametrization of the group will also not be global. The set of points $k_0 + k_4 > 0$ together with the map (52) draws a map on the cone, which we denote by through $\mathbb{C}_1$.

The coordinates of the fixed point $\overset{\circ}{k} = (1/2, \vec{0}, 1/2)$: $\tau = 1,\ \vec{a} = \vec{0}$.

Wigner operator:

$$h(k) = A(\vec{a})D(\tau), \tag{53}$$

where

$$D(\tau) = g_{04}(\alpha) = \begin{pmatrix} \cosh\alpha & \vec{0}^{\intercal} & \sinh\alpha \\ \vec{0} & I_3 & \vec{0} \\ \sinh\alpha & \vec{0}^{\intercal} & \cosh\alpha \end{pmatrix}, \qquad \tau = e^{\alpha} \tag{54}$$

$$A(\vec{a}) = \begin{pmatrix} 1 + a^2/2 & \vec{a}^{\intercal} & a^2/2 \\ \vec{a} & I_3 & \vec{a} \\ -a^2/2 & -\vec{a}^{\intercal} & 1 - a^2/2 \end{pmatrix} \tag{55}$$

The matrices $A(\vec{a}\,)$, as well as the matrices $B(\vec{z}\,)$ from (48) form a 3-parameter abelian subgroup. Since, stationary subgroup is the group $\mathfrak{W}$ described in the previous subsection from (46) and (48) we get the expansion, which is valid *almost for all* $g \in SO(4,1)$:

$$g = A(\vec{a}\,)D(\tau)R(r)B(\vec{b}\,) \tag{56}$$

In order to obtain a parametrization for any element of the group, it is necessary to have an atlas on the cone without vertex.

The next map of $\mathbb{C}_2$, consisting of the region $k_0 - k_4 > 0$ and mapping:

$$\begin{aligned} k_0 &= \lambda\frac{1+x^2}{2}, \\ \vec{k} &= \lambda\vec{x}, \\ k_4 &= -\lambda\frac{1-x^2}{2}; \\ x^2 &= \vec{x}^2, \quad \lambda > 0. \end{aligned} \tag{57}$$

complements the map $\mathbb{C}_1$ to the atlas.

Now we see that outside the coordinate system $\mathbb{C}_2$ remains the intersection of the cone with the hyperplane $k_0 - k_4 = 0$, and that the maps $\mathbb{C}_1$ and $\mathbb{C}_2$ make an atlas on the cone. The transition functions from one card to another are as follows:

$$\begin{aligned} \tau &= \lambda x^2; \qquad \lambda = \tau a^2, \\ \vec{a} &= \vec{x}/x^2; \qquad \vec{x} = \vec{a}/a^2. \end{aligned} \tag{58}$$

The formulas (58) show that we have established a smooth structure on the cone.

Now we need to construct the Wigner operator corresponding to the map (57). From (42)-(43) it follows that the matrix $\eta \in SO(4,1)$, so you can enter the following boost:

$$h_2(\vec{k}) = B(\vec{x})\eta D(\lambda). \tag{59}$$

Thus, we obtain the following parametrization of $SO(4.1)$:

$$g = B(\vec{x})\eta D(\lambda)R(r)B(\vec{y}). \tag{60}$$

It follows from the corresponding statements for the cone that the parameterizations (56) and (60) cover the entire group space. We also get that the expansion (56) is valid for all $g \in SO(4,1)$, except for the elements $\{g \in SO(4,1) : \vec{x} = 0\}$, and (60) is valid for all $g \in SO(4,1)$, except for elements $\{g \in SO(4,1) : \vec{a} = 0\}$.

Here it is necessary to make a few remarks:

(1) The elements $\vec{a} = 0$, i.e. elements of the form

$$p = D(\tau)R(r)B(\vec{b}) \tag{61}$$

constitute a subgroup, namely, a minimal parabolic subgroup P. This subgroup plays an important role in the construction of induced representations [36].

Accordingly, the expansions (56) and (60) can now be rewritten as:

$$g = A(\vec{a})p_1, \qquad p_1 = D(\tau)R(r)B(\vec{b}); \tag{62}$$

$$g = B(\vec{x})\eta p_2; \qquad p_2 = D(\lambda)R(r)B(\vec{y}). \tag{63}$$

(2) Below are the formulas for the transition between these parameterizations:

$$\begin{aligned} p_1 &= D(x^2)R\left(\pi; \overset{\circ}{\vec{x}}\right) B\left(-\frac{\vec{x}}{x^2}\right) p_2; \qquad \vec{a} = \vec{x}/x^2, \\ p_2 &= D(a^2)R\left(\pi; \overset{\circ}{\vec{a}}\right) B\left(\frac{\vec{a}}{a^2}\right) p_1; \qquad \vec{x} = \vec{a}/a^2. \end{aligned} \tag{64}$$

Here, we denote by $R(\pi;\cdot)$ the rotation by an angle π around the vectors $\overset{\circ}{\vec{x}} = \vec{x}/x$ and $\overset{\circ}{\vec{a}} = \vec{a}/a$, respectively.

It is easy to see that P is a stationary subgroup the north pole of the 3-sphere. Therefore:

$$S^3 \simeq SO(4,1)/\mathsf{P}.$$

(3) Maps $\mathbb{C}_i$, $i = 1,2$ induce on a submanifold $\omega = 1$ cone, i.e. on the 3-dimensional unit sphere, the local maps $\mathbb{V}_i$, $i = 1,2$, respectively. The map $\mathbb{V}_1$ (respectively, $\mathbb{V}_2$) consists of points of a sphere with a punctured southern (respectively, northern) pole and coordinate systems:

$$\upsilon_\alpha = \frac{2a_\alpha}{1+a^2}, \qquad \upsilon_4 = \frac{1-a^2}{1+a^2}; \tag{65}$$

respectively,

$$\upsilon_\alpha = \frac{2x_\alpha}{1+x^2}, \qquad \upsilon_4 = -\frac{1-x^2}{1+x^2}. \tag{66}$$

As can be seen, these coordinates coincide with the stereographic projection 3-dimensional sphere from its poles to E_3.

(4) The Wigner operators $h_i(\upsilon)$, $i = 1,2$ corresponding to the maps $\mathbb{V}_i$, will be defined as follows:

$$h_1(\upsilon) = A(\vec{a}), \qquad h_2(\upsilon) = B(\vec{x})\eta. \tag{67}$$

(5) The mappings (53), (59) and (67) are infinitely differentiable.

In conclusion this section, we give some information about invariant measures on the group $SO(4,1)$ and its minimally parabolic subgroup. The de Sitter group, like any connected semisimple group, unimodular, i.e. on it there exists a two-sided invariant measure Haar dg. Below are the expressions for dg in different parameterizations (the numbers in parentheses on the left indicate the numbers of the corresponding parameterizations):

$$\begin{aligned} &(50): && e^{3\beta} du d\beta (d\vec{z}),\\ &(62): && \tau^2 d\tau (d\vec{a}) dr (d\vec{b}),\\ &(63): && \lambda^2 d\lambda (d\vec{x}) dr (d\vec{y}), \end{aligned} \tag{68}$$

where

du is an invariant normalized measure on $SO(4)$,

dr is an invariant normed measure on $SO(3)$;

$(d\vec{a})$, $(d\vec{b})$, $(d\vec{x})$, $(d\vec{y})$ - volume elements in 3-dimensional Euclidean space.

The subgroup P, in contrast to the group $SO(4,1)$, is not unimodular. Below are the expressions for the right-invariant measures $d_r(p)$, the left-invariant measure $d_l(p)$, and also the module $\delta(p)$:

$$\begin{aligned} \delta(p) &= \tau^3,\\ d_l(p) &= \frac{1}{\tau} d\tau dr \left(d\vec{b}\right),\\ d_r(p) &= \tau^2 d\tau dr \left(d\vec{b}\right) = \delta(p) d_l(p). \end{aligned} \tag{69}$$

Finally, from the comparison (68) with (69) we get:

$$\begin{aligned} dg &= dh_i d_r(p), \qquad i = 1, 2; \\ dh_1 &= (d\vec{a}), \\ dh_2 &= (d\vec{x}). \end{aligned} \tag{70}$$

References

[1] Wigner-Inönü, Proc. Nat. Acad. Sci.(USA), **39**, 510, 1953; **40**, 119 (1954).
[2] A.O. Barut, R. Raczka, (1977), Theory of Group Representations and Applications, Warsaw.
[3] Ström S., Arkiv für Fysik, **40**, 1, 1961.
[4] Ström S., Arkiv für Fysik, **30**, 5, 1965.
[5] Michelsson J., Niederle J., Commun.Math.Phys., **27**, 3, 1972.
[6] Drechsler W. Group contraction in a fiber bundle with Cartan connection - J.Math.Phys., 1977, v.18, No.7, p.1358-1366.
[7] B.A. Rajabov, Trans. Nat. Acad. Sci., Azerbaijan, series of phys.-math. sciences, No.**6**, (1983), pp.58-63; (in Russian).
[8] N.A. Gromov, Contractions of the classical and quantum groups, Fizmatlit, Moscow, 2012 (in Russian)
[9] Nachtmann G., Commun.Math.Phys., **6**, 1, 1967.
[10] Nachtmann G., Zeit. für Physik, **208**, 113-115, 1968.
[11] Börner O., Dürr V., Nuovo Cimento, **64A**, 669, 1969.
[12] N.D. Birrell, P.C.W. Davies, Quantum Fields in Curved Space, Cambridge University Press, 1982
[13] V.A. Ryabov, V.A. Tsarev, A.M. Tskhovrebov, The search for dark matter particles, Uspekhi Fizicheskikh Nauk 178 (11) 1129 – 1163 (2008) (in Russian)
[14] Martín López-Corredoira, Tests and problems of the standard model in Cosmology, arXiv:1701.08720v1 [astro-ph.CO], 2017, p.64
[15] The XENON1T Dark Matter Experiment, arXiv:1708.0751v1 [astro-ph.IM], 2017, P.22
[16] Dark Energy Survey Year 1 Results, arXiv: 1708.01530v1 [astro-ph.CO], 2017, p.31
[17] New Ideas in Dark Matter 2017, arXiv: 1707.0459v1 [hep-oh], 2017, p.113
[18] Gerlach W., Stern O. Der experimentelle Nachweis der Richtungsquantelung im Magnetfeld. Zeitschrift fr Physik, 9:349352 (1922).
[19] G. E. Uhlenbeck, S. Goudsmit. Spinning Electrons and the Structure of Spectra, Nature,–1926, v.117, p.264–265.
[20] Thomas L. H. The motion of the spinning electron, Nature.–1926, v.117, p.514.
[21] Schiff, L.I.(1968), Quantum Mechanics, 3rd edition, McGraw-Hill, New York.
[22] J.D. Bjorken and S.D. Drell, Relativistic Quantum Mechanics, Mc Graw – Hill Book Company, 1964, 312 p.
[23] E. Wigner, On unitary representations of the inhomogeneous Lorentz group, Nuclear Physics B(Proc.Suppl.), 6, (1989), 9-64; Ann. Math., **40**, 149 (1939)
[24] V. Bargmann, E.P. Wigner, Group theoretical discussion of relativistic wave equations, Proc.Nat.Acad.Sci.(USA), **34**(5), (1948), 211-223.
[25] A. Einstein, Collected works, vol. 1-2, Nauka, Moscow, 1965-1966 (in Russian)
[26] N. Straumann, The history of the cosmological constant problem, arXiv:gr-qc/0208027v1, (2002), p.12
[27] C. O'Raifeartaigh, M. O'Keeffe, W. Nahm and S. Mitton, One Hundred Years of the Cosmological Constant: from "Superfluous Stunt" to Dark Energy, arXiv:1711.06890 [physics.hist-ph], (2017), p.62
[28] S. Weinberg, Gravitation and Cosmology, John Wiley and Sons, Inc., New York–London–Sydney–Toronto, 1972
[29] Møller C., The theory of relativity, 2nd ed., Clarendon Press, Oxford, 1972

[30] R.C. Tolman, Relativity, Thermodynamics and Cosmology, Clarendon Press, Oxford, 1969
[31] F.Gürsey, Introduction to Group Theory, in "Relativity, Groups and Topology", eds. C. DeWitt, B. DeWitt, New York-London, 1964.
[32] Rajabov B.A. Non-degenerate representations of the group de Sitter $SO(4,1)$ and the contraction of their matrix elements - Preprint **1**, Institute of Physics of Azerbaijan National Academy of Sciences, Baku, (1979), p.20, (in Russian)
[33] Rajabov B.A. Wigner coefficients of non-degenerate representations of the group de Sitter - Preprint **5**, Institute of Physics of Azerbaijan National Academy of Sciences, Baku, (1979), p.9, (in Russian)
[34] Kirillov A.A. Elements of the theory of representations, 2nd ed., Nauka, Moskow, 1978, p.344, (in Russian)
[35] Mackey G.W., On Induced Representations of Groups, American Journal of Mathematics, **73**, 3, (1951), pp. 576-592
[36] M.B. Mensky, The method of induced representations: space-time and particle's concept, Nauka, Moscow, 1976, p.288, (in Russian)
[37] P.Moylan, Unitary representations of the $(4+1)$-de Sitter group on irreducible representation spaces of the Poincaré group, J. Math. Phys., **24**, No.12, 2706-2721, 1983.
[38] Rajabov B.A., The contraction of the representations of the group $SO(4,1)$ and cosmological interpretation, arXiv:1801.10004, (2018), p.12

Astronomy & Astrophysics (Caucasus) 3, (2018)

INVESTIGATION OF THE ATMOSPHERE OF THE STAR HD164136 (F2II)

Z. A. SAMADOV [1,2], U. R. GADIROVA [1]

[1] ANAS, Shamakhy Astrophysical Observatory Named after N. Tusi
AZ5626, Shamakhi d., Y. Mammadaliyev sett.
E-mail: zahir.01@mail.ru

[2] Baku State University
E-mail: ulkergadirova@gmail.com

Abstract

The HD164136 (F2II) star was investigated on the basis of the atmospheric models of Kuruch and the spectra derived from the 2m telescope of the ShAO. The following prices have been obtained for the effective temperature and surface gravity of the star: $Teff = 6670 \pm 200K$, $logg = 2.45 \pm 0.2$. The velocity of microturbulent motion was studied based on the FeII lines. The velocity of the microturbulent motion was calculated as 3.5 km/sek. According to FeII spectral lines, the iron abundance in the atmosphere of the star has been determined and compared with the same amount in the Sun.

Keywords: Fundamental parameters, the velocity of microturbulent motion, chemical composition.

Introduction

According to the modern evolution theory of the stars, the process of mixing a deep substance was observed in supergiant and giant stars of A, F, G spectral classes. As a result, CNO-circulating nuclear reaction products should be brought into the atmosphere and should cause a change in the amount of C, N and O in the atmosphere. Indeed, in the atmosphere of A, F, G spectral classes, it was found that C is less, N is more and O is slightly less (Boyarchuk A.A.et.al.,1981; Boyarchuk A.A.et.al.,1983; Lyubimkov L.S. et al., 2009)

It has also been found that excess Na is observed in addition to the amount of deviations in C, N, and O in the atmosphere of supergiant and giant stars of A, F, G spectral classes. (Boyarchuk A.A. et al., 1983). The opinion suggests that excess Na is a consequence of the transformation of Ne into Na in NeNa-cyclic reactions. Na is removed into the atmosphere in the deep ingredients mixing process. Thus, the study of the atmosphere of supergiant and giant stars of A, F, G spectral classes is important from the point of view of the evolution of stars. It has also been discovered that excess Na was observed in addition to the amount of deviations in C, N, and O in the atmosphere of supergiant and giant stars of A, F, G spectral classes.

In this study, the fundamental parameters of ν Her = HD164136 = HR6707 star - the effective temperature, surface gravity and the iron abundance in the atmosphere were determined. In our subsequent studies, we plan to determine the chemical composition of the star, in particular, the amount of elements C, N, Na.

OBTAINING AND USING OBSERVATION MATERIALS

$vHer = HD164136 = HR6707$ star's spectral class is F2 II, visual magnituda is $m_V = 4^m$, 48, absolute magnituda is $M_V = -0^m, 7$. The galactic width of the star *is* $b = 24^\circ$, the galactic length is $\ell = 56^\circ$ (Rufener F., 1976).

The spectrum of the star was obtained by means of a modern CCD receiver, which was installed in the Cassegrain focus of the 2 m telescope of the Shamakhi Astrophysical Observatory. Observation materials cover the spectral area of $\lambda\lambda 4500 - 6800$ Å. Four spectra of stars were obtained overnight in this region. Spectrum was centered in the night because there was no strong variability in the spectrum of the star. The observed lines in the spectrum were made identical and their intensities ($W\lambda$) were calculated. The spectrum research was carried out through the DECH-20 program packages, provided by (Galazitdinov A.G.,1992).

DETERMINATION OF EFFECTIVE TEMPERATURE AND SURFACE GRAVITY

It is known that in order to analyze the chemical composition of the stars, it is necessary to know their two fundamental parameters: the effective temperature (T_{eff}) and surface gravity (g) in the star atmosphere. T_{eff} and logg parameters are necessary to calculate atmospheric models and based on these models, the chemical composition of the star is being determined. Also, by knowing T_{eff} and logg, we can evaluate other parameters of the stars, like their mass M, radius R, brightness L and age t. Effective temperature and surface gravity were determined by using the following criteria:

1. Comparison of the observation and theoretically calculated values of $[c1]$ index. $[c1]$ index in four-color, narrow lane uv by photometric system is determined with $[c1] = c1 - 0.2(b - y)$ formula. This quantity is independent from the influence of absorption in interstellar medium. Therefore, it is reasonable to use this quantity for the determination of interstar fundamental parameters by the model method. For this quantity, the following results were obtained from the observations: $b - y = 0.267$, $c1 = 0.913$ (Hauck B. et al., 1998) and $[c1] = 0.86$ was calculated. Theoretical value of $[c1]$ was taken from Castelli and Kuruch (Castelli F. et al., 2003) Kuruch.

2. Comparison of observation and theoretically calculated values of Q index. Q index is determined in photometric system of $UBV : Q = (U-B) - 0.72(B-V)$. This quantity has a great importance because it is also independent from absorption in interstar space as $[c1]$ index. Values obtained from observation for this quantity are: $B - V = 0^m.38$, $U - B = 0^m.18$ (Fernie J.D., 1983) and Q=-0.094 was calculated. Theoretical values of Q index was taken from Castelli and Kuruch (Castelli F. et al., 2003).

3. Comparison of the measured and theoretically calculated prices of index β. β index determines the intensity of the Balmer series line of $H\beta$ in hydrogen. β index of observation value is $\beta = 2.67$ (Hauck B. et ., 1998), theoretical value was taken from Castelli and Kuruch (Castelli F. et., 2006).

4. Application method of parallax. This technique is a new method to determine the star's fundamental parameters (logg, T_{eff}) that are not related to star atmosphere models. Observation values of annual parallax of HD164136 star is $\pi'' = 0.00379$ (Leeuwen V.F.,

2007). The application method of parallax is interpreted in (Lyubimkov L.S., 2009).

logg, T_{eff} diagram assigned with the above-mentioned methods is set up (Fig 1).

The effective temperature and the surface gravity of the star are determined according to the geometric center of the intersection of the graphs in the T_{eff} - log g diagram: $T_{eff} = 6670 \pm 200K$, $logg = 2.45 \pm 0.2$. For comparison purposes, the results of other authors are shown in Table 1.

DETERMINATION OF MICROTURBULENT VELOCITY AND AMOUNT OF IRON

Most modern and accurate technique used for the determination of the microturbulent velocity is the atmospheric model method. This technique is based on the studies of large number lines with the intensity ($W\lambda$) range of atom and ion of any element.

By giving different values to the microturbulent velocity ξt for each line,

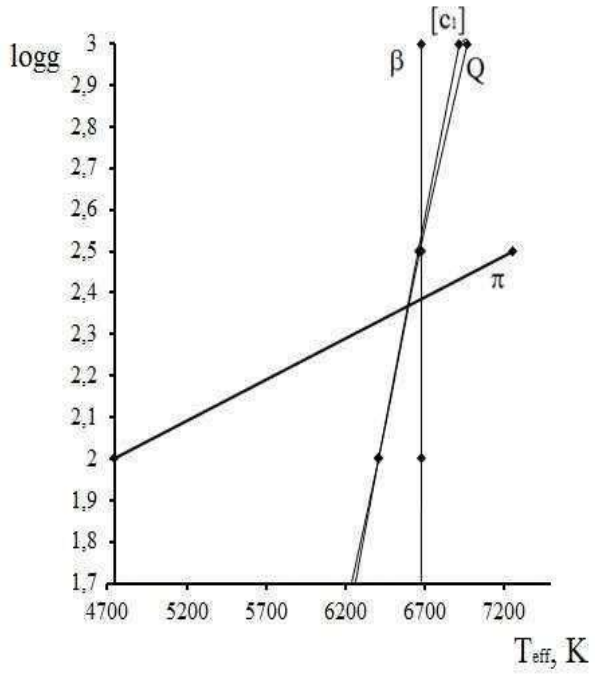

Fig. 1. logg- T_{eff} diagram

Table 1. Calculated values for T_{eff} and logg.

T_{eff}	logg	Authors
7140	3,87	Prugniel P. (Prugniel P. et. al.,2011)
6575	2.00	Luck R.E. (Luck R.E. et. al, 1995)
6803	3.33	Luck R.E. (LuckR.E.,2014)
6799	2.63	Cenarro A.J. (Cenarro A.J. et.
6811	3.40	Kipper T. (Kipper T., 1969)
6500	2.20	Adelman S.J. (Adelman S. J. et.al.,
6483		Kovtyukh V.V. (Kovtyukh V.V.,
6700	2.50	Alfaro (Alfaro B.H. et. al.,1997)
6465	2.00	Hauck (Hauck B.et.al.,1998)
6670	2.45	Our results

the amount of the corresponding element according to measured intensity $W\lambda$ is calculated and corresponding value for ξ_t is selected so that no systematic change with the increase in $W\lambda$ is observed in the value of the selected $\xi_t, log\varepsilon$.

The most commonly observed lines in the spectrum of HD164136 star belong to FeI, FeII lines. Appreciable departures from local thermodynamic equilibrium (LTE) may occur for Fe I lines, while Fe II lines are not seriously affected by departures from LTE; therefore, the microturbulent parameter and the iron abundance were determined from FeII lines on account of their insensitivity to non LTE effect.

For HD164136 star, a model (Kuruch R., 1993) with the parameters T_{eff} = 6670 K, $logg$ = 2.45 was chosen and based on this model, the iron abundance $log\varepsilon(FeII)$ was calculated in the different values of the microturbulent velocity. The iron abundance $log\varepsilon(FeII)$ was determined according to relatively weak lines ($W\lambda \leq 200m$Å). These lines were formed on the deep layers of the atmosphere. These layers were in LTT and the affect of amount of determination errors of microturbulent and damping values are not considered too weak lines. Calculation of the abundance of element was carried out on the basis of observation and theoretically calculated intensity of spectral lines. The theoretically intensity of spectral lines was calculated through the DASA program developed in the Crimean Astrophysics Observatory. It was established that there is no correlation between $log\varepsilon$ and $W\lambda$ when microturbulent velocity ξ_t, = 3.5 km/sec (Fig. 2).

During the analysis of microturbulent velocity according to FeII lines, the iron abundance

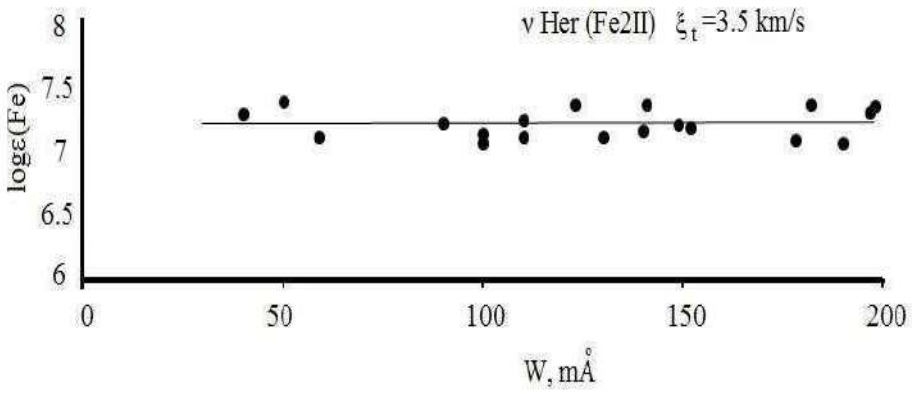

Fig. 2. Determination of the microturbulent velocity based on FeII lines in the atmosphere of the HD 164136 star: ξt, = 3.5 km/sec.

is determined: $log\varepsilon = 7.21 \pm 0.11$. Metallic indication of the star $[Fe/H] = \delta log\varepsilon = log\varepsilon*(Fe) - log\varepsilon\odot(Fe) = 7,21 - 7,45 = -0,21$, the iron abundance in the Sun: $log\varepsilon\odot(Fe)$ = 7.45 (Scott1 P. et al., 2015). Atomic data of spectral lines VALD-2 (Kupka F.N. et al., 1999) were taken from the database.

CONCLUSION

1. Fundamental parameters of HD164136 star have been determined:
$Teff = 6670K$, logg=2.45.
2. By using lines of FeII, the microturbulent velocities of star's atmosphere were determined: $\xi t, = 3.5 km/s$.
3. The iron abundance in the atmosphere of the star was calculated and compared to the amount in the Sun.

REFERENCES

1. Adelman S. J., Cay I.H., Tektunali H.G., Gulliver A.F. and Teker A., Astron.Nachr., 2008, № 1, 4-9.

2. Alfaro B.H., Ferro A.A., Schuster W.J., Publication of the Astronomical Society of the Pacific, 1997, № 109, 958-968

3. Boyarchuk A.A., Lyubimkov L.S., Izvestiya KrAO, 1981, № 64., 3. (in Russian)

4. Boyarchuk A.A., Lyubimkov L.S., Izvestiya KrAO, 1983, № 66., 130. (in Russian)

5. Castelli F., Kurucz R.L., in "Modeling of Stellar Atmospheres" (IAU Simp. No. 210), eds N.E. Piskunov, W.W. Weiss and D.F. Gray, Poster A20, 2003.

6. Castelli F., Kurucz R.L., Astron. and Astrophys. 2006, № 454., 333.

7. Cenarro A.J., Peletier R.F., Sanchez-Blazquez P., Selam S.O., Toloba E., Cardiel N., Falcon-Barroso J., Gorgas J., Jimenez-Vicente J., Vazdekis A., 2007, №374,. 664-690.

8. Fernie J.D., Astrophys. J., Suppl. Ser., 1983, № 52., 7-22.

9. Galazitdinov A.G., Preprint SAO RAN, 1992, № 92, 3-51. (in Russian)

10. Kipper T., Tart Astrof.Obs.Teated, 1969, №21., 65-78.

11. Kovtyukh V.V., Mon.Not. R. Astron. Soc. 2007, №378., 617-624

12. Kupka F.N., Piskunov T., Ryabchikova A., Stempels H.C., Weiss W.W.,

13. Astron. And Astrophys, Suppl.Ser., 1999, № 138, 119.

14. Kurucz L.S., CD-ROM 13, ATLAS9 Stellar Atmosphere Programs and 2km/s grid. Cambridge, Mass.; Smithsonian Astrophys. Obs., 1993.

15. Leeuwen V.F., Astron.Astrophys., 2007, №474., 653-664.

16. Luck R.E., Wepper G.G., Astron.J., 1995, №110, 2425-2456.

17. Luck R.E., Astron.J., 2014, № 147., 137.

18. Lyubimkov L.S., Rachkovskaya T.M., Poklad D.B., Astrofizika, 2009, № 52, 237. (in Russian).

19. Hauck B., Mermilliod M., Astron. Astrophys., Suppl. Ser., 1998, № 129., 431-433. Prugniel P., Vauglin I., Koleva M., Astronomy and Astrophysics, 2011, №531 A., 165.

20. Rufener F., Astron. Astrophys. Suppl, 1976, №26., 275-351.

21. Scott1 P., Asplund M., Grevesse N., Bergemann M. and Sauval A.J., Astron. and Astrophys 2015, № 26, 573.

Astronomy & Astrophysics (Caucasus) 3 (2018)

Key Words

Analytical modeling
Asymmetry changes
Asymmetry
Binary stars
CCD-observations
Chemical composition
Classification
Contraction
Dark energy
Dark matter
De Sitter world
Degree of polarization
Dispersion lines
Eclipsing, stars
Elementary systems
Emission-lines
Fraunhofer lines
Front and rear hemispheres
Full asymmetry
Fundamental parameters
Gamma- ray bursts (GRBs)
Infrared triplet lines Ca II
Lightcurves periods
Line profiles
Luminous Blue Variable Stars
Multiple supernovae outbursts
Nucleus of galaxies
Oblique rotator.
P Cygni
Polarization
Profiles
Pulsating stars
Rate of star formation
Solar spectrum
SO(4, 1) group,
Spectrophotometric characteristics
Spectrum
Spherically symmetrical,
Supernova (SNe),
Stars
The Sun
The velocity of microturbulent motion
Unitary irreducible representations
UBV photometry
Wigner-In¨on¨u limit,

Astronomy & Astrophysics (Caucasus) 3 (2018)

Author Index for Volume 3

A
Alısheva K.İ 16
Aliyeva, Z.F 16
Ayvazyan ,V 49

B
Beradze ,S 30, 39
Blinnikov, S. 49
Burkhonov, O. 49

C
Chigladze,R 1, 23, 61

E
Ehgamberdiev, S 49

G
Gadirova, U. R 3, 91
Gulahmedova S.N 10

I
Inasaridze, R 49
Inasaridze G. 49

K
Khramtsov, V 61
Klunko, E 49
Kochiashvili I. 30, 39
Kochiashvili,N. 30, 39
Krugly, Y 49
Kuli-Zade, D.M 10,16
Kvaratskhelia, O 49

M
Mamedov, S.G 91
Mazaeva, E 49
Mikhalchenko, O 61
Molotov, I 49

N
Natsvlishvili, R 30, 39

P
Pannicke, A. 30, 39
Pozanenko A. 49
Pruzhinskaya M. 49

R
Rajabov, B.A. 74
Rajabova Sh.S 10
Reva, I. 49
Rumyantsev, V 49

S
Salmanov, I.R 67
Samadov, Z. A 91
Sartipzade, R.K. 16
Shevchenko, V 61
Shustarev, P.N 67
Slyusarev, I 61

T
Tateshvili, M. 23

V
Vardosanidze M. 30, 39
Volnova, A 49

Astronomy & Astrophysics (Caucasus)

Scientific paper Submission

The submitted article's technical parameters are the same as in the USA leading international scientific journals.After the positive review only astronomy and astrophysical original articles will be published in this journal.

The manuscript should be presented in A4 format. The size of the article ,including bibliography and other types of enclosure should not exceed 20 pages printed with 1interval and 12 sized font.

It is possible to submit the online version of the manuscript but is should be written only in English. (Text must be typed in Times New Roman, MS word or Pdf file)

The text should be written on the whole page and not separately on twocolumns,the same as in this journal.

Structure of the paper:

Title of the paper:

Author/authors:

Name of the author/authors,firstname,secondname, working place,country and online address must be presented below the manuscript title.

Abstract

The abstract must be informative.Shouldrepresent the content of the paper,describe the goal of the research,symmerize results of the survey and show its theoretical and practical importance.The abstract should not exceed more than 250words,nearly one page.

Key words: Authors should provide key words,which are relevant to the topic.Maxium amount of the words should be 8 . Use only commonly used shortenings .

Introduction: Authors should highlight the essence of the problem, their sub-aims,what is their hypothesis,importance of their paper and what have been done peviously in this field.

Methods: The article should be build methodologically correct way. It should reflect the usage of modern research methods.

Results: Results must be described clearly and briefly**.** Each illustration should have its inscription**.** Number the tables used in the text consistently.

Analysis: This paragraph should investigate the importance of the paper results.You should compare your result to the previous ones**.**

Conclusions: The main conclusion can be written in this paragraph**.**

Acknowledgment: At the end of the paper on the separate chapter you should express your gratitute to those people who helped you during the research.

Literature citation: Consider that every source you have used in this paper is also indicated in the bibliography or vice versa.

Sources Reference Style: The literature quoted in the scientific publication should be indicated with round brackets.(Sort version:name of the author and the rule of the article publication**.**

Reference: Nominated literature where the author's identity is indicated fully,the date of the publication and appropriate page should be arranged alphabetically.

It will be published twice in a year.

The paper should be send to the following e-mail address: astronomy@sjuni.edu.ge

CONTENTS

1. Academician Evgene Kharadze
Chigladze R.

3. INVESTIGATION OF THE ATMOSPHERE OF THE STAR HD164136 (F2II)
Samadov Z. A. and Gadirova U. R.

10. THE FRAUNHOFERS LINES CLASSIFICATIONS ON ASYMMETRY CHANGES INSIDE THE PROFILES IN SPECTRUM OF THE SUN
Kuli-Zade D.M.,Gulahmedova S.N., Rajabova Sh.S

16. ON THE FULL ASYMMETRY OF THE WHOLE FRAUNHOFER LINES PROFILE IN SPECTRUM OF THE SUN
Kuli-Zade D.M., Mamedov S.G., Aliyeva Z.F., Alısheva K.İ., Sartipzade R.K.

23. Results of Observations over Jupiter's Galilean Satellites
Chigladze R., Tateshvili M.

30. Spectral and Photometric Data of Be star, EM Cep
Kochiashvili N., Natsvlishvili R., Kochiashvili I., Vardosanidze M., Beradze S., Pannicke A.

39. Photometric and Spectral Observations of P Cygni, the Luminous Blue Variable
Kochiashvili N., Beradze S., Natsvlishvili R., Kochiashvili I .,Vardosanidze M., Pannicke,A.

49. Observations of Supernovae associated with Gamma-Ray Bursts
Volnova A., Pozanenko A., Pruzhinskaya M., Blinnikov S., Mazaeva E., Inasaridze R., Ayvazyan V.,Inasaridze G.,Reva I.,Burkhonov O. , Ehgamberdiev S., Kvaratskhelia O. , Rumyantsev V.,Krugly Y., Klunko E.,Molotov I.

61. New observations of variable stars at the Astronomical Institute of Karazin Kharkiv National University
Shevchenko V.,Mikhalchenko O.,Slyusarev I., Khramtsov V.,Chigladze R.

67. Ca II INFRARED TRIPLET LINE PROFILES IN THE SOLAR PRECTRUM
Sartibzade R., Kuli-Zade D.M., Aliyeva Z.F.

74. THE CONTRACTION OF THE REPRESENTATIONS OF THE GROUP SO (4; 1) AND COSMOLOGICAL INTERPRETATION
Rajabov B.A.

91. INVESTIGATION OF THE ATMOSPHERE OF THE STAR HD164136 (F2II)
Samadov Z. A., Gadirova U. R.

97. Key Words

98. Author Index for Volume 3

99. Scintific paper Submission

100. Contents

Publishing Groupi: **L. Gurgenidze**
L. Zedginidze

Correctional: T. Dolidze

SAMTSKHE-JAVAKHETI STATE UNIVERSITY PRESS

Akhaltsike, Rustaveli Street №106
Tel.: 0(365)22-19-90, 591-41-12-78
E-mail: astronomy@sjuni.edu.ge